



UNIVERSITÀ DEGLI STUDI DI PADOVA

Corso di laurea in Scienze Forestali e Ambientali

*Monitoring and modeling of the debris flows in the  
Fiames area*

Relatore

Dr. Carlo Gregoretti

Correlatori

Dr. Massimo Degetto

Ing. Gianpietro De Vido

Laureando

Giacomo Crucil

Matricola n. 1016288

ANNO ACCADEMICO 2012 - 2013









# TABLE OF CONTENTS

1. Abstract .....	7
2. Riassunto .....	9
3. Introduction .....	11
4. Description of the phenomenon .....	15
5. Description of the case study .....	21
5.1. Geographic framework .....	21
5.2. Climatic framework .....	22
5.3. Geology and tectonic .....	23
5.4. Geomorphologic characteristics .....	24
5.5. The "c08" debris flow .....	25
5.6. The case study event .....	27
6. Materials and methods .....	31
6.1. Description of the hydrological model .....	31
6.1.1. Definition of the CN (Curve Number) .....	31
6.1.2. Pre-processing phase 1 (TerrainPro) .....	34
6.1.3. Pre-processing phase 2 (GeoPro) .....	36
6.1.4. Computation of the runoff hydrograph .....	38
6.2. Description of the Triggering model .....	42
6.2.1. Debris flow solid phase concentration .....	51
6.2.2. Input and output data of the "Debris flow hydrograph" model .....	54
6.3. The "automata" numerical model for simulation of routing and deposition phases of a debris flow .....	57
6.3.1. Principles of the Automata cellular model .....	57
6.3.2. Input data files and parameters and output files .....	60
6.4. PAI methodology for magnitudo estimation .....	62
6.5. Field surveys .....	63
6.5.1. Introduction to field surveys .....	63
6.5.2. GPS technology .....	64
6.5.3. Remotely sensed data .....	66
6.5.4. Individuation of the triggering area .....	67
6.5.5. Characterization of the topography of the channel .....	69
6.5.6. Grain size analysis .....	72

6.6.	Analysis of precipitations.....	73
6.6.1.	Use of rain gauges .....	73
6.6.2.	Rainfall data analysis .....	74
6.7.	Preliminary GIS analysis.....	78
6.7.1.	Introduction to GIS processing .....	78
6.7.2.	Data filtering.....	79
6.7.3.	Creation of the DTM for pre and post event.....	81
6.7.4.	Creation of erosion/deposition maps.....	85
7.	Results and discussions .....	87
7.1.	The hydrological model.....	88
7.1.1.	Hypothesis 1 .....	88
7.1.2.	Hypothesis 2 .....	101
7.2.	The triggering model .....	102
7.2.1.	Hypothesis 1 .....	103
7.2.2.	Hypothesis 2 .....	106
7.3.	The event simulations with the Automata model.....	106
7.3.1.	Hypothesis 1 .....	106
7.3.2.	Hypothesis 2 .....	124
7.3.3.	Final considerations.....	125
8.	Modelling of a design scenario.....	127
8.1.	Introduction to the design scenario .....	127
8.2.	Modeling the design scenario .....	128
9.	Conclusions.....	133
10.	Bibliography.....	137

# 1. ABSTRACT

A numerical model working on the freeware GIS platform ADB Toolbox, comprising a runoff hydrological model, a debris flow hydrograph model and an automata cellular model (modified by Gregoretti, 2012) have been used for estimating the solid-liquid hydrograph and simulating the routing and deposition phases of the debris flow occurred in the evening of the 4<sup>th</sup> of July 2011 on the "c08" channel at Fiammes (Km 109 SS51), Cortina d'Ampezzo, in the Italian Dolomites. The area is in a delicate situation, in which the much busy national road SS 51 "Alemagna" could be soon encountered by future dangerous debris flow from the same channel, or from the eleven adjacent ones, as occurred in the last year.

A set of field data, made by both GPS dataset acquired just after the debris flow occurred and Lidar dataset, have been used to estimate the sediment material entrained by the case study event, and to build the digital surfaces on which to run the models. Rainfall data, from a network of rain-gauges, have been acquired to describe the precipitation that generated it and use them in the model.

The simulations have the main objective of finding the best combination of input files and parameters to fit the output data with field measurements: this operation, testing the capability of the model to simulate a known event, provided the parameters to be used for simulating a project event and open the way to the creation on hazard and risk maps according to the methodology proposed in Italy by the PAI "Piano stralcio per l'Assetto Idrogeologico - Plan for the Hydrogeological Arrangement" (Autorita' di Bacino dei Fiumi Isonzo, Tagliamento, Livenza, Piave, Brenta-Bacchiglione, 2007).

The search for the parameters to simulate the event of the 4<sup>th</sup> of July 2011 took the necessity of producing a set of results to be tested, corrected and re-tested with an iterative procedure involving all the three models at the same time, using the not satisfying results as a basis for new simulations: the best parameters have been used to simulate three design events corresponding to the return periods: 30, 100, 300 years. The three simulations provided the magnitudo maps that were used to build the hazard map. The work should help to improve hazard management strategies for infrastructures and human settlements protection in the Dolomitic and, in general, in the Alpine areas.



## 2. RIASSUNTO

Un modello numerico, operante sulla piattaforma GIS freeware "AdB Toolbox", comprendente un modello idrologico per il calcolo dei deflussi superficiali, un modello idrologico per la stima delle condizioni di innesco di una colata detritica ed un modello agli automi cellulari, sono stati impiegati per stimare l'idrogramma solido-liquido e per simulare le fasi di scorrimento e deposito di una colata detritica avvenuta nella sera del 4 Luglio 2011 nel canale "c08" di località Fiames (Km 109 SS51), Cortina d'Ampezzo, nelle Dolomiti italiane. L'area è in una delicata situazione, nella quale la Strada Statale 51 "Alemagna", molto trafficata, potrebbe essere presto interessata da future colate detritiche generate dallo stesso canale o dagli undici altri canali adiacenti, come occorso in passato.

Dei rilievi sul campo, comprendenti rilievi GPS condotti subito dopo l'avvenimento della colata e rilievi Lidar, sono stati usati per stimare le quantità di sedimento mobilizzate dall'evento studiato e per generare le superfici digitali sulle quali far operare il modello. Dati di precipitazione sono stati registrati da una rete di pluviometri per studiare le piogge che hanno generato l'evento e usarle come input nel modello.

Le simulazioni hanno avuto l'obiettivo principale di trovare le migliori combinazioni di file e parametri di input i cui risultati coincidessero con quelli dei rilievi sul campo: questa operazione, testando le capacità del modello di simulare un evento noto, hanno fornito i parametri da utilizzare per simulare un evento di progetto, aprendo la strada alla creazione di mappe del pericolo e del rischio, basandosi sulla metodologia proposta in Italia dal PAI, Piano stralcio per l'Assetto Idrogeologico.

La ricerca dei parametri per simulare l'evento del 4 Luglio 2011 ha richiesto la necessità di produrre diversi set di risultati da testare, correggere e ri-testare seguendo un processo iterativo comprendente tutti e tre i modelli, usando i risultati non soddisfacenti come base per nuove simulazioni: i parametri migliori per simulare l'evento studio sono stati usati in seguito per simulare tre eventi progetto corrispondenti ai tempi di ritorno di 30, 100 e 300 anni. Le tre simulazioni hanno permesso di ottenere le mappe di magnitudo, in seguito usate per costruire la mappa del pericolo. Questo lavoro dovrebbe rappresentare un importante aiuto nelle strategie di gestione del rischio per la protezione di infrastrutture e insediamenti umani nelle aree dolomitiche e, in generale, alpine.

Uno speciale ringraziamento a mamma e papà  
che hanno reso possibile questo traguardo

### 3. INTRODUCTION

Debris flows are solid-liquid mixtures of water, mud, sediment and woody debris that are generated mainly in the alpine environment in the channel incised on the slopes at the base of the cliffs. Once that the mixture is mobilized, it propagates in the downstream direction until the reduced slope or the presence of defensive structures lead to the deposit of the solid phase and the subsequent stop of the debris flow.

Since debris flow are triggered and route downstream in few minutes, (it is an impulsive phenomenon), they are very dangerous for the speed that they can reach (even up to 10-12 m/s), for the large volumes of sediment that they can mobilize (debris diameter also of 4-5 m, in masses of many thousand s of cubic metres) and for the impact they can have on any obstacle they encounter. The routing path of a debris flow is usually obliged and coincides with the channel in the upper part of the fan but in the medium part it can deviates (Takanashi et al., 2007) and in the lower part, where terrain slope diminishes, can spread (Rickenman, 2005; Berti & Simoni, 2007).

The spreading of these phenomena in areas interested by human settlements, in the case in which the defensive structures are absent on the territory or are not able to intercept or contain the solid-liquid mobilized volume, entails serious consequences from the socio-economic point of view: loss of life, damage to buildings, interruption of infrastructures, etc..

The analysis of the threat for the safety measures against this type of phenomena is therefore necessary and is usually carried out through the simulation of possible future scenarios. The models since now used to simulate a potential threat scenario are:

- Empirical (Aulitzky 1973);
- Numerical of the empirical-statistical type (Berti & Simoni, 2007);
- Numerical based on the topographic gradient (Gruber, 2007);
- Numerical based on the integration of motion equations (Brufan et al., 2000; Armanini et al., 2009);
- Numerical SPH “Smooth Particle Hydrodynamics” type (Pastor et al., 2008);
- Numerical based on Cellular Automata (Deangeli & Segre 1995; d’Ambrosio et al., 2004);

Numerical models, in particular, are a mathematical-physics tool of fundamental importance for the definition of watershed plans. The one-dimensional hydraulic models are widely used internationally in practical applications of wave propagation in riverbeds

characterized by a simple shape. In these models, the simulation of the hydraulic motion is carried assuming a constant speed inside the single section but variable along the watercourse from section to section. The two-dimensional hydraulic models are naturally more complex than one-dimensional as they require more topographical, hydraulic and geo-morphological information and a greater computational effort on the computer. In this type of models, in order to respond more inherently to the physical reality of the problem, the speed in each section is characterized by two planimetric components so that it is possible to take into account the so-called "cross-current". These models respond effectively to the problem of the propagation of flood waves in complex riverbeds characterized by considerable topographical, hydraulic and geo-morphological variations. Specific hydraulic problems in which are widely used two-dimensional hydraulic models are represented by bodies such as lagoons of great extent, sea and coastal areas. The complexity of special hydraulic problems requires the application of advanced three-dimensional models of the latest generation into which it is considered also the third velocity component in the vertical direction. In this way it is possible to take into account all the velocity components in the three spatial dimensions. Typical problems of application of three-dimensional models are represented by the propagation of liquid masses characterized by different values of density, like the intrusion of sea water in a sweet watercourse, or solid/liquid/air mixtures like debris flows.

The aim of this work is to test the capability of a new three-dimensional numerical model, that operates in GIS environment, to predict the routing and the deposition phases of a debris flow and the conditions that generated it. In the specific, the model works on an open source GIS platform, AdB Toolbox, and it is based on Cellular Automata method and Bagnold Theory for dilatant fluids (Segree and Deangeli, 2005), modified by Gregoretti (2012) to take into account an input hydrograph and velocity computation through Tsubaki relationship. The model is composed of three main parts:

- a model to simulate the runoff hydrograph on the triggering area of the debris flow;
- a model to transform the liquid hydrograph into a solid-liquid hydrograph, accounting for the runoff conditions able to trigger the movement of sediment material in the channel-bed and for the availability of sediment;
- a model to simulate the routing and deposition phases of the debris flow on a provided digital surface (a DTM, Digital Terrain Model), given the input of the solid-liquid hydrograph.



The test has been conducted on a case study debris flow, whose monitoring allowed to obtain a set of data suitable to describe the mass movement that occurred during the specific event and then to compare them with the output of the numerical model. The test in particular has been conducted to simulate a debris flow event that occurred on the evening of the 4<sup>th</sup> of July 2011 in the test bed area of Fiames (Km 109 SS51), Cortina d'Ampezzo, in the Italian Dolomites: rainfall data have been obtained by a network of rain-gauges installed in the surroundings, to simulate the runoff hydrograph that triggered the event; Lidar data have been used to build a DTM of the watershed and of the fan, to estimate the contributing area for the runoff and to serve as basis for the routing simulations; on field GPS data have been acquired to describe the morphological variation in the channel bed and in the deposition area in order to estimate the quantity of sediment entrained and deposited by the debris flow.

The simulations have the main objective of finding the best combination of input files and parameters to fit the output data with field measurements: this operation, testing the capability of the model to predict a known event, provide the parameters to be used for simulating a project event and open the way to the creation on hazard and risk maps. In particular, the PAI methodology for the magnitude estimation of a debris flow event has been considered in this work.

This work is part of the "Alpine Space PARAMount ("imProved Accessibility: Reliability and security of Alpine transport infrastructure related to mountainous hazards in a changing climate") that aims at improving hazard management strategies for infrastructure protection by the adaptation of existing tools and practices to the transport sector (debris-flow, avalanche, rockfall). The project developed because transport security and accessibility are essential for a balanced and sustainable development of the Alpine region. Due to current climatic trends, the vulnerability of transport infrastructure to natural hazards has increased, but the specific threats to transport infrastructure have not yet been tackled in a systematic joint effort. Therefore the goal of PARAMount is to improve risk management strategies for infrastructure protection by the adaptation of existing tools and practices to these special requirements (Paramount statements, 2007).



## 4. DESCRIPTION OF THE PHENOMENON

Debris flows are natural events between a dry landslide and a flood event: they consist of a mixture of water and debris that propagates downstream along steep slopes or channels, by the action of the force of gravity. Their triggering can be caused by the mobilization by sliding of loose material on steep slopes or by the mobilization of debris accumulation on the bottom of streams and natural channels; in this work only the latter type of debris flow will be dealt. The occurrence of these phenomena is related mainly to brief and intense precipitation events, which provide large amount of surface runoff able to mobilize partially or totally the sediment material accumulated on the bottom of the channel bed. These deposits are due to earlier failures of the channel banks due to erosion of the channel-bed itself or by the superficial erosion (shallow landslides, rill and interill erosion). A debris flow occurs when runoff mobilize debris deposits accumulated on the bottom of the channel. The formation of runoff is related to the permeability of the basin, that is related to its land-use and geological and morphological characteristics. The debris flows is considered, as a type of event, a kind of solid mass transport (see Table 4-1) in which the movement of the debris is originated by the component parallel to the direction of the force of gravity and by the hydrodynamic force of the current, and is supported both by the exchange of momentum between the elements of the solid phase and by the interaction between solid and liquid phases; in ordinary solid transport instead, the movement of the debris is due to and supported by the hydrodynamic force of the current.

Table 4-1 Classification of mass solid transport (Takahashi, 1981)

	<b>Transport mechanism</b>	<b>Interstitial fluid</b>	<b>Speed and routed distance</b>	<b>Brief description</b>
<b>Landslide</b>	sliding, overturning, collapse	Air and water	from 2-3 mm/year to free fall	The particles of the terrain move slowly with little internal deformations. The water content is below the saturation threshold
<b>Sturzstrom</b>	Interaction between grains	air	from 200 m to 10 km	The debris flows on a sub-horizontal bed with high velocities
<b>Debris flow</b>	Interaction between grains and floatage	Water and clayey mud	from 0,5 m/s to 20 m/s, from 200 m to 10 km	Rapid downstream flux of a mixture of water and poorly sorted debris material

A debris flow is distinguished from other forms of sediment transport triggered by surface runoff, and from the landslides, for the role played by water, which forms with the debris an inconsistent mixture, whose behaviour is mainly related to the grain size characteristics of the material and to the morphological characteristics and runoff amount. The particle size of the solid fraction largely influence the rheological behaviour of a debris flow: assortments with a strong presence of fine-grained sediments (sand, silt, clay) favour a macro-viscous behaviour, while a uniform particle size allows sediments to collide more easily, thus favouring a grain-inertial behaviour. Another characteristic of debris flows is the speed at which they propagate downstream, up to values between 0.5 m/s and 20 m/s; the magnitude of the force of impact associated with the push of the fluid is of the order of some  $\text{kN/m}^2$ , while the dynamic actions due to the collision of large boulders in the front of the debris flow reach values of 102-104  $\text{kN/m}^2$ . A debris flow generally occurs with a main front formed by the coarser material, followed by the body and the tail consisting of solid material with decreasing dimension and concentration while increasing the distance from the front.

Debris flows were rarely observed directly, but recently, several shots taken with cameras allowed the observation of some special features. They occur as a series of waves or impulses (Li and Luo, 1981; Pierson, 1980) characterized by a tilted front containing the larger boulders, and by a less viscous rear part containing, however, a greater amount of water and grains of smaller dimensions (Johnson, 1970; Pierson, 1980) (Figure 4.1).

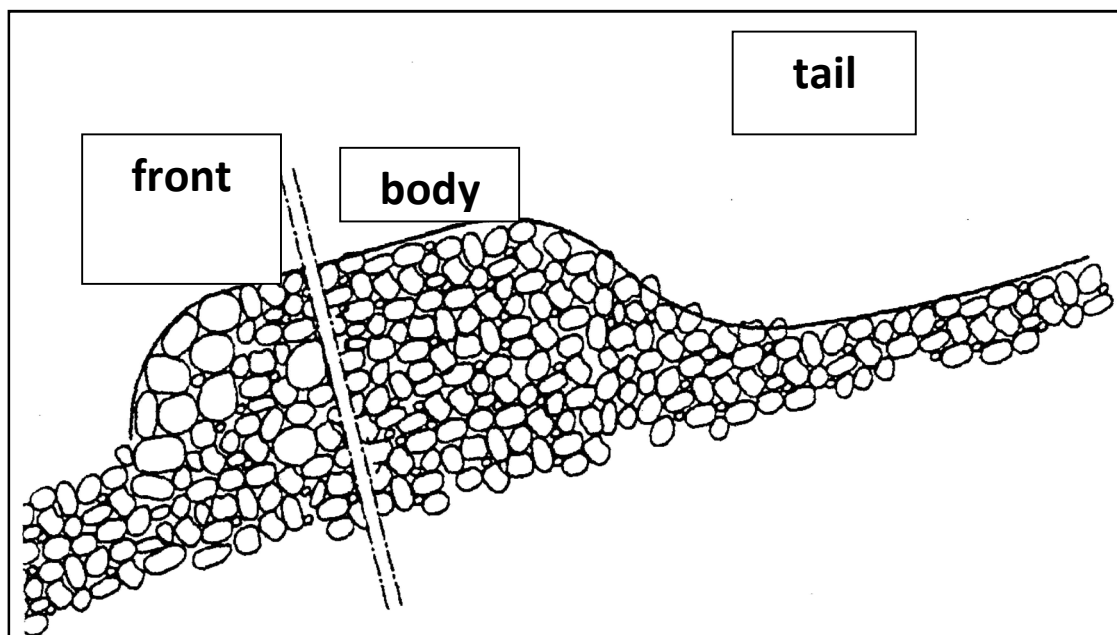


Figure 4.1 Scheme of the longitudinal section of a debris flow (from Bagante, 1999)

The density of the debris flow ranges between  $1400 \text{ kg/m}^3$  (Okuda et al., 1977) and  $2530 \text{ kg/m}^3$  (Curry, 1966), which correspond to volumetric concentrations respectively of 25% and of 70-80%. Among the waves, more fluid/wet phases may occur, characterized by turbulent flow with a high content of sediments but with a smaller number of blocks of medium-large dimensions (Genevois et al., 1999). Sometimes the character of the flow is very turbulent, with boulders suspended and floating on the surface (Okuda et al., 1980; Pierson, 1981).

The debris flow have a very distinct morphology: the length is generally greater than the width; relationship length/width frequently reported in the literature are in the range of 10:1 to 50:1 (Van Steijn, 1988).

Three elements are distinguishable in the morphology of a debris flow channel: the source zone or triggering area, the transport/excavation channel and the depositional fan.

The source areas are most frequently represented by topographical concavities or depressions in the upper part of mountain catchments, characterized by a geometry which favors the accumulation of debris and the convergence of the sub-surface and/or surface flow, required to mobilize them. In the source area, the removal of the sediment prevails on deposition: it is generally an area with steep slope, little or no vegetated, with a sufficient accumulation of debris on the surface. The sediment is especially neo-glacial moraine material and groundwater resulting from the retreat of glaciers and mechanic alteration of rock forming the substrate and the common rock walls above the slope.

Two main groups of source areas or detachment areas for debris flows can be defined, each one divided into sub-types:

- "Slope" type source area, divided into sub-types 1 and 2:
  - sub-type 1: the detachment area is located on a steep and poorly consolidated slope made of debris, with average slopes between 51 and 78 % ( $27 - 38^\circ$ );
  - sub-type 2: the detachment zone is located in the area of contact between a rock cliff and a steep detrital slope. The slope is similar to that of the previous type. Often a concentrated surface runoff originates in a channel of the rock wall and the water seeps in large extents within the debris cover. The debris flow takes its origin in the channel not far from the cliffs surface, causing a progressive erosion;

- "Channel" type source area, divided into sub-types 3,4 and 5
  - sub-type 3: the triggering area is located in a rocky gorge occupied by debris. The rocks in the bed and on the slope limit erosion. Often these masses of debris are covered with ice. The slope varies between 45 and 70% (24 - 35 °);
  - sub-type 4: large and temporary accumulations of debris in a channel are suddenly mobilized under the condition of increased runoff. The slope varies between 23 and 65% (13 - 23 °).
  - sub-type 5: last type of source of debris flow is represented by the collapse of a dam in a natural valley. This process can take different forms: from instability of the embankment; from overflows and progressive removal of surface layers; from subsequent collapses.

To these forms, other causes may then be added such as the siphoning in the mass or the liquefaction of this. The collapse of a natural dam in the river bed is perhaps, among the possible events, the most dangerous. The dam can in fact be created by landslides or flows from the slope during heavy weather events.

Hampel (1968) developed a classification of streams interested by debris flows, differentiating them according to flow on alluvial deposits or rock. The former can be destabilized even by events with a low return period, related to phenomena of intense rainfall followed ,immediately after, by a return to normal conditions of flow. The latter require on the other side a gradual accumulation of debris between a triggering rainfall event and the next and thus can be considered stable, at the end of the debris flow event, until the filling of material is sufficiently high to achieve another one. In this case, therefore, rainfall events very short but extremely intense will be responsible for the instability, preceded by periods of low intensity rainfall when material accumulates. Hampel (1968) argues, therefore, that the frequency of debris flow events does not coincide with the frequency of occurrence of maximum rainfall, but is dependent on the morphology and shape of the area.

Downstream the source area there is the transport zone, where the processes of erosion and deposition are more or less balanced. This area is normally in a channel, bounded or not by natural levees, located on the floor of a valley, in a ravine, or on the surface of a detrital slope. Question, in this case, of channels very often of ephemeral nature, subjected to changes and shifts of course according to the amount of rainfall and to, very often, changeable hydrological conditions. The flow normally follows pre-existing drainage lines and the main path commonly presents sections with a "V" or rectangular shape.

Where the slope begins to decrease, the transport zone gradually changes into a deposition zone, where this process dominates the erosion. The upper part of the deposition zone often consist of a channel bordered by natural levees and often is hardly distinguishable from the transport zone. The levees have a high angle of inclination from the horizontal and often show a reverse classing of the grain size, with the coarsest diameters at the top of the banks and out of them.

The material of a debris flow usually shows a wide range in particle size, ranging from clay to boulders of medium to large (even up to several tens of m<sup>3</sup>). Normally also a small but significant amount of clay material is present. Van Steijn (1989) reported an average particle size distribution for debris flow in the French Alps with bimodal distribution, with peaks in the fine fraction (<1 mm) and in the coarse fraction of the debris. The material of such deposits often includes the material of the triggering area. In many cases also organic material of different kinds can be incorporated in the detrital mass (Sauret, 1987).

A typical composition is, for example, according to Nasmith (1972):

- 30% rock with sizes up to 1 m
- 15% sand
- 35% silt and clay
- 20% of trees and wood in general

The peculiar characteristics of a debris flow, however, changes from region to region, depending on local geology. The following table summarizes the values of some physical properties of the materials constituting a debris flow (Figure 4.2):

<i>Table 2.3</i> Physical properties of debris flows (partly based on Hovius 1990).				
Property	Notation	Minimum	Maximum	Unit
Average grain size	$\phi$	-1.8	1.5	$\phi$
Trask grain-size sorting coefficient	$SO_T$	2.6	25	-
Debris-flow material density (bulk)	$\rho_b$	1.4	2.6	Mg·m <sup>-3</sup>
Debris-flow material density (matrix)	$\rho_m$	1.5	2.0	Mg·m <sup>-3</sup>
Volumetric solids content (bulk)	$c_s$	0.25	0.86	-
Volumetric solids content (matrix)	$c_i$	0.40	0.60	-
Volumetric clay content	$c_c$	0.005	0.20	-
Strength	$\tau_r$	0.3 <sup>a</sup>	5.0·10 <sup>4</sup>	Pa
Newtonian viscosity	$\eta_N$	10 <sup>b</sup>	8.0·10 <sup>3</sup>	Pa·s
Bingham viscosity	$\eta_B$	0.01 <sup>c</sup>	700	Pa·s
Average flow velocity	$u_m$	0.1	30 <sup>d</sup>	m·s <sup>-1</sup>
Length	$l$	0.2	1.2·10 <sup>5e</sup> 6.0·10 <sup>5f</sup>	m
Volume	$V$	1·10 <sup>-3</sup>	1·10 <sup>12f</sup>	m <sup>3</sup>

<sup>a</sup> Li and Luo (1981)  
<sup>b</sup> Morton and Campbell (1974)  
<sup>c</sup> Zhang et al. (1985)  
<sup>d</sup> Zeng et al. (1992)  
<sup>e</sup> Martinez et al. (1995)  
<sup>f</sup> subaqueous debris flows described by Masson et al. (1992)

Figure 4.2 Physical properties of debris flows (from Blijenberg 1998)

A wide particle size distribution is essential to have high values of density and volumetric concentration in the materials constituting the debris flow. From numerical simulations for the arrangement of spheres of different sizes, Johnson and Rodine (1976) concluded that a mixture of spheres of three different measurements can reach a volumetric concentration up to 0.98. In a moving fluid, the combination of particles will take place above a certain concentration. In agreement with Johnson and Rodine (1976), this causes an increase of both the internal friction angle of the material and the apparent cohesion. For real debris flow they established that the volumetric concentration can be up to 0.95 without significant combinations of particles. Nevertheless Takahashi (2007) states  $0.9C^*$  the superior limit of volumetric concentration, where  $C^*$  is the dry sediment volumetric concentration of sediment at rest.

Another important effect of large particle size distribution is a very rapid dissipation of pressure excess of interstitial fluid. In a mixture of solid particles and fluid, a part of the weight of the solid particles is counterbalanced by the fluid through the buoyancy. The pressure of the fluid increases with respect to a hydrostatic distribution because of the exchange of momentum with the solid phase, creating an excess of pressure in the voids that increases the interstitial fluid pressure over the hydrostatic value.

In a mixture containing a wide variety of particle size, the voids between the larger grains are occupied by the smaller grains and the interstitial fluid. Only the gaps between the smaller grains are occupied by the interstitial fluid. Thus, the connections between these voids are very small. However, the interstitial fluid often contains a bit of clay, which makes it more viscous. Thus, It has a net effect, that is a very slow flow of interstitial fluid through the pores and a slow dissipation of the pressure excess due to the exchange of momentum of the grains if they are dispersed.



## 5. DESCRIPTION OF THE CASE STUDY

### 5.1. Geographic framework

The study area (Figure 5.1 and Figure 5.2) is located along the west and south-west slopes of the Pomagagnon and Pezories massif, between 2 and 3 km north from Cortina d'Ampezzo. The area, that lies on the section between the km 106 and the km 110 of the SS 51 "Alemagna" includes twelve debris flow channels, active straight toward the S/S 51 and the river Boite. The latter events in some channels date back, before this study, to 2004 and 2006, and recently, to summer 2011.

On the Regional Technical Map of the Veneto Region, it falls within the Section 1:10000 n° 029020 (Chiave), and within the elements 1:5000 n° 029021 (Zurlon), 029022 (Chiave), 029023 (Cadin di Sopra), 029024 (Fiammes).

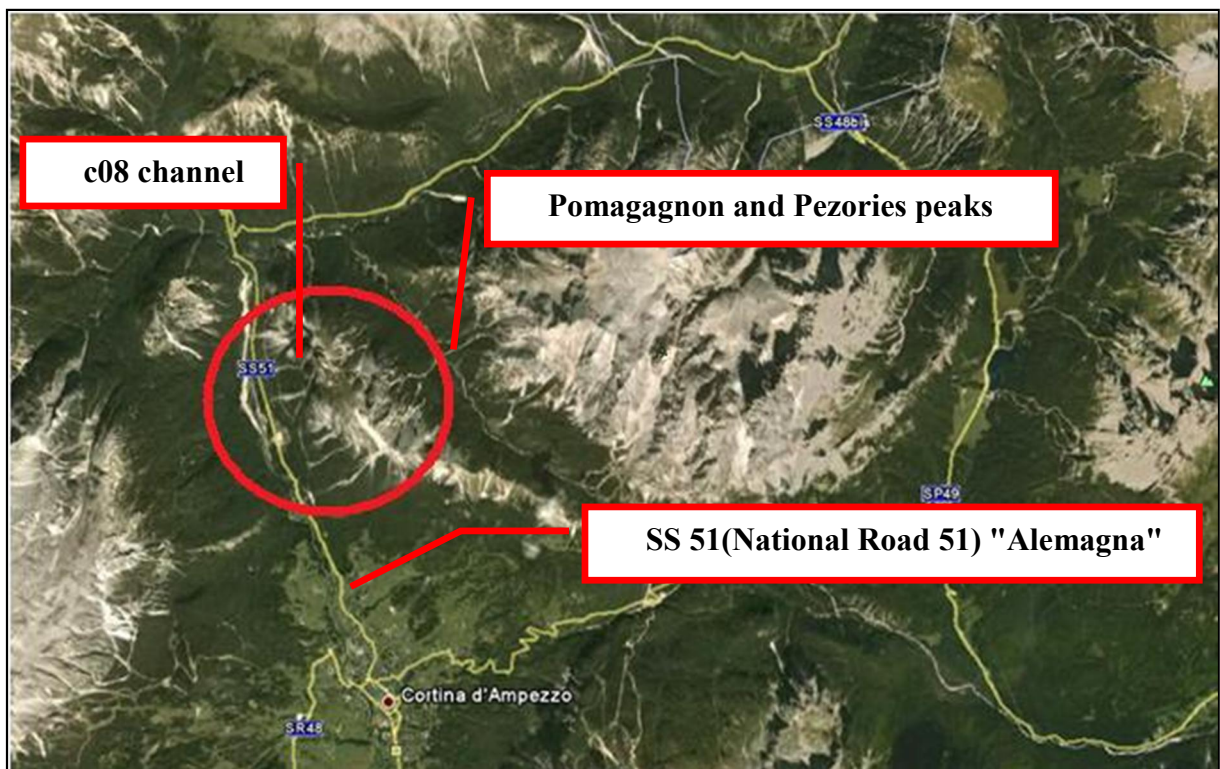


Figure 5.1 The localization of the case study area. The town of Cortina d'Ampezzo and the SS 52 "Alemagna" national road are indicated.

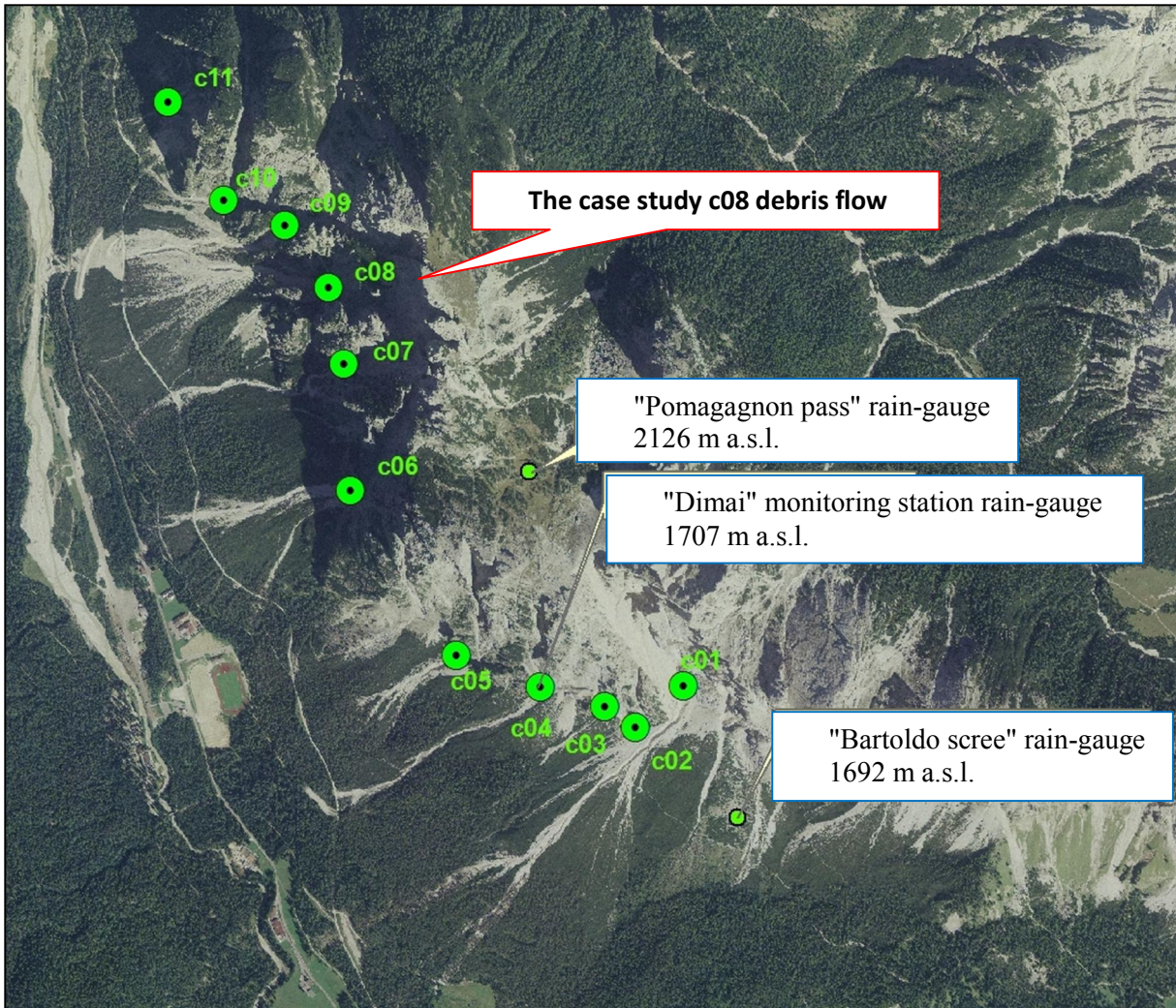


Figure 5.2 The Pomagagnon and Pezories S-W sides, with the eleven active debris flow channel and their respective triggering areas. The location of the three used rain-gauges for the acquisition of rainfall data is provided.

## 5.2. Climatic framework

In order to characterize the climatic framework of the hollow of Cortina d'Ampezzo, the rain and thermometric data coming from the Cortina meteorological station (1230 m a.s.l.) of the "Ufficio Idrografico del Magistrato alle Acque di Venezia", have been analyzed by a previous study (Convenzione tra La Regione Veneto E L'IRPI – CNR per lo studio della colata detritica di Fiames (Cortina d'Ampezzo, BL)), considering the interval between the 1938 and the 1994. The area is characterized by a meso-thermic wet climate, with the average temperature of the coldest month between  $+18^{\circ}\text{C}$  and  $-3^{\circ}\text{C}$ , by the absence of a dry season, and with the average temperature of the warmer month inferior to  $22^{\circ}\text{C}$ .



The characteristics of precipitation of the study area are derived from the data of the 5 existing weather stations in the town of Cortina d'Ampezzo Cortina, Misurina, Falzarego, Podestagno, S. Vito. The data series do not cover the same period for all 5 stations, in particular, the data of the recent years are missing. The average annual rainfall of the study area, as snowfall from November to May, is generally between 1100 and 1150 mm, with the exception of Podestagno, the highest station, and is distributed in 11-115 days per year (Figure 5.3). The mean monthly rainfall excess the 100 mm from May to November, with a peak in the June-July period.

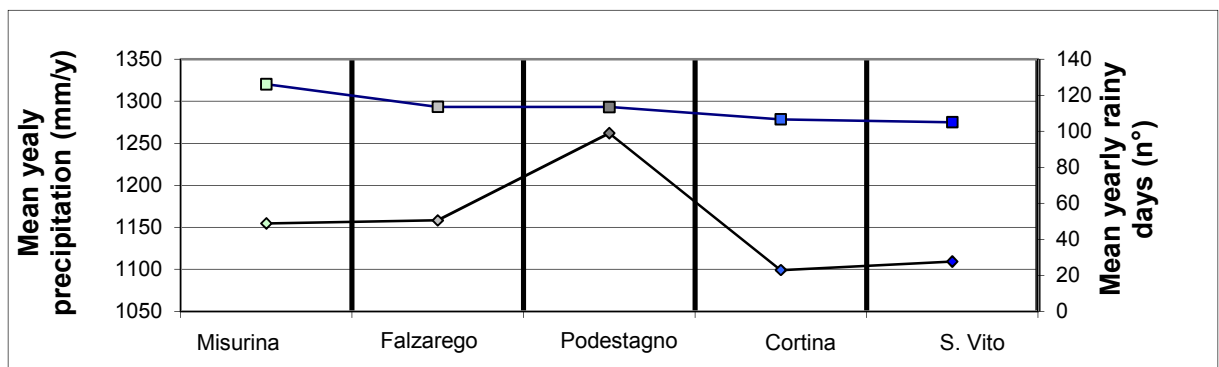


Figure 5.3 Mean annual rainfall and number of rainy days in the stations of Cortina, Misurina, Falzarego, Podestagno, S. Vito.

### 5.3. Geology and tectonic

On a wide spatial scale the area of Fiammes is set in the Eastern Dolomites, Southern Alps, south to the Insubrica tectonic line, that separates the northern metamorphic alpine layer from the southern alpine layer made principally by sedimentary rocks.

The geologic layers forming the mountain group of the Pomagagnon are listed as follow, from the most ancient and deep: 1) San Cassiano formation, Cassiana and Durrenstein Dolomitic Limestone formation; 2) Raibl and Primary dolomites; 3) Dachstein Limestones, Grey Limestones, Fanes Encrinites, Ammonitico Rosso, Biancone, silty red limestones, Puez marl, flinty red limestones, flysch Ra Stua, Ruiobes de Inze formation, Antruilles formation, Mt Parei conglomerates.

Over the described formations, deposits of the quaternary area laying: they consists mainly of debris deposits of gravitative origin, produced from mechanic and meteoric degradation of rock cliffs.

Two main tectonic movements interested and modified the pre-quaternary rocks:

- in the pre-oligocene over-thrust fault movements and folds acted toward West and strike-slip faults acted in NNE-SSW direction. This tectonic phase made the Raibl formation of the mount Pomagagnon thrust over the Primary Dolomite of the Tofane mountains, giving the origin to the upper Boite valley with a N-S direction

- during the Neogene, over-thrust movements toward S, folds with E-O direction and two main systems of joined faults with NO-SE and NE-SO direction deformed the aforementioned structures, making the Dacshtein limestones and the Primary dolomite of the mount Croda d'Ancona over-thrust the Primary dolomite of the Cristallo mountain

## **5.4. Geomorphologic characteristics**

The morphology of the area is strongly influenced by the geologic structure, characterized by the alternation of rigid and plastic formations.

The diving of the layers involved in over-thrust movement created, on the left side of the Boite valley, the sub-vertical hanging wall cliffs of the Croda d'Ancona and Pomagagnon mountains, made up by the Noric formations of Primary Dolomite. Here, the weathering of the limestones and of the dolomites gave origin to a dense debris layer (at least 40 meter, according to recent surveys) that covers almost completely the hillslope, not allowing the surfacing of the bedrock. The debris is originated on cliffs characterized by an intense fracturing, caused by the action of crio-clastism and rock falls, and is made up by material sorted from fine silt particles to big rocks and boulders (3-4 m of diameter), with slopes going from 30-40° just under the cliffs to 10-20° on the lower portions.

The hillslope is often interested by debris flow events, in correspondence to channels within big fractures of the cliffs and ledges. Much of them are occurring on the hillslope, changing direction on each event, many others are very channelized but with very frequent avulsions. On the basis of photo-interpretation and field surveys (Convenzione tra La Regione Veneto E L'IRPI – CNR), more than 300 debris flows have been founded in the municipality of Cortina d'Ampezzo, distinguishing the rock catchment, the triggering area, the flowing channel and the depositional fan.

## 5.5. The "c08" debris flow

The co8 channel takes origin within a deep cove in the S-W Pomagagnon mountain side, surrounded by sub-vertical rock cliffs. There, at 1736 m of elevation, a drainage area of about 0.147 km<sup>2</sup> give soon origin, just where the rocky walls end, to a channel that cuts the upper layer of fine sediments and silt and the down below layer of very coarse sediment and big boulders.

Two triggering areas have been identified, one (called A) at 1637 m a.s.l., 180 m downstream the head of the channel, one (called B) at 1592 m a.s.l, 260 m downstream, where the availability of poorly sorted sediment can easily matches the critical discharge conditions for its mobilization. There the slope varies between 40% and 50%. Assuming as outlet the triggering sections, the relative catchment area of A and B has been calculated, as resumed in table (Table 5-1): it varies of 0.012 km<sup>2</sup> among the two.

At 1580 m a.s.l. the channel gets outside the rock cliffs and runs on a gentle detrimental hillslope, with the old main channel proceeding westward and the new channel, opened during the 4/07/2011 debris flow event, proceeding WWS direction. There the channel host a huge quantity of sediment up to the banks and outside them, where the smoothness of the channel itself and of the hillslope allows for frequent and abundant avulsions, on slopes between 20% and 40%.

At 1385 m a.s.l. the channel reaches the "Cortina-Dobbiaco" bicycle path that runs South to North. In the portion of the hillslope under the bicycle path a huge detention basin should protect the "SS 51 d'Alemagna" national road from the discharge of debris flow events. It is composed of two big walls, about 5 m tall, made of recovered material from the debris flow: one, semi-circular, just beneath the cycling lane, creates a pool, the other lays N-S on about 260 m just above the national road (in correspondence of the Km 109 SS51). The total volume of the retention basis in roughly 100000 cubic metres.

Table 5-1 Channel 08 main parameters

Channel 08 main parameters	
Total lenght	780 m
Average slope	48.6%
Average slope on the fan	42.2 %
Slope in triggering area A	42.70%
Slope in triggering area B	49.41%
Catchment area to triggering A	0.135 km <sup>2</sup>
Catchment area to triggering B	0.147 km <sup>2</sup>

The watershed contributing to the triggering section (Figure 5.4) develops deeply, with a quite elongated shape, within the Pomagagnon massif. His morphology, characterized by high sub-vertical cliffs, is able to channel low altitude meteorological perturbations greatly increasing his capacity to catch precipitation and generating runoff. The high Melton number (1.97) indicate a basin and a fan with great propensity for the formation of debris flows. His main parameters are resumed in table (Table 5-2).

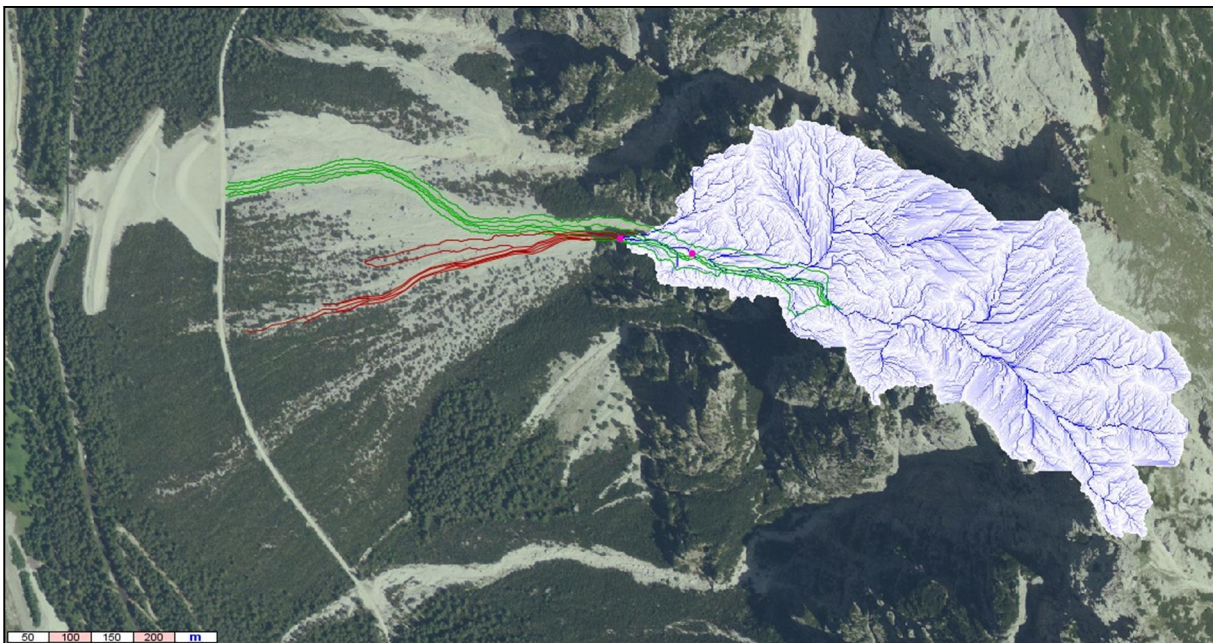


Figure 5.4 Orthophoto of the c08 channel and, overlapped, the drainage area to the triggering section B.

Table 5-2 c08 basin parameters

Area 2D	0.147 km <sup>2</sup>
Area 3D	0.417 km <sup>2</sup>
Upper height	2345 m
Lower height	1591 m
Average height	1980 m
Melton number	1.97

Observing the debris flow area, both on the field and on a orthophoto, the huge quantity of sediment deposited till to the national road by previous events, demonstrate that the c08 basin is able to mobilize, during storms characterized by larger return times, many thousands of cubic metres of sediment material, representing a great risk for the infrastructure downstream. The SS 51 "Alemagna" is characterize during great part of the year by an intense traffic of cars and huge loads, being the only link to the most famous touristic hot spot of the area, Cortina d'Ampezzo, and proceeding to Austria.

## 5.6. The case study event

In the evening of the 4<sup>th</sup> of July 2011 a storm event triggered a debris flow by channel-bed failure on the c08 channel, mobilizing a quantity of sediment ranging from 4700 to 6700 cubic meters (according to the results of the GIS analysis on the field survey dataset). The dynamic of the event is not completely clear since no direct observation of the event occurred and the channel has been not covered by surveys since many weeks. From the inspection of the area seems that the material flowing from the triggering section first obstructed the old channel, or founded it already obstructed by an event previous to the 4th July, and deviated towards the WWS direction, along a path left by an old event, digging a new active channel in that direction. From GIS analysis of the DTM of the area resulted that the new active channel deviated toward the steepest slope path. The debris flow then stopped the deposition of material 500 m downstream, after passing over the bicycle path.

The GIS volume computation, that gave a total of 6700 m<sup>3</sup> of deposit, net of erosion, has been done considering that the old channel has been blocked by the material of the same debris flow event. On the other hand, the volume computation considering the channel already blocked by a previous event lead to a result of about 4500 m<sup>3</sup> mobilized by the 4<sup>th</sup> July event.

The rain-gauge positioned on the Dimai channel, positioned about 1,7 Km South, (see ch. 6.6.1) registered the storm event of precipitation, showing a peak of intensity of 64.8 mm/h at time 21:40 (Figure 5.5).

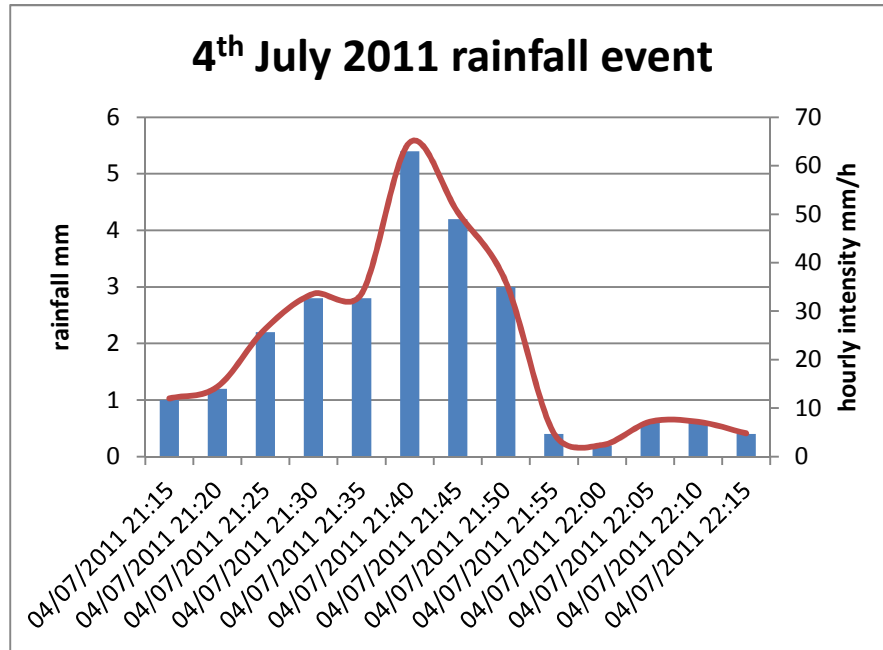


Figure 5.5 Yetograph of the 4th July 2011 precipitation registered at the Dimai rain-gauge.

In the meanwhile the rain-gauge positioned behind the Fiames peak, positioned about 1,2 Km South-East, didn't registered high values of intensity, and this is possibly due to the very variable and spatially limited nature of the storm events in the mountain area, in particular close to high peaks and big rock cliffs, where the effect of wind can strongly influence the distribution of precipitations within few hundreds of meters.

The orthophoto in figure (Figure 5.6), dated to 2008, shows the c08 channel before the 4 July 2011 event, figure (Figure 5.7) shows a orthophoto of the channel taken in November 2011: it is possible to recognize the old channel (green enhanced) and the new active channel (red enhanced). At the time at which the second orthophoto was taken, other two debris flow events occurred on the new active channel, modifying the topography and the sediment distribution on the area, but no data are now available.



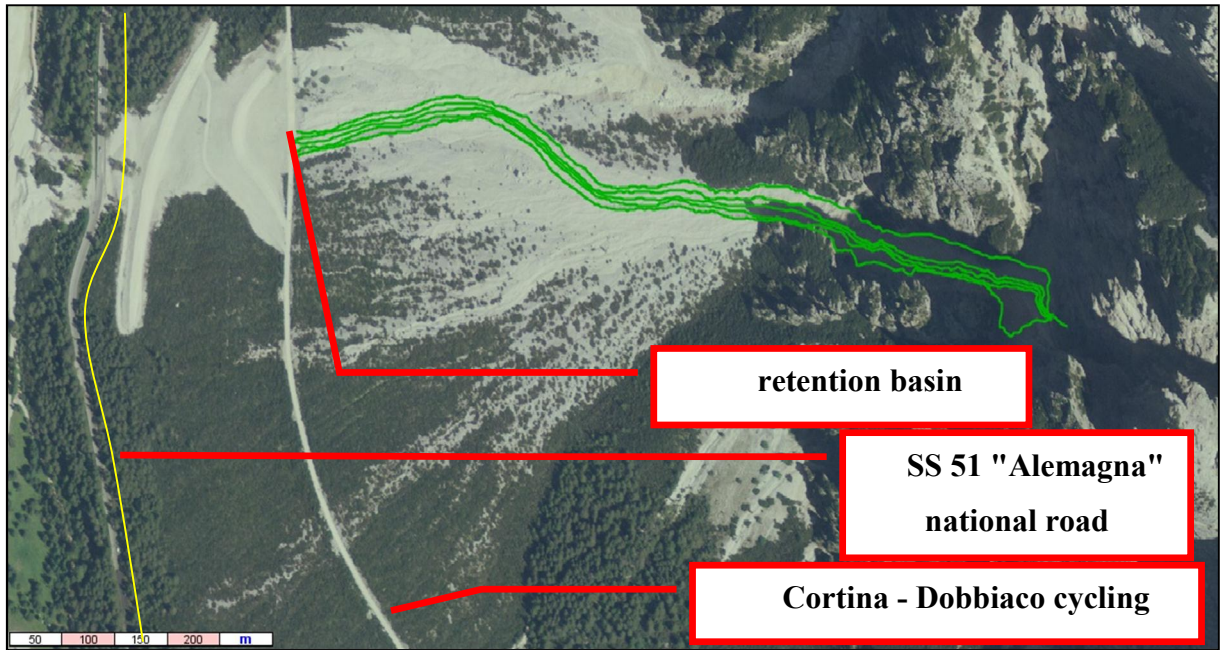


Figure 5.6 The c08 past active channel, before the 4<sup>th</sup> July 2011 event, is indicated in green. After exiting the rock walls and routing on the fan, it was directed west-ward, toward the retention basin protecting the SS 51 "Alemagna" national road.

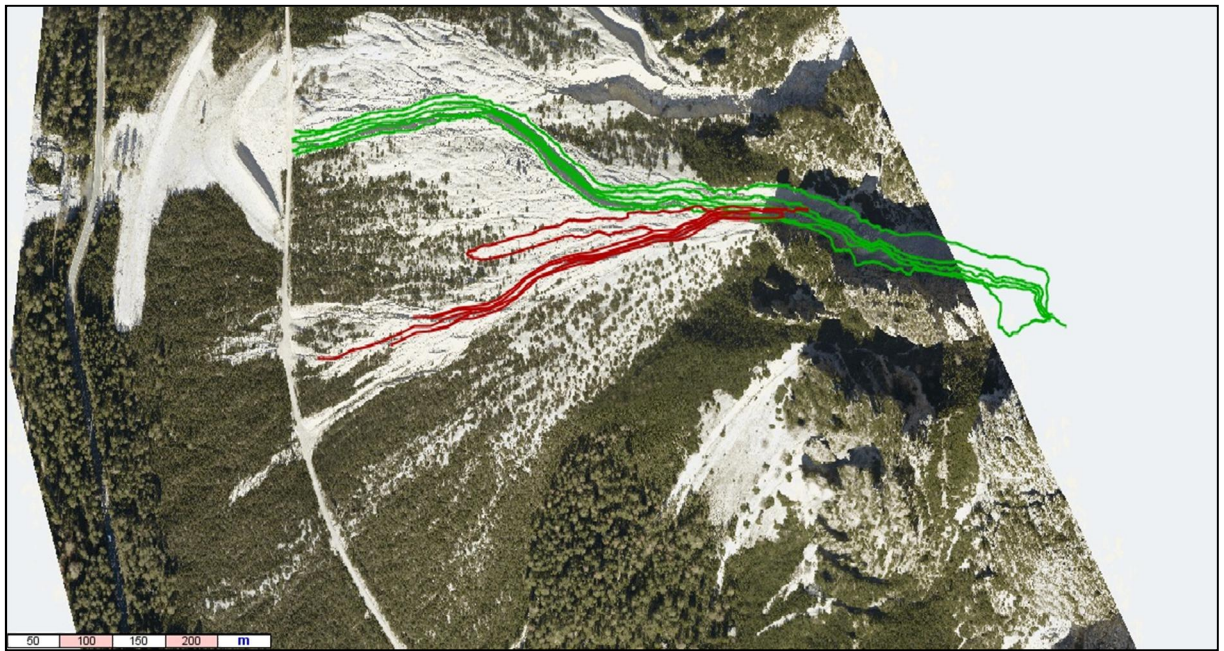


Figure 5.7 The c08 new active channel, after the routing of the 4<sup>th</sup> July 2011 event, is indicated in red (in green the old active channel). To be noted that the new routing direction is avoiding the retention basin, toward the SS 51 "Alemagna" national road.



## 6. MATERIALS AND METHODS

### 6.1. Description of the hydrological model

The Hydrological model allows the creation of the liquid hydrograph by which it is possible to calculate the solid-liquid hydrograph of the debris flow, that represents the main input of the model for the simulation of the routing and deposition phases of a debris flow on a fan: the Automata model.

The bibliography referring to chapters 6.1, 6.2 and 6.3 is available in Degetto and Gregoretti (2012). and in Gregoretti and Degetto (2012).

The hydrological model, that is implemented in the GIS software AdB-ToolBox, is composed of four distinct steps:

1. Definition of the CN (Curve Number)
2. Pre-processing phase 1 (TerrainPro): Extraction of the DEM of the watershed starting from a DEM of a larger extension area and its hydrological refinement.
3. Pre-processing phase 2 (GeoPro): Determination of the morphological parameters used by the model to simulate runoff.
4. Computation of the runoff hydrograph

#### 6.1.1. Definition of the CN (Curve Number)

The curve number CN is a parameter relative to the attitude of a soil to produce runoff and is used by the SCS (Soil Conservation Service) method for computing excess rainfall or direct runoff. The SCS method divides the total precipitation  $P$  by three contributes, according to the scheme of Figure 6.1:  $P_e$  = excess precipitation,  $I_a$  = initial abstractions and  $F_a$  = infiltration loss.

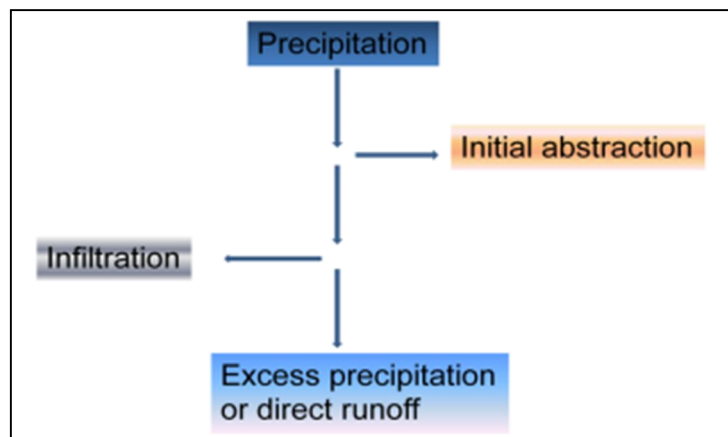


Figure 6.1 Schematic view of SCS method for computing excess precipitation.

The continuity equations yields:

$$P = Pe + Ia + Fa \quad (6.1)$$

The SCS method is based on the hypothesis that the ratio between  $Fa$  and the potential maximum retention  $S$ , that is the soil saturation volume per unit of area, is equal to the ratio between  $Pe$  and  $P-Ia$ :

$$\frac{Fa}{S} = \frac{Pe}{P - Ia} \quad (6.2)$$

Assuming for mountain watershed  $Ia = 0.1 S$  the combinations of equations (6.1) and (6.2) provides:

$$Pe = \frac{(P-0.1S)^2}{P+0.9S} \quad (6.3)$$

Then excess precipitation  $Pe$  depends on total precipitation  $P$  and  $S$ :  $P$  is a datum while  $S$  must be estimated. The parameter  $CN$  is then introduced with the purpose to estimate  $S$ .  $CN$  is a synthetic parameter that quantifies the capability of a soil of producing runoff and is related to  $S$  according to the following relationship:

$$S = S_0 \left( \frac{1000}{CN} - 10 \right) \quad (6.4)$$

where  $S_0$  = scaling factor equal to 25.4 mm. The higher the  $CN$  value the higher the  $Pe$  value: for a value of  $CN = 100$  ( $S = \infty$ , impermeable soil) all the precipitation is converted to runoff, for a value of  $CN = 0$  the high hydraulic conductivity of the soil do not allow the presence of excess rainfall, so there is no direct runoff.

The Curve Number raster map is obtained by overlapping a Land-cover raster map and a Hydrologic Groups raster map through an automatic procedure of reclassification implemented in the software: according to a conversion table (ASCE, 2009; Debris Flow Modeling Tool- Reference Manual, 2012) the Land-cover and Hydrologic Groups are converted to a fixed value of  $CN$ .

The Land-cover map is obtained from orthophoto interpretation.

The hydrologic groups of soils are based on their infiltration and transmission rates, that depend on size of grains, size of pores, surface tension or suction, soil texture, soil structure, hydraulic conductivity, initial moisture content and slope. To build a hydrologic groups map an overlay of different layers is needed: pedology-map, geo-lithology map, rocky outcrops and scree map, geotechnical map, slope map (with the same soil property, a soil with a greater steepness has a bigger surface flow, so that an “apparent” lower infiltration results: for slopes lower than 30% the hydrological class remain the same, while for slopes greater than 30% the hydrological class assigned is scaled to a class proceeding from class A to class D). To define

the different hydrological groups the following values in are applied (Table 6-1, Table 6-2, Table 6-3).

Table 6-1 Hydro-groups a

Hydrologic Group	Infiltration rate when thoroughly wetted	Infiltration rate cm/hr	Initial Potential infiltration rate - Horton (mm/hr)	Asymptotic Potential Infiltration rate – Horton (mm/hr)	Permeability (cm <sup>2</sup> )
<b>A</b>	High and very high	0.762 - 1.143	250	25.4	$10^{-7} - 10^{-2}$
<b>B</b>	Moderate	0.381 – 0.762	200	12.7	$10^{-9} - 10^{-7}$
<b>C</b>	Low	0.127 – 0.381	125	6.3	$10^{-11} - 10^{-9}$
<b>D</b>	Very low	0.000 – 0.127	76	2.5	$10^{-14} - 10^{-11}$

Table 6-2 Hydro-groups b

Hydrologic Group	Water Transmission rate	Saturated Hydraulic Conductivity (m/s)	Water runoff potential	Drainage	Soil depth
<b>A</b>	High	Soil depth >1.0m: $> 4 \cdot 10^{-5}$	Low and very low	Well or excessively drained	Deep soils
<b>B</b>	Moderate	Soil depth <0.5m: $1 \cdot 10^{-5} - 4 \cdot 10^{-5}$ Soil depth >0.5m: $4 \cdot 10^{-6} - 1 \cdot 10^{-5}$	Moderately low	Moderately drained	Deep soils but less than those in A
<b>C</b>	Slow	Soil depth <0.5m: $1 \cdot 10^{-6} - 1 \cdot 10^{-5}$ Soil depth >0.5m: $4 \cdot 10^{-7} - 4 \cdot 10^{-6}$	Moderately high	Poorly drained	Shallow soils or deep soils with an impermeable layer
<b>D</b>	Very slow	Soil depth <1.0m: $< 1 \cdot 10^{-6}$ Soil depth >1.0m: $< 4 \cdot 10^{-7}$	High and very high	Very poorly drained	Shallow soils or deep soils with an impermeable surface layer

Table 6-3 Hydro-groups c

Hydrologic Group	Texture 1	Texture 2	Indicative Geo-lithology
<b>A</b>	Gravels and Sands (>90%) Silt and Clays (<10%) Texture: medium-coarse with skeleton	Gravelly, sandy-gravelly and sandy soils. May fall into this soil category: silt loam, loamy sand, loam with good structure or with skeleton >35%.	Highly fractured rocks, debris and pebbles on minor slopes, inconsistent tuffs, sand, gypsum, ash, lapilli, cinders, not compact limestone, rock fragments more or less cemented
<b>B</b>	Gravels and Sands (50-90%) Silt and Clays (10-20%) Texture: medium-coarse	Sandy loamy soils. May fall into this soil category: loam, silt loam, silt, sandy clay loam with good structure or with skeleton >35%.	Rather fractured rocks, morfine and glacial deposit on minor slopes, conglomerates, breccias, cemented sands
<b>C</b>	Sands (<50%) Silt (>10%) Clays and colloids (20-40%) Texture: medium-fine	Loam, silt loam, sandy clay loam, clay loam, silty clay loam soils low in organic content May fall into this soil category: sandy clay, silty clay, clay with good structure or with skeleton >35%	Fractured rocks, compact sedimentary rocks, marl, sandstone, pumice, debris and pebbles on steep slopes, dolomitic compact limestone
<b>D</b>	Sands (<50%) Silt (<10%) Structured and homogeneous clays (>40%) Texture: fine	Silty clay, clay soils. They are swellable clay soils. Fall into this soil category all those who have an impermeable surface layer (depth < 0.5m) or who have permanent high water table (depth < 0.6m). Rocky outcrops, Scree with relative thin layer on slightly permeable layer on steep slope.	Slightly fractured rocks, igneous rocks, shale, lacustine deposits, metamorphic rocks, gneiss, mica-schist, quartzite, phyllite, schist, talc-schist.

As a summary, the "CN" tool requires as input:

- the landcover raster map
- the hydrologic groups raster map
- the CN conversion table

to give as output:

- the CN distribution raster map

### 6.1.2. Pre-processing phase 1 (TerrainPro)

The DEM of the catchment area can have pixels (raster cells) that are surrounded by pixel of higher elevation: this kind of situation generates, for the algorithms that calculate flow accumulation and flow direction, a pixel called "pit", because of its property of serving as a well for the simulation of routing water, precluding its way to the outlet. In such a situation is not possible for the routines of the phases 3 and 4 to determine a path from that pixel to the outlet.

To solve this problem the "DEM depit" routine compares the elevation of each cell with those of the eight cells surrounding it, then it applies one of two possible methods:

- the excavation of a channel from the "pit", to the nearest pixel with a lower elevation (solver): the solution increases the elevation of the pit cell up to 0.001 m less than the lowest of the surrounding cells and a pixel with an elevation lower than the pit (solver), and along the steepest path, is searched. The solver is searched in a window 500x500 pixels that can be modified by the user: then the height of all the cells between the pit and the solver is lowered, creating a channel. This solution is suggested in the case of converging flows (as in valleys) because it usually maintains the morphology of the terrain.
- the filling of the pit, increasing its elevation: the solution fills the pit providing a new elevation 0.001 m larger than the lowest of the surrounding cells. This solution is suggested in the case of divergent flows (as on cones or fans); it can also be used as a support for the first solution in the case of unresolved pits.

In the case of DEMs of large extension the procedure should be repeated twice. In the case of unresolved pits that cannot be eliminated by both the methods, a map is generated for individuating them, allowing to correct them manually.

To summarize, the "DEM depit" tool requires as input:

- DEM map Digital Elevation Model (raster file). The value of each pixel corresponds to the pixel elevation (m);
- Selection of the method to solve pits Channel excavation or filling;

to give as output:

- Depitted DEM map - Refined or proper hydrological Digital Elevation Model;
- Pit map - Raster of the resolved pits: 1 for no pit cells, 3 for solver, 5 for channel, 6 for pit originated during the iterations and 8 for pits;

- Operation file (text file, .log) - Text file listing all the resolved pits and excavated channels.

Then, using a "depitted" and hydrologically correct DEM the tool "Upslope area 1" provides for each pixel the flow accumulation area or upslope area (area of the watershed draining by the pixel) using the D8 method. In the output raster file each cell has a value assigned, corresponding to the number of pixels that constitute the drainage area upstream the cell itself. The counting is automatic and happens summing, along the flow directions, the number of pixels included between the cell originating the flow and the considered cell. The source cells will have, draining no pixels upstream, a value of 1; the cell at the outlet section, draining the entire upstream area, will have a value corresponding to the entire number of cells.

"D8 classic" is the traditional algorithm for the computation of the flow direction: the slopes between one pixel and each of those surrounding it are computed on the base of the differences in elevation (from the DEM values) and the distance between the centers (pixel size for the cardinal directions and pixel size  $\times 2^{0.5}$  for the diagonal directions) It is indeed assumed that runoff occurs along the direction with the steepest slope.

To summarize, the "Upslope area 1" tool requires as input:

- the depitted DEM raster map;

to give as output:

- the upslope area 1 raster map: flow accumulation file in which the value of each pixel corresponds to 1 + the number of pixels that drain to it (the contributing area to the pixel is expressed in the form of pixels number).

Once the outlet is specified, the "watershed" tool identifies the pixels of the initial DEM belonging to the watershed by means of flow directions algorithm (D8 method). A raster map of the watershed is built, associating a constant value of 1.0 to the pixels of the watershed, while "no data" to the other outer cells. The raster is then cut into the minimum extension, obtaining a new raster with the pixels belonging to the watershed and a single border line of outer cells (nodata).

To summarize, the "Watershed" tool requires as input:

- the depitted DEM raster map;
- the x;y coordinates of the outlet (manual insertion)

to give as output:

- the watershed mask raster map (mask of the watershed cut to the minimum extension).

### **6.1.3. Pre-processing phase 2 (GeoPro)**

The tool "Upslope area 2" provides the flow accumulation area or upslope area for each pixel (area draining to the pixel), the flow directions versus the surrounding pixels and the path length from each cell to the outlet. The flow directions can be computed selecting one of four different algorithms for runoff distribution.

- D8 classic;
- Multiple flow;
- D-infinite;
- D8 facets;

The "Upslope area 2" tool requires as input:

- the depitted DEM raster map;
- the selection of the model for runoff distribution;

to give as output:

- the upslope area 2 raster map: flow accumulation file in which the value of each pixel corresponds to 1 + the number of pixels that drain to it (the contributing area to the pixel is expressed in the form of pixels number);
- the flow direction raster map: the value of each pixel corresponds to the flow direction angle (cardinal or diagonal ones) from one pixel to that with the steepest slope among the surrounding ones.
- the flow distance raster map: each cell has a value corresponding to the length of the flow path, calculated starting from the source and assuming as unit of length the pixel width.

Then the "Routing" tool provides, for each pixel, the routing time along the hillslope to the network (hillslope routing time) and the routing time along the network to the outlet (network routing time). The sum of the hillslope routing time and the network routing time is the routing time of direct runoff from the pixel to the outlet (isochronous map). The flow path is determined choosing the flow direction with the steepest slope.



The land use file is used to divide the flow path along the hillslope in a number of segments equal to the number of land types of the watershed, in the way that the length of each segment corresponds to the length of the flow path along a land type. Each land use type influences the hillslope velocity (land use codes and respective hillslope velocities are reported in the Debris Flow Modeling Tool - Reference Manual, 2012)

The velocity of overland flow (hillslope velocity) and the network velocity (Figure 6.2) are used to compute the routing times of runoff along the hillslope and the network for each pixel. The overland velocity value depends on the land type. (i.e. the direct runoff velocity over a rocky surface is greater than on wooded area).

The network cells are individuated using a threshold upslope area, defined by the user (minimum value 5000 m<sup>2</sup>).

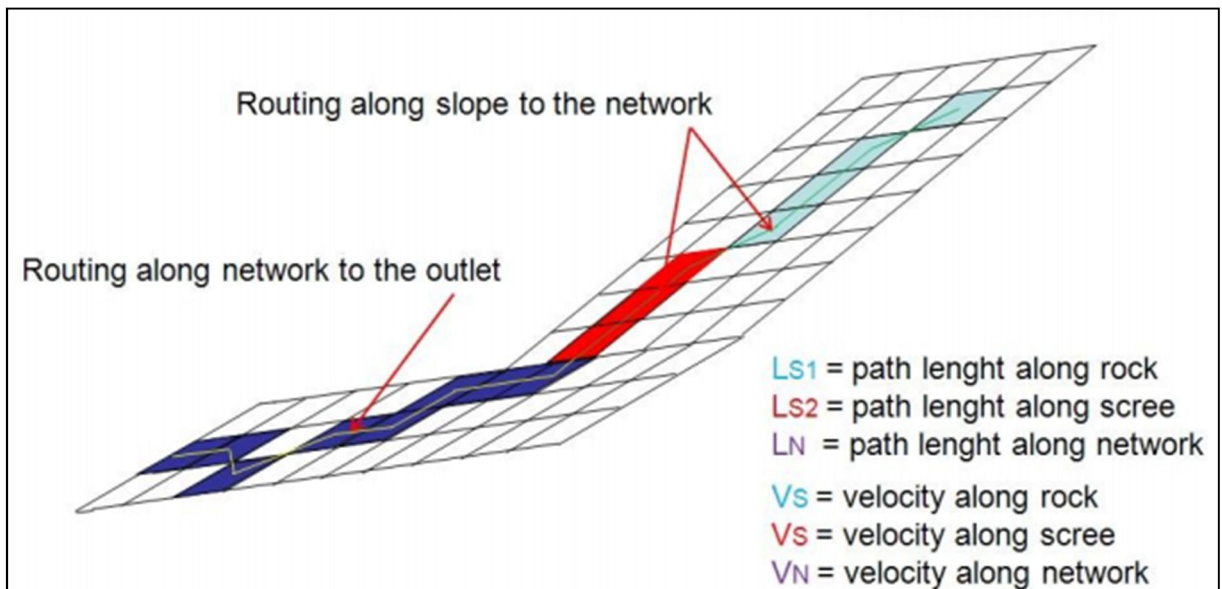


Figure 6.2 Schematic view of flow paths.

The routing time for the runoff to reach the outlet is given =  $\frac{Ls1}{Vs1} \frac{Ls2}{Vs2} \frac{Ln}{Vn}$

To summarize, the "Routing" tool requires as input:

- the flow direction raster map;
- the upslope area 2 raster map;
- the land cover raster file (cut to the watershed extension);
- the value of network flow velocity: values range between 1.0 and 4.0 m/s, with closer approximation between 1.5 and 2.5 m/s in Alpine regions;
- the threshold area: threshold drainage area ( $\text{m}^2$ ) to identify the synthetic network;
- slope velocity value: values of flow velocity on the hillslope (m/s) for each land cover type;

and provides give as output:

- the routing time along hillslope raster map: the value of each pixel corresponds to the routing time (hours) along the hillslope till to the reaching of the network;
- the routing time along network raster map: the value of each pixel corresponds to the routing time (hours) along network from the access point of direct runoff to the outlet;
- the flow velocity raster map: the value of each pixel is the velocity (m/s) corresponding to the land type if the pixel belongs to the hillslope or the network velocity if the pixel belongs to the network.
- the synthetic network raster map: the value of each pixel is 10.0 if it belongs to the network, 0 otherwise.

#### **6.1.4. Computation of the runoff hydrograph**

The simulation of the runoff hydrograph at the outlet section is carried out through the Kinematic Routing Excess Rainfall Model (KRERM).

The excess rainfall of each pixel is routed along the steepest slope to the outlet using hillslope velocities, depending on land cover, and network velocity equal to the average velocity in the outlet cross section corresponding to the peak value of simulated runoff or to a value given by the user. This model has been used by Gregoretto and Dalla Fontana (2008) for simulating runoff that triggered 30 occurred debris flow in the Dolomites.

KRERM uses the SCS method based on Curve Number parameter (CN) to compute the excess rainfall for each pixel and routes it to the outlet. Each pixel is surrounded by other 8 pixels (kernel) and therefore there are 8 possible flow directions depending on the height of the kernel pixels. The excess rainfall or direct runoff is routed along the steepest slope to the outlet. The tool "Routing" already provides the routing times from each pixel of the watershed

to the outlet. The contributes of excess rainfall that reach the outlet in the same time step are summed and this sum is the value of runoff associated to the time step.

The  $M$  cells of the watershed contributing to runoff at the outlet in the time step  $n\Delta t$  are those for which the routing time is  $n\Delta t$  (eq. 6.4):

$$m_k\Delta t + \sum_{j=1}^{N_{soil}} \frac{L_{SJi}}{V_{SJ}} + \frac{L_{Ni}}{V_N} = n\Delta t \quad (1 \leq m_k < n) \quad (6.4)$$

where  $m_k$  is a generic antecedent time step ( $m_k < n$ );  $N_{soil}$  is the number of different land covers,  $L_{SJi}$  is the length of the flow path of pixel  $i$  along land cover  $J$ ;  $V_{SJ}$  is the flow velocity corresponding to land cover  $J$ ;  $L_{Ni}$  is the length of flow path of pixel  $i$  along the network;  $V_N$  is the flow velocity along network. The runoff  $Q$  at time step  $n\Delta t$  is then (eq. 6.5):

$$Q(n\Delta t) = \sum_{i=1}^M P_i(m_k\Delta t) \quad (1 \leq m_k < n) \quad (6.5)$$

where  $P_i(m_k\Delta t)$  is the excess rainfall precipitated on pixel  $i$  at time  $m_k\Delta t$ . Network velocity is assumed equal to the average velocity in the outlet section, corresponding to the peak value of simulated runoff. In this case the average velocity is computed by the uniform flow law of Gauckler-Strickler. This value is compared automatically with that used for network velocity and if the relative difference is larger than a tolerance value, the routing times corresponding to the network are computed again and another simulation is carried on. Again the average velocity is computed and compared with the network velocity. The iterations stops when the relative difference is smaller than the tolerance value. This automatic iteration is needed to be coherent with the triggering criteria used for debris flow initiation. The choice of network velocity equal to the average velocity corresponding to the peak value of simulated runoff, descends from the analyses of runoff that triggered debris flows due to channel-bed failure carried out by Gregoretti and Dalla Fontana (2008). These authors found that most of the 30 historical debris flows they analyzed were triggered at a time close to the simulated runoff peak time.

The runoff is computed using an internal time step equal to the ratio between cell size and the maximum value of hillslope velocity. This assumption descends from the Computational Fluid Dynamics (CFD condition) and avoids that runoff route from cell to cell faster than the maximum slope velocity.

The infiltrated precipitation that does not contribute to runoff is routed to the outlet as subsurface flow. Subsurface flow is computed using the linear storage model.

The choice of AMC value is a function of moisture conditions prior to the simulated event, as shown in Table 6-4.

Table 6-4 AMC values (Chow et al., 1988; Hawkins et al., 2009)

	Height of rainfall during the 5 days preceding	
	Dormant season	Growing season
AMC = 1 (dry)	$h < 12.7 \text{ mm}$	$h < 35.6 \text{ mm}$
AMC = 2 (normal)	$12.7 \leq h \leq 27.9 \text{ mm}$	$35.6 \leq h \leq 53.3 \text{ mm}$
AMC = 3 (wet)	$h > 27.9 \text{ mm}$	$h > 53.3 \text{ mm}$

The value of AMC may be constant (equal to the input value) or variable: in the second case it changes with time, following the values of rainfall and seepage losses.

The AMC value changes the values of curve number raster map according to the following relation (eq. 6.6):

$$CN(AMC) = \frac{aCN_n}{10 + bCN_n} \quad (6.6)$$

where  $a = 2.08454 e^{(0.80709)AMC - 0.47225}$ ;  $b = (a - 4.2)/100 - 0.58$ ; and  $CN_n$  is the curve number value of CN raster map.

Rainfall input can be represented by a hyetograph, depth-duration frequency curves and intensity duration curves (obtained empirically).

The "Hydrograph" tool requires as input:

- the routing time along hillslope raster map: the value of each pixel corresponds to the routing time (hours) along the hillslope till to the reaching of the network;
- the routing time along network raster map: the value of each pixel corresponds to the routing time (hours) along network from the access point of direct runoff to the outlet;
- the CN raster map;
- the flow velocities raster map;
- the "Advanced parameters":
  - rainfall input data: a text file with rainfall data associated to time (data coming from rain-gauges);
  - hyetograph shape: Alterned blocks, constant intensity, instantaneous intensity, triangular, Wallingford;
  - peak position: position of the maximum intensity in the interval of duration of the hyetograph (0-1);
  - rain step: time steps used to generate the synthetic rainfall input
  - out step: output time step for the hydrograph generation

- AMC: Antecedent Moisture Condition of the watershed, according to the classification made in Table 6-4. Can be set constant or variable during the simulation;
- base flow discharge in  $m^3$ : initial discharge or base flow. Can be set by the user or calculated automatically with  $Q_0 = 0.05 \times A$  (basin area  $Km^2$ );
- recession Constant: linear storage coefficient, expressed multiplied by  $10^6$ , ranges between 6 and 8 in the Alpine region;
- reduction factor: ratio between contributing area of the basin and basin area (the contributing area is that considered to estimate the rainfall duration when using the depth-duration frequency curves or the empirical threshold: in this case using all the basin area could lead to hydrograph with anomalous shape and very large runoff volume without a non negligible increasing of the peak discharge value respect to a lower contributing area);
- initial abstraction coefficient;
- max value of slope velocity (m/s): also used in the "Routing" tool;
- outlet characteristics:
  - initial network flow velocity (can be chosen the same used in the Routing tool);
  - channel slope in the outlet: channel bed slope in the triggering section, calculated on the DEM with AdB Toolbox;
  - channel width: channel width in the triggering section, calculated with field measurements;
  - right and left bank side slope: right and left side slopes in the triggering section, calculated on the DEM with AdB Toolbox. Side slope = height of the side/length of the side;
  - Gauckler-Strickler roughness coefficient ( $m^{1/3}/s$ );
  - Tolerance: tolerance relative to the iterative procedure for assigning the mean velocity corresponding to the peak runoff value as network velocity. (0.01-0.05)

to give as output:

- the hydrograph simulation file (.sim), to be used as input in the "Triggering" tool;
- the resuming excel file.

## 6.2. Description of the Triggering model

The "Triggering model" or "Debris Flow Hydrograph model" determines the debris flow occurrence for an assigned runoff. In positive case it also computes the runoff hydrograph contributing to the debris flow and the corresponding debris flow hydrograph. The figure below shows the conceptual phases of the processing (Figure 6.3).

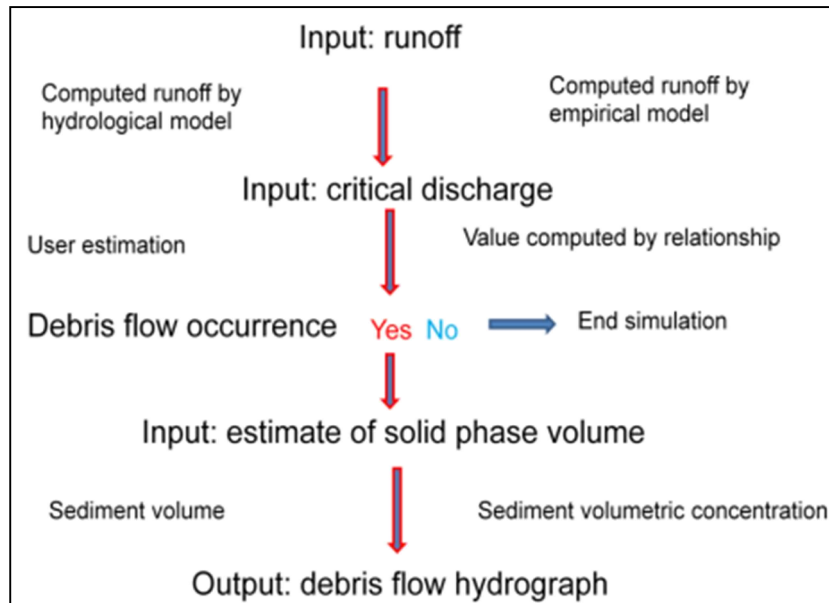


Figure 6.3 Scheme of the Triggering model

The triggering model is based on the capability of the surface runoff descending from cliffs and rock walls to mobilize sediments laying in the channels, incised on the detrimental hillslope at their foot. A number of studies (Griffiths et al. 1997; Tognacca et al, 2000; Gregoretti, 2000; Berti and Simoni, 2005; Griffiths et al.2004; Godt and Coe, 2007; Coe et al, 2008a, 2008b; Gregoretti and Dalla Fontana, 2008; Tecca and Genevois, 2009; Kean et al., 2011), relate the triggering of a debris flow on either incised channels or on a hillslope, to the erosion power of the water stream flowing over the sediment bed. Also videotape recordings of occurred debris flows (Berti et al., 2000) show that the mobilization of channel-bed material occurred only when surface runoff appeared and caused small failures in the steep channel-bed deposits: as the material mobilized, it scoured and entrained additional debris and progressively increased the solid concentration of the flow.

The runoff hydrograph descending from cliffs can be computed by a hydrological model or, considering a triangular shape, can be assigned by providing the peak value, the corresponding time and the hydrograph duration.

The triggering model derives from the method proposed by Gregoretti and Dalla Fontana (2008) to determine the critical runoff that triggers debris flow due to channel-bed failure. In

particular Gregoretti and Dalla Fontana (2008) compared the peak value of the runoff simulated by the distributed kinematic hydrological model KRERM with the critical discharge value computed by an empirical relationship. If the runoff peak value exceeds that given by the empirical relationship, the debris flow occurs. The present model allows the use of two different unit-width critical discharge empirical relationships, the former given by Tognacca et al. (2000) and the latter by Gregoretti and Dalla Fontana (2008). As an alternative, a unit-width critical discharge value can be inserted by the user. The relationship given by Tognacca et al. (2000) and Gregoretti and Dalla Fontana (2008) are respectively (eq. 6.7 and 6.8):

$$q_{crit} = 4d_M^{1.5} \tan \vartheta^{-1.17} \quad (6.7)$$

$$q_{crit} = 0.78d_M^{1.5} \tan \vartheta^{-1.27} \quad (6.8)$$

where  $q_{crit}$  = unit-width critical discharge;  $d_M$  = mean sediment size;  $\vartheta$  = bed slope angle. It can be observed that the value of  $q_{crit}$  computed by equation (6.7) given by Tognacca et al. (2000) is about four times that computed by equation (6.8) given by Gregoretti and Dalla Fontana (2008). Debris flow is triggered if the runoff discharge  $Q_r$  is larger than  $Q_{crit} = q_{crit} B$ , being  $B$  the channel width in the triggering section. The runoff potentially contributing to the debris flow is then all the runoff for  $t > t_{crit}$ , time corresponding to  $Q_{crit}$  (shaded area in Figure 6.4).

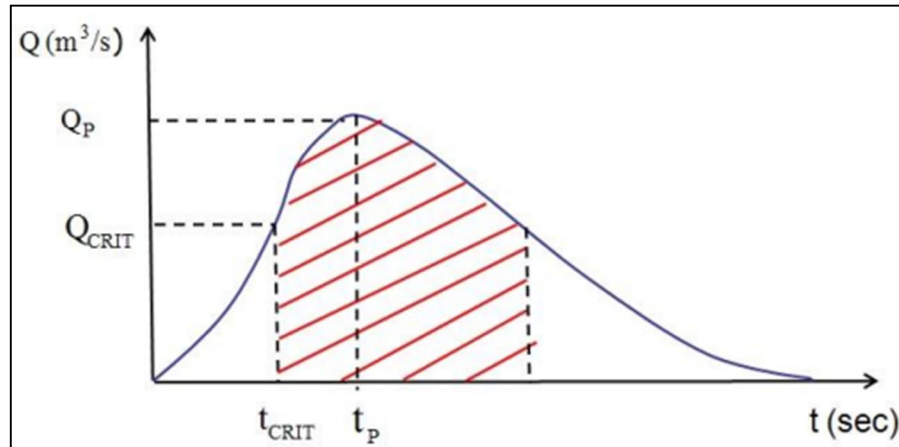


Figure 6.4 The potential runoff contributing to debris flow (shaded area)

The debris flow hydrograph can be both that originated during the triggering phase or that resulting after its routing in the channel, before spreading or depositing on the fan and/or impacting.

In the first case the debris flow hydrograph shape is the same of that of the contributing runoff (see the Figure 6.4 above). In the second case the shape of the debris flow hydrograph is different from that in the Figure 6.4. During the routing phase, debris of larger size usually accumulates in the front and the routing velocity should decrease due to the increase of flow resistance caused by momentum exchange between solid and liquid phases; these two concomitant phenomena change the hydrograph shape and the peak discharge position moves towards the beginning of the hydrograph so that debris flow peak discharge corresponds to the front advance. Debris flow hydrograph in this last case can be assimilated to a triangular shape with a very steep rising branch: as it results from field measurements (Zanuttigh and Lamberti, 2007), flow depth values rise to the maximum and then decrease. Consequently, runoff contributing to debris flow is assumed to have the same shape. In the Figure 6.5, the runoff contributing to debris flow for the two cases (options). In the first one (option 1) runoff is that of the Figure 6.4. In the second one (option 2) runoff has a triangular shape with the peak value at the beginning and its duration is computed dividing the double of the runoff volume corresponding to the previous case by the peak value. The runoff volume of Figure 6.4 is that potentially contributing to debris flow hydrograph. It could be smaller than that of figure Figure 6.4 because observed debris flow hydrographs are shorter in time (usually shorter than 10-15 minutes) than simulated runoff hydrographs: this fact is mainly due to the lack of erodible sediments, potentially entrainable. A more reliable estimation of runoff contributing to debris flow can be approached by reducing the duration of the hydrograph time after occurrence or considering only runoff able to entrain a fixed value of sediment volume for a-priori established value of sediment volumetric concentration.



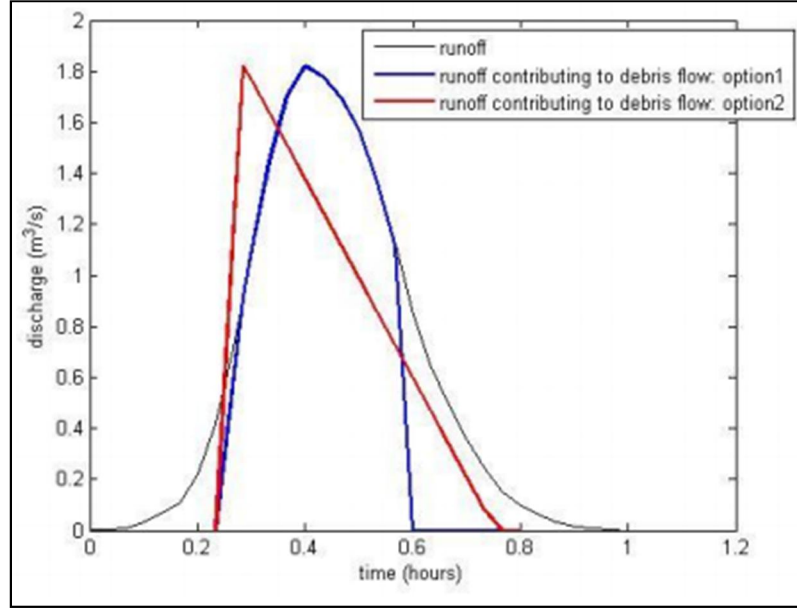


Figure 6.5 The two possible shapes for potential runoff contributing to debris flow: case 1 in the triggering area, case 2 after routing.

The building of the debris flow hydrograph follows two different paths according to the two cases: in the first case, the debris flow wave has the same shape of simulated runoff and sediment volumetric concentration is assumed constant; in the second case debris flow wave has a triangular shape and sediment volumetric concentration is assumed linear and decreasing after peak discharge. The assumption of same shape of runoff and constant sediment concentration leads to:

$$Q_T = \frac{V_T}{V_R} Q_R \quad (6.9)$$

where  $Q_T$  = debris flow discharge;  $V_T$  = volume of debris flow;  $V_R$  = volume of runoff contributing to debris flow. Equation (6.9) ignores or neglects all the inertia terms relative to the sediment entrainment (i.e. the erosion velocity and momentum exchange between solid and liquid phases, that changes the flow resistance and then the routing wave velocity). The ratio  $V_T/V_R$  can be expressed both by the computation of volumes of solid and liquid phases of the debris flow or by the sediment volumetric concentration. By using the volumes, the simple mass balance is considered:

$$V_T = V_S + V_R + V_W \quad (6.10)$$

where  $V_S$  = solid volume;  $V_W$  volume of interstitial water associated to the mobilized sediment volume:

$$V_W = (1 - v^*)SV_S/v^* \quad (6.11)$$

where  $v^*$  = bed dry sediment volume concentration and  $S$  = sediment deposit saturation degree. Substituting the second member of eq. (6.11) for the term  $V_W$  in eq. (6.10) and then

the second member of eq. (6.10) for the term  $V_T$  in eq. (6.9), the following equation for the solid-liquid hydrograph is obtained:

$$Q_T = \frac{V_S \left(1 + \frac{(1-v^*)S}{v^*}\right) + V_R}{V_R} Q_R \quad (6.12)$$

The solid volume should then be a datum and it could be provided by field measurements, geo-morphological estimations or empirical relationships, as subjective estimations of the sediment volume ( $V_S/v^*$ ). Anywhere, it must coherently correspond to the debris flow hydrograph type. In other words, if debris flow hydrograph is relative to the triggering area then the correct sediment volume value should come from estimations relative only to the source sediment areas in the triggering zone. The solid-liquid hydrograph can be also obtained through the mean sediment volumetric concentration. The mean sediment volumetric concentration,  $v_D$ , by definition, is:

$$v_D = \frac{V_S}{V_S + V_R + V_W} \quad (6.13)$$

Substituting the second member of eq. (6.11) for  $V_W$  in eq. (6.13), after clarifying  $V_R$ , the following equation is obtained:

$$V_R = \frac{1 - (1-S)v_D - v_D/v^*S}{v_D} V_S \quad (6.14)$$

Substituting the second members of eq.s (6.11) and (6.14) for the terms  $V_W$  and  $V_R$  in eq. (6.10) and the second member of eq. (6.10) for  $V_T$  in equation (6.9), the following equation is obtained:

$$Q_T = \frac{V_S + \frac{1 - (1-S)v_D - v_D/v^*S}{v_D} V_S + (1-v^*)S V_S/v^*}{\frac{1 - (1-S)v_D + v_D/v^*S}{v_D} V_S} Q_R \quad (6.15)$$

After some arrangement, equation (2.9) becomes:

$$Q_T = \frac{1}{1 - (1-S)v_D - v_D S/v^*} Q_R \quad (6.16)$$

that is the solid-liquid hydrograph expressed by means of  $v_D$ . Equations (6.12) and (6.16) are equivalent: assigning,  $v_D$  and  $v^*$  values the same ratio  $Q_T/Q_R$  is computed by the equations above, because  $V_S$  is linked to  $v_D$  and  $v^*$  by equations (6.14). Resuming, debris flow discharge can be computed by the solid volume through equation (6.12) or by the mean sediment volumetric concentration through equation (6.10). If  $S = 1$  (saturated bed sediment), equation (6.16) becomes:

$$Q_T = \frac{1}{1 - v_D/v^*} Q_R \quad (6.17)$$

Equation (6.17) is equal to that proposed by Takahashi (1978; 1991; and 2007) for saturated bed too. In Figure 6.6 a comparison between the equations (6.17) and the experimental data of Lanzoni and Tubino (1993): equation (6.17) provides values of  $Q_T/Q_R$  larger than those obtained from experiments. This is due to the contribution of runoff to the bed sediment seepage flow and to the water storage in the rear portion of the debris flow, for which the measured sediment concentration is not the mean sediment concentration but the front sediment concentration. Using an empirical approach two new equations are provided:

$$Q_T = 0.73 \frac{1}{1-v_F/v^*} Q_R \quad (6.18)$$

$$Q_T = \frac{(1-\frac{v_F}{2})}{1-v_D/v^*} Q_R \quad (6.19)$$

where  $v_F$  = sediment front concentration. Equation (6.18) fit well experimental data while equation (6.19) provides, on average, values slightly larger than those corresponding to the previous equation and seems more conservative than the previous one. As a matter of fact, in observed debris flow waves sediment concentration is highest at the front and decreases upstream, while in laboratory debris flow experiments sediment concentration is nearly constant because of steadiness of liquid discharge and therefore the symbol  $v_F$  should be substituted with  $v_{FC}$  in equations (6.18) and (6.19). Considering that the reduction coefficients 0.73 (or  $1-v_D/2$ ) were obtained for debris flow of uniform grain sediment size and saturated bed conditions, their value can change depending on the frequency distribution of sediment grain sizes and bed saturation conditions. For this reason, a free value of the reduction coefficient (RC) can be set according to the end user necessities and equations (6.18)-(6.19) could be grouped in a unique form:

$$Q_T = RC \frac{1}{1-v_{FC}/v^*} Q_R \quad (6.20)$$

In the case of partially saturated bed, equation (2.14) can be rewritten in the following form:

$$Q_T = \frac{RC}{1-(1-S)v_{FC}-v_{FC}S/v^*} Q_R \quad (6.21)$$

Equations (6.20) and (6.21) relate the total debris flow discharge to the runoff discharge by means of the sediment front concentration and the quantities  $S$  and  $v^*$ . Therefore these equations cannot be used to directly compute the debris flow hydrograph in the triggering area (option 1) because they correspond to a well developed debris flow wave. Nevertheless they can be used for estimating the physical plausibility of the values of  $V_S$  and  $v_D$  used in equations (6.12) and (6.16). In fact, by using equation (6.21), the front sediment concentration

$v_F$  can be computed after substituting the discharges  $Q_T$  and  $Q_R$  with the corresponding volumes  $V_T$  and  $V_R$  because of the assumption of constant sediment concentration:

$$v_{FC} = \frac{1}{1-S+\frac{S}{v^*}} \left(1 - RC \frac{V_R}{V_T}\right) \quad (6.22)$$

Equation (6.22) can be used to check the effective capability of runoff volume to mobilize the input solid volume or that corresponding to the input  $v_D$ . If it results  $v_{FC} > 0.9 v^*$  it means that the input sediment volume can be mobilized only partially or the input sediment concentration is too large. Then it is assumed  $v_{FC} = 0.90 v^*$  (Takahashi, 2007;) and the new reduced total debris flow volume  $V_{RID}$  is computed through equation (6.22) after substituting  $v_{FC}$  with  $0.9 v^*$ :

$$V_{RID} = \frac{RC}{1-0.9(1-S)v^*-0.9S} \quad (6.23)$$

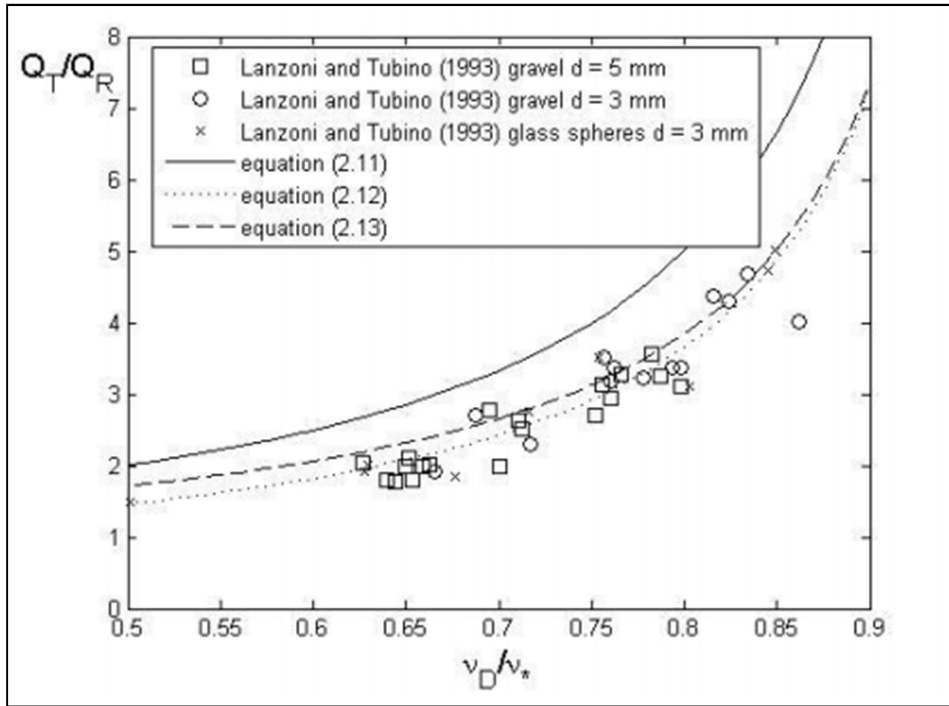


Figure 6.6 Comparison between values of  $Q_T/Q_R$

Then the reduced sediment volume,  $V_{SRID}$ , and sediment concentration,  $v_{RD}$ , can be computed; the first from eq. (6.10) after the substitution of the second member of eq. (6.11) for the term  $V_W$ :

$$V_{SRID} = \frac{V_{RID}-V_R}{1+(1-v^*)\frac{S}{v^*}} \quad (6.24)$$

the second by definition:

$$v_D = V_{SRID}/V_{RID} \quad (6.25)$$

Then the solid-liquid hydrograph can be computed through one of the following two equations:

$$Q_T = \frac{V_{RID}}{V_R} Q_R \quad (6.26)$$

$$Q_T = \frac{1}{1-(1-S)v_{RD}-v_{RD}S/v^*} Q_R \quad (6.27)$$

Finally, if the front sediment concentration  $v_F$  is provided rather than the mean sediment concentration  $v_D$ , the total debris flow volume is computed through equation (6.21) after substituting  $Q_T$  and  $Q_R$  with  $V_T$  and  $V_R$  respectively (according to equation (6.9) ratios  $Q_T/Q_R$  and  $V_T/V_R$  are equal) and the solid volume by equation (6.24) after substituting  $V_{RID}$  and  $V_{SRID}$  with  $V_T$  and  $V_S$  respectively. The mean sediment concentration is then given by the ratio  $V_S/V_T$ .

In the second case, that is the well developed debris flow, the solid-liquid hydrograph is computed through the peak value of debris flow discharge and the total debris flow volume. Compared to the previous case (solid-liquid hydrograph in the triggering area), sediment concentration is not constant but has a linear distribution and there are three input possibilities: solid volume, debris flow front concentration, or both.

Considering the first possibility of input data, the peak debris flow discharge,  $Q_{PT}$ , is computed by using eq. (6.21):

$$Q_{PT} = \frac{1RC}{1-(1-S)v_F-v_F S/v^*} Q_P \quad (6.28)$$

where  $Q_P$  = peak value of runoff discharge. Now it is possible the computation of the hydrograph duration  $D_T$  ( $V_T$  is given by eq. (2.4):

$$D_T = 2 \frac{V_T}{Q_{PT}} \quad (6.29)$$

The sediment concentration is assumed to be equal to  $v_F$  until the peak time  $t_p$ , and then it decreases linearly (from  $t_p$  to  $D_T$ ). The decreasing rate of sediment concentration,  $\Delta v = v_F/(D_T-t_p)$ , depends on both the decreasing rate of debris flow discharge,  $\Delta Q = Q_{PT}/(D_T-t_p)$  and the solid volume  $V_S$ . The solid discharge,  $Q_S$ , by definition is  $vQ_T$ . Substituting  $v = v_F - \Delta v t$  and  $Q_T = Q_{PT} - \Delta Q t$ , it is possible the computation of solid discharge for  $t > t_p$ :

$$Q_S = (v_F - \Delta v t)(Q_{PT} - \Delta Q t) \quad (6.30)$$

The integration of  $Q_S$  by time in the interval  $D_T - t_p$ , added to  $0.5 v_F Q_{PT} t_p$  (solid volume corresponding to the interval  $0-t_p$ ) leads to the computed solid volume  $V_{SC}$ :

$$V_{SC} = \Delta v \Delta Q (D_T - t_p)^3 / 3 - (v_F \Delta Q + \Delta v Q_{PT}) ((D_T - t_p)^2 / 2 + v_F Q_{PT}) (D_T - t_p) + 0.5 v_F Q_{PT} t_p \quad (6.31)$$

The only unknown,  $\Delta v$ , is then explicated, after substituting  $V_{SC}$  with  $V_S$ :

$$\Delta v = \frac{V_S - 0.5v_F Q_{PT} t_P - v_F (D_T - t_P) + 0.5v_F \Delta Q (D_T - t_P)^2}{\Delta Q (D_T - t_P)^3 / 3 - Q_{PT} ((D_T - t_P)^2 / 2)} \quad (6.32)$$

The first check is on the solid volume that the runoff is able to mobilize. As in the previous case

eq. (6.22) is used and  $v_{FC}$  must be smaller than  $0.9 v^*$ . In this case the computed value of the front sediment concentration  $v_{FC}$  could be smaller than  $v_F$  because the former corresponds to a constant runoff discharge while the latter to an unsteady runoff discharge (in real observed debris flow, flow depth is decreasing). The second check is on the value of  $v_F$ : it must be smaller or equal to  $0.9 v^*$ . The third check is on  $\Delta v$  (or  $V_{SC}$ ): it should results smaller or equal to  $v_F / (D_T - t_P)$  otherwise sediment concentration assumes negative values. If  $\Delta v$  results larger than  $v_F / (D_T - t_P)$ , the input front sediment concentration  $v_F$  is progressively lowered until  $\Delta v = v_F / (D_T - t_P)$ . Moreover,  $\Delta v$  must result positive: in the case in which the input value of  $v_F$  were too low, sediment concentration is assumed constant and equal to  $v_F$ ; in this case sediment volume  $V_{SC}$  results smaller than  $V_S$ . Data on sediment volume used to estimate the input value of  $V_S$  should come from estimations relative to the sediment volume entrainment along the whole routing path from the triggering area to the point where the solid-liquid hydrograph should be provided.

If only the sediment volume is provided, the total volume is computed by the following equation:

$$V_T = V_S (1 + (1 - v^*) S / v^*) + V_R \quad (6.33)$$

The front sediment concentration can be then computed through equation (6.22), it is  $v_{FC}$ , and the procedure of the previous possibility is followed. If only the sediment front concentration is provided, total debris flow volume is computed through equation (6.21) after substituting  $Q_T$  and  $Q_R$  with  $V_T$  and  $V_R$  respectively (according to equation (6.9) ratios  $Q_T / Q_R$  and  $V_T / V_R$  are equal) and the solid volume by equation (6.24) after substituting  $V_{RID}$  and  $V_{SRID}$  with  $V_T$  and  $V_S$  respectively. Again, the procedure of the first possibility is followed.

### 6.2.1. Debris flow solid phase concentration

The debris flow solid phase concentration can be computed according to the expression proposed by Takahashi (1978) and updated by Lanzoni and Tubino (1993), or those proposed by Ou and Mizuyama (1994) and Lien and Tsai (2003). By using the ratio between the basal shear and normal stresses, in hypothesis of hydrostatic fluid pressure distribution and normal stress equal to the Bagnold dispersive stress, Takahashi (1978) proposed the following relationship for debris flow sediment concentration in uniform conditions:

$$v_D = v_F = \frac{\tan \vartheta}{(\frac{\rho_S}{\rho})(\tan \varphi - \tan \vartheta)} \quad (6.34)$$

Being  $\varphi$  and  $\vartheta$ , respectively, the static friction angle and the bed slope angle. Egashira et al. (1997) obtained the same relationship considering the dynamic condition at the bottom. To be more realistic, the angle  $\varphi$  should be substituted by the dynamic friction angle, that is the ratio between shear stress and normal stresses close to the bottom. Experiments of Lanzoni and Tubino (1993) showed that equation (6.34) satisfactorily fits data only if the quasi-static friction angle,  $\varphi_S$ , is used. This angle according to Allen (1970) and verified by Lanzoni and Tubino (1993) is usually  $5-7^\circ$  (dilatancy angle) less than  $\varphi$  in the case of gravel. Ou and Mizuyama (1994), elaborating data of flume experiments, proposed the following relationship for sediment concentration that is reported by Lien and Tsai (2003):

$$v_D = \frac{4.3v^* \tan \vartheta^{1.5}}{1 + 4.3v^* \tan \vartheta^{1.5}} \quad (6.35)$$

This equation was empirically obtained by flume data averaging sediment concentration values both in the front and in the rear part of the debris flow. The higher liquid volume in the rear part of debris flow explains the lower values of sediment concentration respect to the previous formula given by Takahashi (1978). Moreover, this equation, in the usual range of application ( $15-25^\circ$ ), is a straight line. Afterwards, Lien and Tsai (2003) developed a method for computing sediment concentration at the equilibrium based on maximizing the entropy of the variable concentration as proposed by Cao and Knight (1997). They obtained the following relationship:

$$v_F = \frac{v^*}{2} [(1 + \chi_3 + \chi_4) \pm \sqrt{(1 + \chi_3 + \chi_4)^2 - 4\chi_3}] \quad (6.36)$$

and

$$\chi_3 = \frac{\tan \vartheta}{v^* (\frac{\rho_S}{\rho} - 1)(\tan \alpha - \tan \vartheta)} \quad (6.37)$$

$$\chi_4 = \frac{\eta}{v^* \cos \vartheta (\tan \alpha - \tan \vartheta)} \quad (6.38)$$

Where  $\alpha$  = dynamic friction angle and  $\eta$  = constant to be determined by experimental results. In case  $\alpha = \vartheta$ , the eq. (6.36) becomes:

$$v_F = \frac{v^* \sin \vartheta}{1 + \eta(\rho_s - \rho)/\rho} \quad (6.39)$$

Using data of  $v_F$  from the experiments of Takahashi (1978) and the sediment concentration profiles of Tsubaki et al. (1972), and assuming  $\alpha = 32.2^\circ$  according to Bagnold (1954), Lien and Tsai (2003) proposed  $\eta = 0.04$ . Figure 6.7 shows the good agreement between Takahashi data with equation (6.36). This comparison is better than that between Takahashi data and eq. (6.34). Figure 6.7 shows also that eq. (6.35) underestimates the debris flow front concentration value of the experiments of Takahashi (1978).

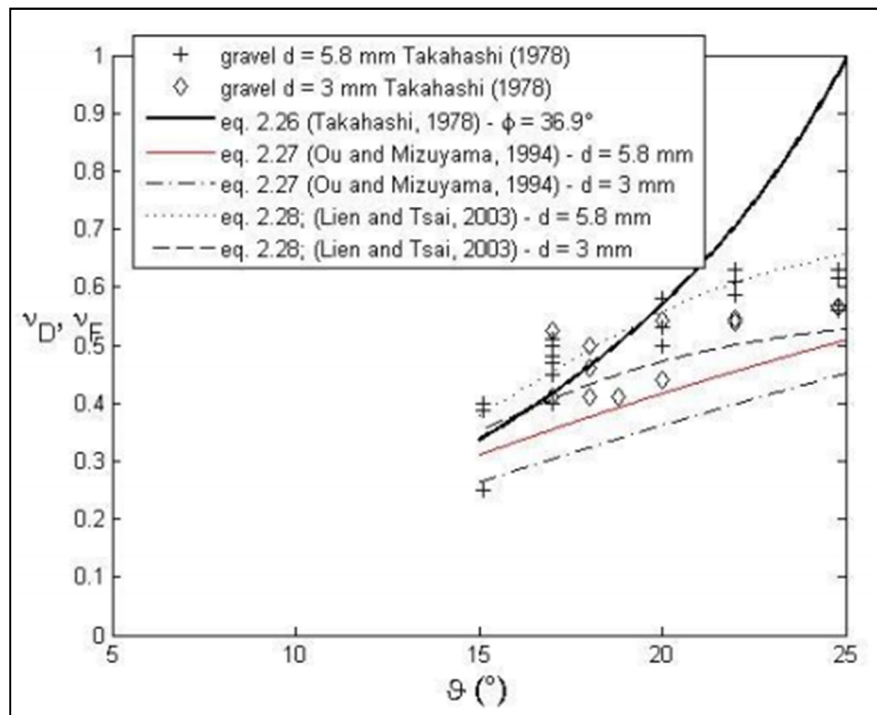


Figure 6.7 Comparison of experimental data of Takahashi (1978) and  $v_F$  values given by equations (6.34), (6.35) and (6.36).

Figure 6.8 shows the comparison between experimental data of Lanzoni and Tubino (1993) with eq. (6.34), (6.35) and (6.36). Comparison is worst as it regards gravel data and eqs. (6.34) and (6.35) while eq. (6.36) with parameter value of Lien and Tsai (2003) is good for gravel  $d = 5$  mm and not for gravel  $d = 3$  mm, whose sediment concentration is underestimated. As it regards sphere glasses, equation (6.34) results with an inferior limit of the experimental values, while eqs. (6.35) and (6.36) underestimate them.

Figure 6.9 shows the comparison of experimental data by Lanzoni and Tubino (1993) with eqs. (6.34) and (6.36) for different parameters values. In particular, the constant  $\eta$  decreases



for matching experimental values simulating with gravel  $d = 3$  mm. Parameters of equation (6.36) to fit experiments of the glass spheres are completely different from those suggested by Lien and Tsai (2003). Equation (6.34) fits, quasi satisfactorily, data by Lanzoni and Tubino using the quasi-static friction angle rather than the friction angle.

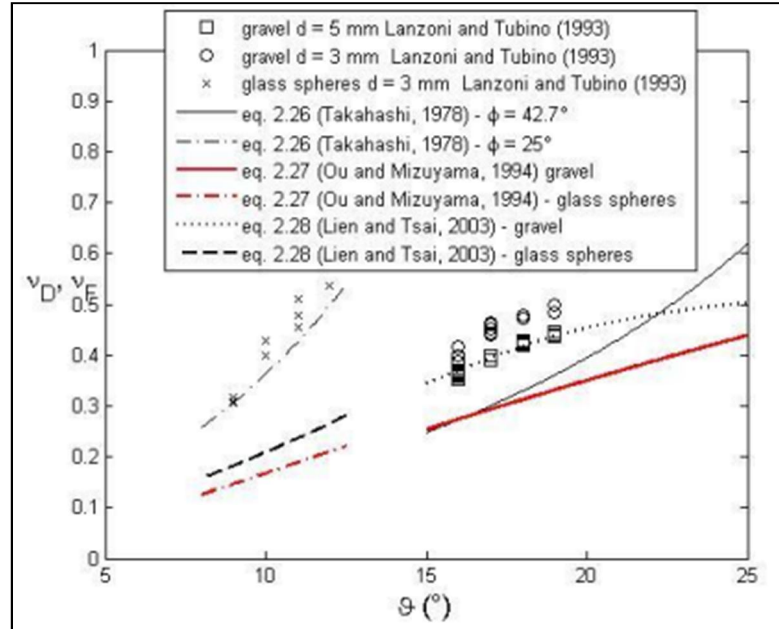


Figure 6.8 Comparison of experimental data of Lanzoni and Tubino (1993) and  $vF$  values given by equations (6.34), (6.35) and (6.36).

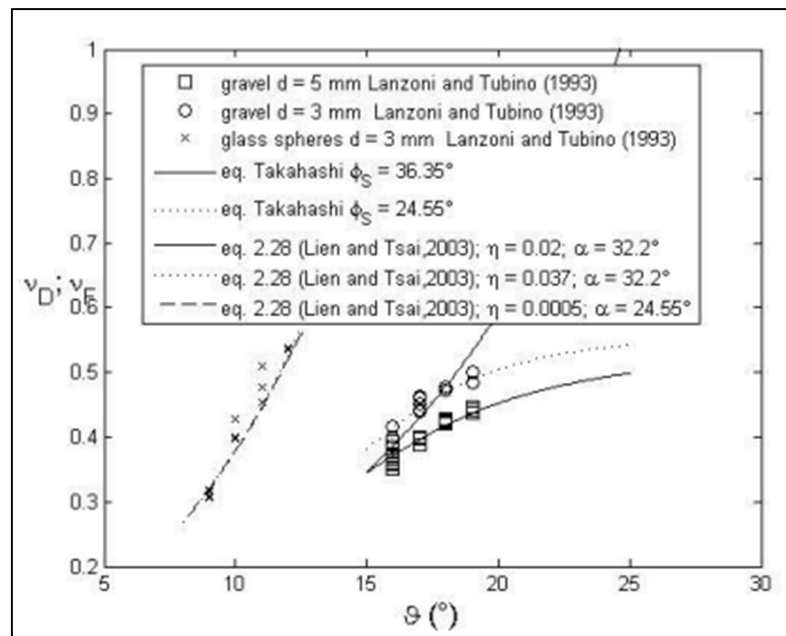


Figure 6.9 Comparison of experimental data of Lanzoni and Tubino (1993) and  $vF$  values given by equations (6.34) and (6.36) with different parameter values.

### 6.2.2. Input and output data of the "Debris flow hydrograph" model

The debris flow hydrograph model or triggering model requires as input:

- the runoff data file: the file with .sim extension produced by the "Hydrograph" tool in the Hydro Model, containing for each time step the total discharge, the direct runoff, the base flow, total precipitation and precipitation excess;
- critical discharge input, that can be represented by:
  - a unit critical discharge ( $\text{m}^2/\text{s}$ )
  - sediment and morphologic data to be used by a unit critical discharge relationship:
    - average grain size diameter (m);
    - channel bed slope in triggering section (%);
    - unit seepage discharge ( $\text{m}^2/\text{s}$ );
    - the choice of the relationship: (eq. 6.8) Gregoretti and Dalla Fontana (2008) or (eq. 6.7) Tognacca (2000).
- Triggering area characteristics:
  - channel bed width (m);
  - dry sediment volumetric concentration (0.5-0.9);
  - sediment saturation degree (%);
- Selection of the hydrograph shape of the contributing runoff:
  - Q1 for the hydrograph corresponding to the triggering area (choice 1 Figure 6.10);
  - Q2 for the hydrograph downstream the triggering area, corresponding to a well developed debris flow (choice2 Figure 6.10) ;

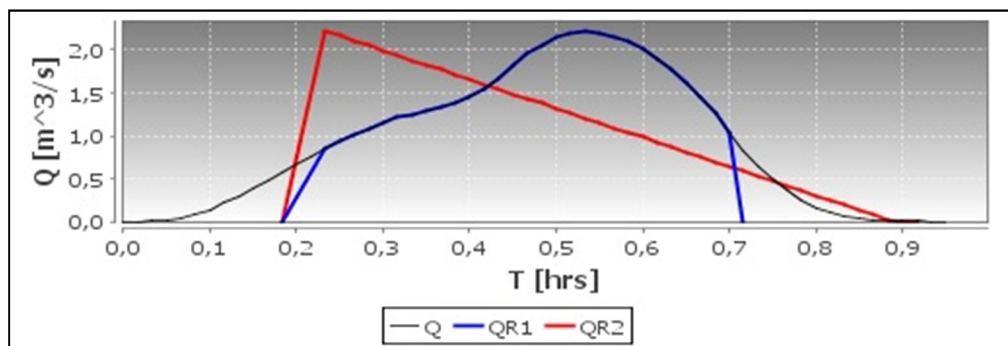


Figure 6.10 QR1 and QR2 shape.

- Runoff reduction by time in debris flow hydrograph: debris flow hydrograph will be built considering only the volume of runoff in the defined time (min);

- Input sediment:
  - a reduction coefficient
  - the choice between:
    - sediment volume ( $m^3$ ): potential sediment volume erodible by a critical event. Can be obtained by field measurements or estimated through four relationships that take into consideration the basin area and the average channel slope:
      - Marchi-D'Agostino (2004) - Eastern Italian Alps
      - Bianco-Franzi (2000) - Italian Alps
      - Rickenmann-Koschni (2010) - Switzerland basin, using also a geological index.
      - Gartner et al (2008) - recently burned basins in the USA, using catchment area with slopes steeper than 30% and 10 min peak of rainfall intensity
    - front sediment volume concentration: can be obtained by field measurements or estimated through three relationships that take into consideration the channel bed slope in the triggering area, internal friction angle, dry sediment volumetric concentration, Eta parameter, dynamic friction angle:
      - Takahashi (1978);
      - Ou & Mizuiama (1994);
      - Lien and Tsai (2003);
    - both sediment volume and front sediment volume concentration;
- time step output of the debris flow hydrograph (min).

Before giving the results, the tool advises the user if with the combination of input data and parameters the debris flow can effectively occur, according to the chosen triggering relationships.

The model then gives as output some resultant text files:

- the "resultant\_ris.txt", that contains all the calculations and the output simulated data, divided in three parts: the runoff elaboration only with the rainfall runoff hydrograph; computation rainfall runoff that contributes to the debris flow; debris flow hydrograph computation

- the "resultant\_ris\_automata.txt", consisting on time, debris flow discharge and sediment concentration data, that is the main input for the "Automata" model for the following step, the simulation of routing and deposition phases.
- the "resultant\_ris\_discharge.txt" with time, water runoff contributing to debris flow, solid discharge and debris flow discharge data.

## 6.3. The Automata numerical model for simulation of routing and deposition phases of a debris flow

### 6.3.1. Principles of the Automata cellular model

Cellular automata model can be successfully used to simulate flow of water and sediments using simple local rules for mass and momentum exchange. The present model is a 3D numerical code based on Cellular Automata Method (Segre & Deangeli 1995; Deangeli & Grasso, 1996; Deangeli & Giani, 1998; Deangeli, 2008; Deangeli et al., 2011). Cellular automata are mathematical idealizations of physical systems in which space and time are discrete, and physical quantities are based on a finite set of discrete values. A cellular automaton consists of a regular uniform lattice (or array), that is usually infinite, with a discrete variable at each site (cell). The state of a cellular automaton is specified by the values of the variables at each site.

A cellular automaton evolves in discrete time steps, with the value of the variable at one site being affected by the values of variables at sites in its neighbourhood at the previous time step. The variables at each site are updated simultaneously, based on the values of the variables in their neighbourhood at the preceding time step, and according to a definite set of local rules (Wolfram, 1987). The numerical code was set up to analyze debris flows over a rigid substratum. The debris flow is assumed to be completely mixed. The model does not take into account variations in vertical direction of the debris properties, by adopting a vertically averaged description. The fan where the debris flow routes is discretized in elementary cells of finite size. In each one the state of the system is specified by the values of some representative quantities.

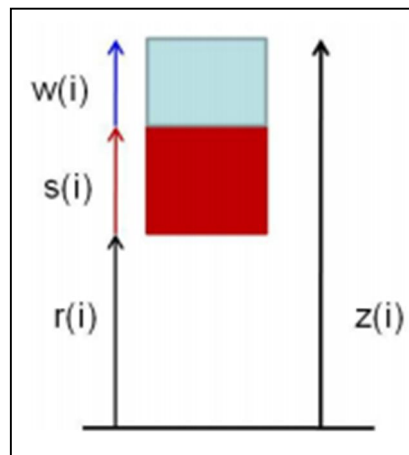


Figure 6.11 Different phases constituting the mixture: schematic view.

These include: the height of the impermeable rigid bed ( $r$ ); the amounts of water ( $w$ ) and gas ( $g$ ) and of granular solids ( $s$ ) in the cell. All the contents are given as partial heights (volumes/ base area of the cell), so that the top height in the cell ( $i$ ) is given by (Figure 6.11):

$$z(i) = r(i) + w(i) + g(i) + s(i) \quad (6.40)$$

The density of the mixture in each cell is given by:

$$\rho = C(i)\rho_s + (1 - C(i))\rho_w \quad (6.41)$$

where  $C$  is the solid volume concentration,  $\rho_s$  is the solid density and  $\rho_w$  the water density.

The lattice geometry implemented in the model is the Cartesian square lattice ( $b=4$ ) (Figure 6.12).

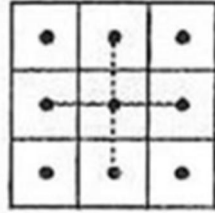


Figure 6.12 Cartesian square lattice

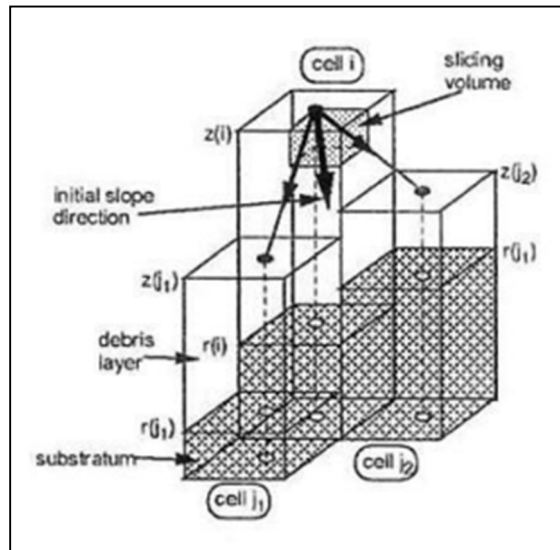


Figure 6.13 Two neighbours partition rule.

Volume and consequently mass conservation are separately imposed for solid and water. Energy and momentum conservation are not enforced here. This is consistent with modeling a process which is dissipative. The assumption that the debris previously in motion can suddenly be stopped within the space of a single cell, depending only on the instantaneous local conditions, is equivalent to the assumption that kinetic energy is readily dissipated,

gravity being the main energy source. Initial conditions for the model are imposed specifying the site topography and the debris distribution at the initial time.

Boundary conditions are easily implemented on any set cells: to realize an open boundary it is just sufficient to force the content of these cells to be always null, while to achieve closed boundaries any resulting out flux is set to zero. Each cell is connected to a number of its nearest neighbouring cells in order to transfer material at each time step.

In a 3D field the whole lattice could be considered as a network of elementary slopes (with inclinations due to different local topography and debris layers). A two neighbours partition rule for the transfer of debris has been implemented, in order to achieve lattice isotropy. A local slope angle  $\theta(i, v)$  is defined in the cell (i) for each pair of adjacent neighbours (jv, jv+1) ( $v=1,..b$  module b) (Figure 6.13).

Evolution rules for the automaton considered the mixture to behave as dilatants fluid, according to Bagnold theory. The propagation of elementary flows in each lattice sector (i,v) occurs if:

$$\rho(i) \tan \theta(i, v) > (\rho(i) - \rho_w) \tan \varphi_D \quad (6.42)$$

where  $\varphi_D$  is the dynamic friction angle. The cross sectional mean velocity  $U$  is a simplified version of that given by Takahashi (1991):

$$U = \beta \sqrt{\rho g h^3 \sin \vartheta} \quad (6.43)$$

where  $\beta$  is a dimensional coefficient grouping all constants and can be considered equal to 0.01. Alternatively there is the expression proposed by Tsubaki (1972):

$$U = C \sqrt{g h^3 \sin \vartheta} \quad (6.44)$$

where  $C$  is a dimensionless Chezy coefficient. Values of  $C$  can be found in Gregoretti (2000). Let quantities  $q$  of material flow out of the cell  $i$  toward its critical neighbours and evaluate  $q$  by putting  $[z(i)-r(i)]-[z(jv)-r(jv)]$  as  $h$  and  $\vartheta(i, v)$  as  $\vartheta$  in Equations 6.43 and 6.44. In the model it has been assumed that  $q(C, \Delta z)$  are constant during the time step and rely on the first order approximation for small values of the time step  $\Delta t$ . The simplified elementary rate is thus:

$$q_k(i, v) = \Delta t \beta h(i) \sqrt{\rho g h^3(i) \sin \vartheta} \quad (6.45)$$

All the computed elementary rates are stored before the simultaneous updating of the lattice.

Instantaneous flow rates  $q(i)$  are evaluated in each cell by vector summing all the incoming flows. The determination of the stoppage travel of a debris flow is still an open problem. On a

practical point of view simulation is stopped when the maximum value of computed velocity in a time step is less than a fixed value chosen by the user (0.025 m/s or less).

The value of  $s(i)$  is the solid height corresponding to the transit of debris flow. In other words it can be both a solid deposition height if condition given by equation (6.42) does not occur and the solid part of flow depth if it occurs. At the end of simulation when maximum velocity is lower than 0.1 m/s,  $s(i)$  can be reasonably assumed as a deposition height of solid phase. The sediment deposition height is obtained by dividing  $s(i)$  by the dry sediment volumetric concentration.

### 6.3.2. Input data files and parameters and output files

The automata cell model requires as input:

- the DTM of the area, with a particular boundary condition: one "no data" line of cells all around the DTM must be present. The boundary conditions can be created automatically with a utility tool already present in the Automata tool;
- a file with (.txt) extension with the coordinates of the raster cells used as input for the simulation;
- the debris flow solid-liquid hydrograph produced with the Triggering model;
- a set of parameters:
  - simulation time: time duration (s) in the reality for the simulation. It should be a little bit greater than the duration of the solid-liquid hydrograph, to allow for all the mobilized material to route and deposit;
  - time step output: intermediate steps (s) at which output files are produced;
  - number of input cells;
  - Courant number (C): reflects the portion of a cell that a solute will traverse by advection in one time step. Designing a model with a small ( $<1$ ) Courant number will decrease oscillations, improve accuracy & decrease numerical dispersion.  $C = \frac{v\Delta t}{\Delta l}$ , where  $\Delta l$  = dimension of the grid cell at each location,  $v$  = average linear velocity at that location,  $\Delta t$  = maximum time step size;
  - initiation angle: dynamic friction angle for the initiation of movement according to Bagnold theory. Flow occurs if slope is larger than this initiation angle;
  - relationship to calculate the cross-section mean velocity
    - Takahashi (1991);



- Chezy a-dimensional relationship, with a coefficient ranging from 1 to 10 (1 for houses, walls, rigid obstacles, dense forest; 2 for instability areas, erosion areas, dense bushy and shrubs, and dense-high herbaceous vegetation; 3 for bed and bank channel pastures, sparse vegetation; 4 for roads, parkings smooth areas);
- ending simulation velocity: the simulation stops under this maximum value of computed velocity during the time step;
- dry sediment volume concentration: dry sediment volume concentration in the deposition area, used to compute the sediment deposition depth.
- Magnitudo: limits of the classes of flow velocity and flow depth, whose combination in a matrix gives the magnitudo of the event, according to PAI methodology.

The output files are:

- solid volume raster map: represent the height (m) of the solid phase;
- the water volume raster map: represent the height (m) of the liquid phase;
- the flow depth raster map: represent the volume of the sum of liquid and solid phase;
- the sediment deposition depth raster map: computed dividing the solid depth by the dry sediment volumetric concentration. Since it represents the deposited material it is the output to be compared with map of the deposits measured on the field;
- the solid flow depth raster map
- the liquid flow depth raster map:
- the velocity raster map: represent the maximum value of outgoing velocity (m/s) for each cell, with respect to the possible directions;
- the max flow depth raster map: represent the maximum value for the entire simulation of the total flowing depth;
- the max velocity raster map: represent the maximum value for the entire simulation of the flow velocity;
- the magnitudo raster map: represent the magnitudo obtained by the max value of the combination of velocity and depth matrix, for the same time step;
- the max magnitudo raster map: represent the magnitudo obtained by the combination of max velocity and max flow depth matrix of the entire simulation, not necessary in the same time step.

## 6.4. PAI methodology for magnitudo estimation

The primary objective of the PAI (Piano stralcio per l'Assetto Idrogeologico - Plan for the Hydro-geological Arrangement) is the reduction of landslide risk within values compatible with the land uses, so as to ensure the safety of people and to minimize the damage to the exposed properties.

The PAI methodology aim at producing a map inventory of the hazardous phenomena as landslide and debris flows, assigning a hazard level to each zone. The procedure is composed by the following steps:

1. The individuation and zoning of the areas interested by landslide and debris flow hazard;
2. The definition of the characteristics of the mass movement (typology, velocity, volumes and/or depths);
3. The estimation of the probability of occurrence of the phenomenon (using, often, the return time of the hydrological or seismic triggering causes);
4. The crossing of the data in matrices (velocity/frequency and magnitudo/frequency) and assignation of the hazard values.

The dangerousness of an area is estimated through:

- velocity thresholds (Table 6-5):
- thresholds of geometric severity (Table 6-5):

Table 6-5 PAI classes of velocity and geometric severity

Intervals of velocity	Velocity class		Depth intervals	Classes of geometric severity
5 m/s	3		> 1m	3
3m/min			0.5 - 1m	2
1.8 m/hour	2		< 0.5m	1
13m/month				
1.6m/year				
16mm/year				
< 16mm/year	1			

Which are combined to define magnitudo classes (Table 6-7):

Table 6-6 PAI magnitudo classes.

Magnitudo matrix		Intervals of velocity		
		1	2	3
Hazard class of geometric severity	1	1	2	3
	2	2	4	6
	3	3	6	9

With the interaction between magnitudo classes and probability of occurrence (return time), the hazard classes are assigned (Table 6-7):

Table 6-7 PAI hazard classes.

Hazard classes (P) related to the magnitudo		Return time (years)			
		1 - 30	30 - 100	100 - 300	> 300
Magnitudo classes	6 - 9	P4	P4	P3	P1
	3 - 4	P3	P3	P2	
	1 - 2	P2	P1	P1	

## 6.5. Field surveys

### 6.5.1. Introduction to field surveys

The principal aim of the field data collection has been to provide data for the elaboration of an accurate representation of the topographic surface of the area interested by a debris flow, both immediately before and after the occurrence of a debris flow event: obtaining such kind of information would allow to identify the areas of erosion, the areas of deposition and the magnitude of these processes related to a specific event. These data are needed to test the numerical model, in particular the values of its parameters whose results would best fit with the field data of deposition depth.

The objectives of the surveys have been:

- the identification of the triggering area of the debris flows;
- the characterization of the topography of the channel, in particular in the triggering zones of the phenomenon and in the part of the channel characterized by propagation and deposition of sediment. The operation serves to:
  - the description and measurement of the volumes eroded and entrained in the triggering and transport reaches;
  - the description and measurement of the volumes of sediment deposited in the deposition areas;
- the characterization of the transported material through the grain size analysis;

The acquirement of the spatial dataset describing the c08 channel has been carried out with GPS instrumentation, while the availability of a Lidar dataset gave the substratum on which to set the field data.

### **6.5.2. GPS technology**

The GPS instrumentation used in the field benefits of the positioning of kinematic type. The kinematic positioning is characterized by the fact that during the measuring operation the receiver is in motion or stopped for a few seconds. The kinematic positioning in real time of a single receiver (absolute positioning) does not require special attentions in the operational phase, but to be able to observe at least four satellites simultaneously. The kinematic positioning also provides relative or differential measures, based on the observation simultaneously of two receivers, which could achieve by far better accuracies than the absolute positioning.

In particular, during the field survey on the c08 channel, the kinematic survey of the DGPS type has been used. The DGPS (Differential GPS) is a technique of GPS positioning which exploits the ability of a receiver to calculate the correction to be made to the measures in order to reduce the errors and to send those corrections to another receiver. The DGPS system is therefore composed of a receiver that is parked in a static position on a M vertex ("master" or "basel" station) and one or more receivers ("rover" or "remote" receiver), usually in motion. Once accurately captured the coordinates of the vertex where it is placed the master receiver, each time the software knows the "exact" distance between the satellites (at least 5) and the receiver and can calculate the overall effect of the different possible errors ( troposphere, clock satellites, orbits, etc..). In differential positioning the master station then make the corrections and send the "clean" coordinates to the rover receiver, via radio and/or GSM,

which compares them with those being surveyed and extrapolates the final values that will be recorded. The accuracy that can be achieved with the detection DGPS goes up to 2-3 cm on the vertical measure, even higher on the horizontal one.

Two different GPS instruments have been used in the field, chosen for the possibility to work with the DGPS system:

1) the receiver "HiPer PRO" and controller "FC 200"

The receiver "HiPer PRO", along with controller "FC 200" is a system consisting of two Topcon GNSS receivers, a mobile called "rover" and a fixed "base", and a device for the system configuration and the acquisition of the points. The handheld "FC 200" has a Windows CE user interface and communicates with the rover and the base station via bluetooth signal. The topographic software installed is "Mercury" of the Geotop company. The "rover" is mounted on a pole in carbon and is used to perform the point acquisition, while the "base" is mounted on a tripod and is used as a reference for the corrections of the coordinates detected by the rover (DGPS-RTK mode). Both the instruments operate at all the frequencies currently used for the transmission of satellite data and exploit both the GPS and GLONASS satellites (the Russian satellite constellation), while communicating with each other via radio waves.

2) the receiver "GRS-1" with Topcon GNSS antenna "PGA-1"

The handheld and receiver "GRS-1" is a GNSS system of the Topcon company, operating at dual frequency, cable connected to a "PGA-1" antenna, both mounted on a carbon fiber pole. The handheld has a Windows Mobile user interface, the topographic software installed is "Mercury" of the Geotop company. It manages all the frequencies currently used for satellites' data transmission and uses both GPS and GLONASS satellites. The DGPS correction is possible through an internet communication between a data type SIM card contained in the receiver and some fixed bases of the Geotop network (in this case the fixed base of Cortina d'Ampezzo has been used).

### 6.5.3. Remotely sensed data

A set of "x,y,z" (geo-referenced with cartesian cartographic coordinates, and provided with geoidic and orthometric elevation) o points dataset coming from a 2006 LiDAR survey has been used to build a DTM of the whole Fiames area, to serve as the basis to run the simulations.

The fidelity of the Lidar dataset in representing the local surface has been tested establishing a set of control points, as suggested by Scheidl et al. (2008). These have been obtained acquiring the coordinates of four fixed and known point (three poles of a fence near the bicycle path and a stump of a tree close to the rock cliffs) with the GPS in DGPS mode for a period of acquisition of 30 minutes. The difference in elevation between the fixed points and the Lidar points in the surrounding (50-70-cm), did not exceeded the 15 centimetres.

Considering the huge amount of data and so the storing memory, this dataset has been reduced through a mask over the channel and deposition area, in order not to overpass the computing limits of the software AdB Toolbox. The analysis of the c08 has been done on a surface of 303700 m<sup>2</sup>, with an average point density of 2.3 points/m<sup>2</sup>. It is however to be considered that the surface specifically of the channel and of the deposits has been built using GPS data acquired on the field just after the observed debris flow events: the surface for the simulation, so, is a collage obtained merging LiDAR and GPS points, as shown in figure Figure 6.14. The average density of only the Lidar data, not considering the GPS points, is 2.45 points/m<sup>2</sup>. The average density of GPS points only on the area covered by the GPS field survey is 0.097 points/m<sup>2</sup>.

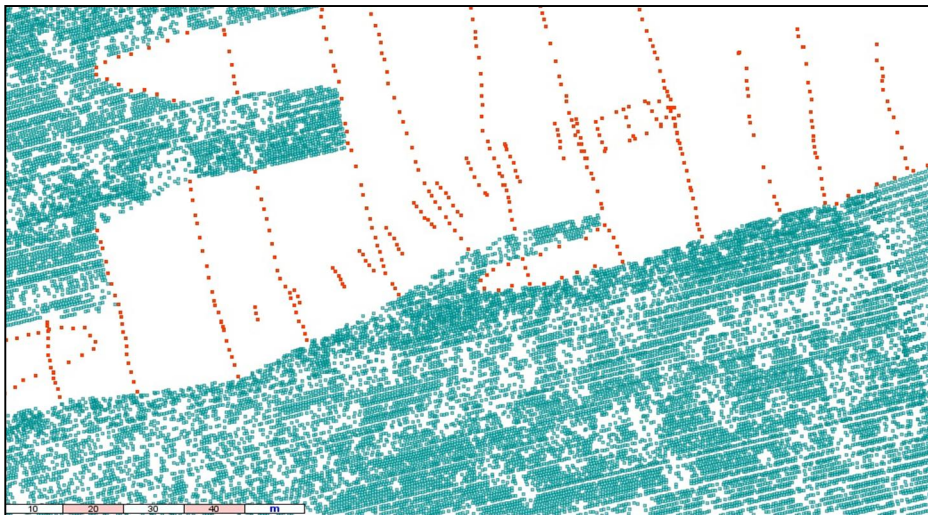


Figure 6.14 The figure shows a particular (90 x 170m) of the vectorial data acquired for the digitalization of the surface of the c08 channel: the blue dots are the Lidar x,y,z points, describing the areas outside the channel, not interested by erosion/deposition processes; the red dots are the GPS points acquired on the field, describing the areas of the channel and outside it, in which the debris flow of the 4<sup>th</sup> of July routed. To be noted the big difference in density among the two dataset.

#### **6.5.4. Individuation of the triggering area**

The identification of the triggering section occurred on the basis of the considerations made by Gregoretti and Dalla Fontana (2008): the triggering areas are characterized by a morphology of the channel that allows both the formation of deposits of debris and the formation of surface runoff; determining the source of the triggering of a debris flow means identifying the context in which the solid and incoherent material is mobilized by the water and transforms its flow from a Newtonian motion of water to a non-Newtonian motion of water and sediment. According to the considerations of Berti et al. (1998), the availability of debris material in the upper part of the channel, where debris flow initiate, does not seem to represent a limiting factor for the occurrence of the phenomenon if the channel is deeply incised in young, weakly cemented, heterogeneous slope deposits (as observed in the c08 channel).

The importance of the triggering zone of the debris flow is carried out, during the GIS analysis, when the detection of the triggering point allows to extract, with computerized procedures, the drainage area that contributes to that point. The operation can then determine, by a simulation (using the appropriate tool "upslope area 2" in the Hydrological model), the runoff hydrograph, to be compared with the critical liquid discharge needed for the triggering of the event, estimated by empirical formulas (Gregoretti and Dalla Fontana, 2008; Tognacca et al., 2000).

Related to the estimation of the liquid critical discharge is the particle size analysis of the material present and available to the transport: the analysis of the grain size makes possible to determine some characteristic diameters ( $D_{\text{average}}$ ,  $D_{50}$ ,  $D_{84}$ ,  $D_{90}$ , etc..) necessary as input data for the numerical model of forecasting of the hydrograph of the debris flow. Dealing with the triggering of a debris flow due to the instability of the channel-bed, the particle size sampling has been always carried out on the surface, because superficial material is initially mobilized by the runoff, thus constituting a hyper-concentrated current who later will transform into a debris flow (Gregoretti and Dalla Fontana, 2008). As explained in chapter 5.5, two possible triggering sections have been identified on the c08 channel: one (called A, Figure 6.15, at 1637 m a.s.l., 180 m downstream the head of the channel, one (called B, Figure 6.16 ) at 1592 m a.s.l., 260 m downstream.





Figure 6.15 Triggering section A, height 1637 m a.s.l.



Figure 6.16 Triggering section B, height 1592 m a.s.l.



### **6.5.5. Characterization of the topography of the channel**

The characterization of the topography of the channel, in particular the triggering zones of the phenomenon and the part of the channel characterized by deposition of sediment, provides the data of the variations of micro-morphology due to its process of deposition, and it consequently allows the estimation of the sediment volumes entrained in the triggering and transport reaches and those deposited, that respectively represent the input and the output of the Automata model for the simulation of routing and deposition phases of a debris flow.

The GPS instrumentation has been employed with the aim of acquiring data for an accurate description of the mobilization of material during a debris flow occurrence, optimizing time and financial resources. As mentioned in chapter 5.6, no direct observation of the event has been done, so, where possible, the distinction of old and new deposits has been described on the basis of the visual interpretation of their "age": usually very recent deposits have a lighter colour than old ones. Where this distinction was not possible, many GPS points have been acquired in order to compare them with the Lidar dataset.

The data acquisition has been done following a common framework:

- the points are acquired in sections along the channel, within it and outside the banks, for as far as sediment has been moved by the studied event; the banks are acquired aside;
- the distance between points in a section is about 0.5 - 1 m: it is not constant because it follows the micro-topography, in order to describe it as precisely as possible;
- the distance among sections is 3-10 m, depending on the degree of variability of the channel: the greater the variability the closest the distance among sections;
- each section has a name and a numerical code;
- within the section, the points indicating left and right bank, left and right bed limit and the talweg (deepest point in the section, important for the water flowing) are marked with the description.

GPS data acquisition (see Figure 6.17, Figure 6.18, Figure 6.19, Figure 6.20) have been carried out starting where the field observation gave evidence of the first out-banks deposits, and this is due to two reasons:

- the Automata model for routing and deposition phases of a debris flow is not able to simulate erosion, so all the simulations have been performed starting from the reach of the channel in which the process of transport of sediment material give way to the deposition process;

- the GPS survey has been carried out only where allowed by the signal conditions between rover-satellites and rover-fixed base: since the transport reach of the channel is contained within high rock cliffs these condition were highly unfavourable or impossible. Laser pulse data have been taken to compensate but their subsequent comparison to the Lidar dataset gave evidence that they were carrying too heavy errors, so they have been discarded at all. As a consequence, the available and useful dataset to calculate deposition and erosion processes do not covers the area of the triggering and transport reaches of the channel.

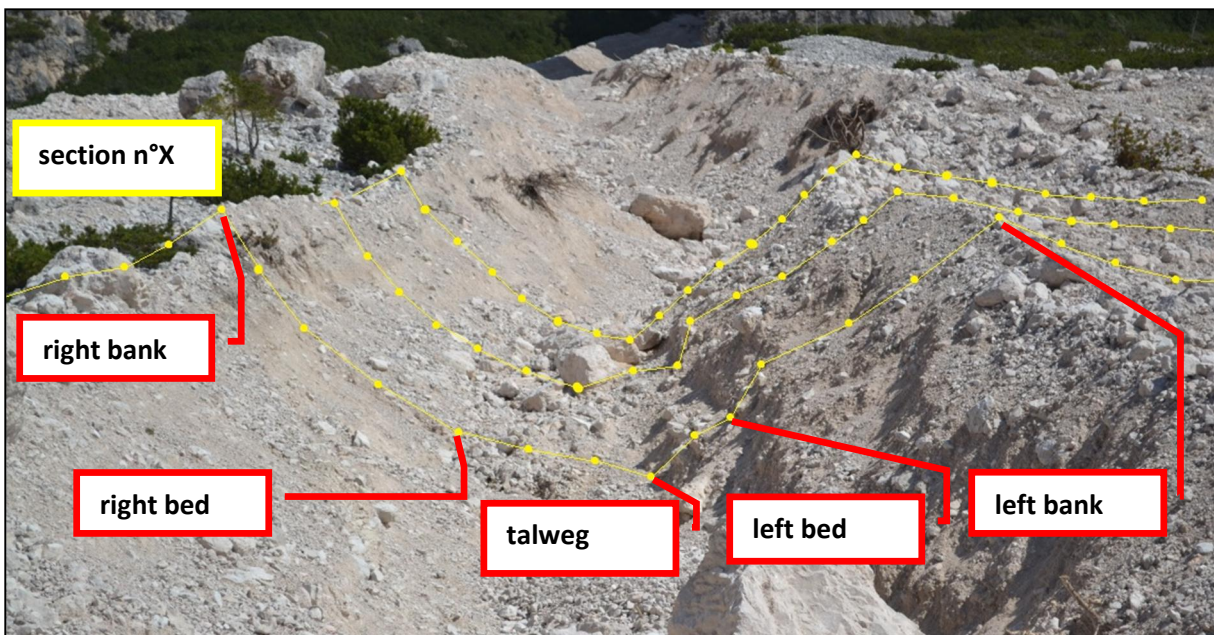


Figure 6.17 Scheme for the acquisition of GPS points (yellow dots) on the channel: the sections are 3-10 m each other, the points in a section 0.5-1 m each other, pivotal points have the description for the post processing.

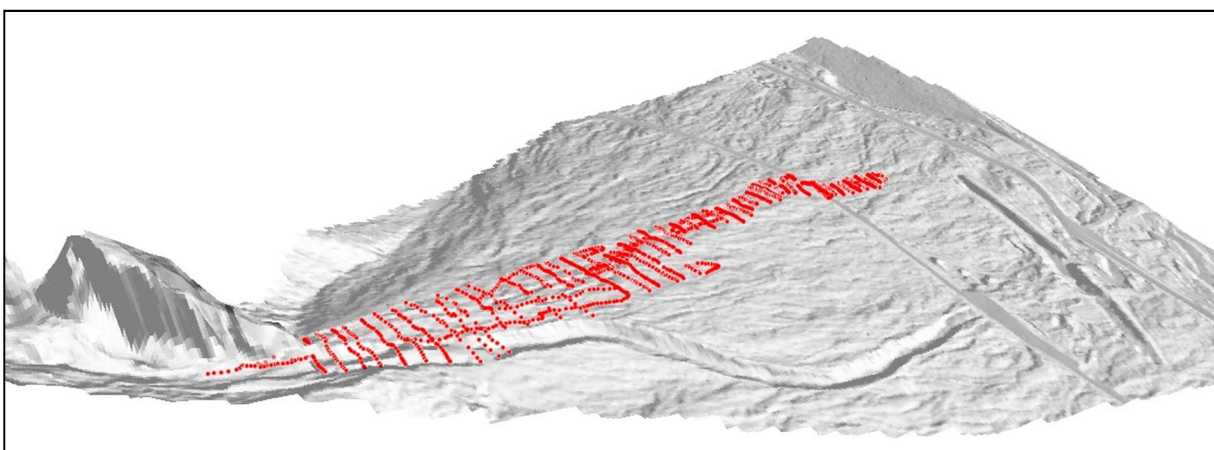


Figure 6.18 North-East view of the DTM of the fan of the c08 channel, colored with hillshade effect. The red dots are the post-event GPS points acquired during the field survey. It's evident their structure in sections.



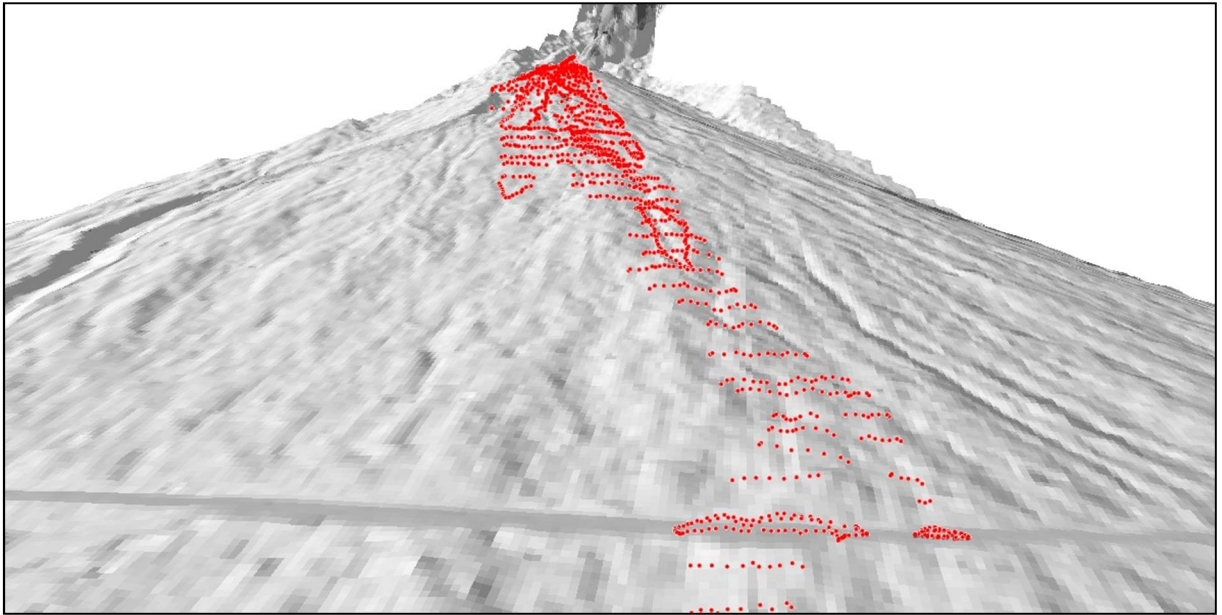


Figure 6.19 Front (West) view of the DTM of the fan of the c08 channel, colored with hillshade effect. The red dots are the post-event GPS points acquired during the field survey. It's evident their structure in sections.

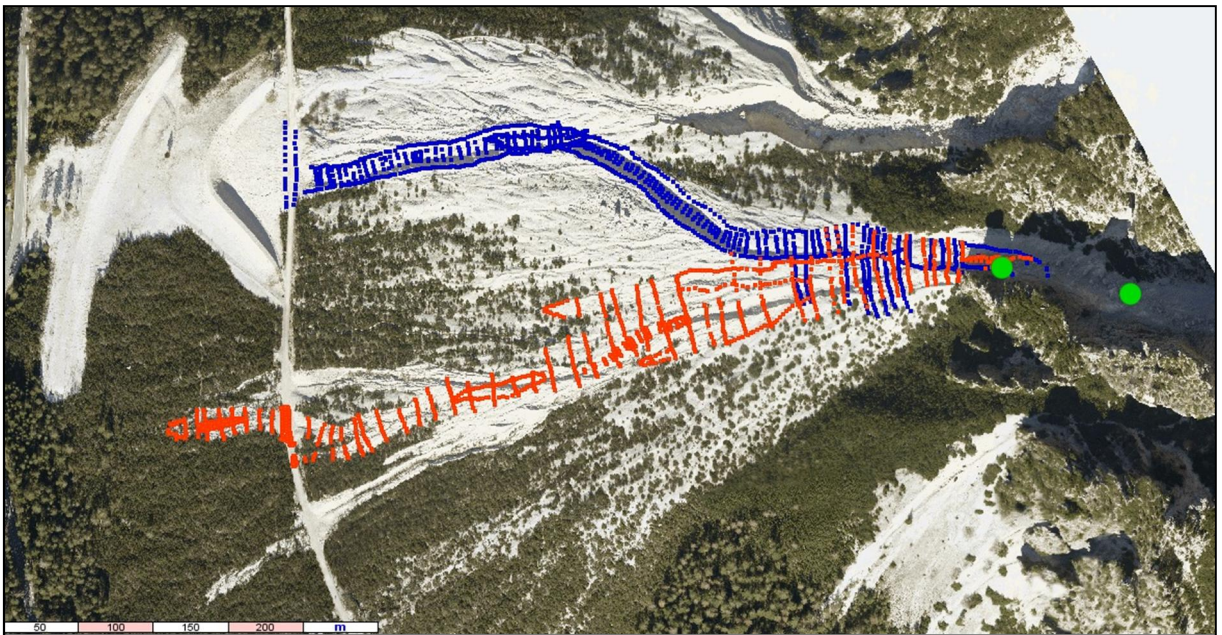



Figure 6.20 Bird watch view of the c08 channel. The red dots are the GPS points acquired in 2010, before the 4th July debris flow event; the red dots are the GPS points acquired immediately after the event; the green dots are the two triggering areas.

### 6.5.6. Grain size analysis

The particle size analysis has been always based on gravel data sampling on the surface bed of the debris flow channel, by the method of the "transect-line" type: this is a sample method that involves the measurement of the diameter of gravel collected at fixed distances along a transect of predefined length. The transects has been built with strap metric lying on 10-15-20 m of length, sampling every 0,20 - 0,25 - 0,40 - 0,50 m (depending on the size of the sediment). For each transect 50-100 elements were measured. The measurement of the diameters has been done with a metal grid with 10 square holes, for 10 diameter classes, listed in the table (Table 6-8). For each rock, the smallest hole through which it passed has been noted, recording the diameter class. The stones larger than the largest class size were measured with a measuring tape along the three dimensions length, width and height. The particle size analysis was performed on a computer using the program "Campion" (Gregoretti, 2010). The program receives as input a file (.txt extension), that contains a strip with the classes of the sampled elements (or size measurement) and generates as output a .txt file with different strips result: diameter of the sampled elements in increasing order, diameter classes with extremes in diameter and in  $\phi$  index (according to the Wentworth scale proposed by the American Geophysical Union), average diameter class, and cumulative and relative frequency of items per class, total average diameter, cumulative curve relative to each element, class average diameter with cumulative frequency, characteristic diameters  $d_{10}$ ,  $d_{16}$ ,  $d_{20}$ ,  $d_{30}$ ,  $d_{50}$ ,  $d_{60}$ ,  $d_{65}$ ,  $d_{70}$ ,  $D_{84}$ ,  $d_{90}$ .

Table 6-8 Classes of diameter of the sieve for the field grain size analysis

N° of riddle of the sieve	Diameter of the sieve (mm)	 <p>The metal sieve use for grain size sampling</p>
1	10.00	
2	15.00	
3	23.00	
4	30.00	
5	43.00	
6	61.00	
7	87.00	
8	126.00	
9	179.00	
10	226.00	

## 6.6. Analysis of precipitations

### 6.6.1. Use of rain gauges

The rainfall data has been provided by a small network of rain gauges consisting of 3 elements that were installed at strategic points on the sides of the mount Pomagagnon.

The rain gauges are of the "tipping bucket" type: a hollow plastic cylinder, with known upper circular area and a funnel on the bottom, conveys the precipitation to two bascules (trays) that move "like a swing" receiving and emptying alternatively the rainwater. Each receiver, in the moment in which empties the water, touches a sensor beneath it and an electrical impulse is sent to the data-logger. The amount of water that generates the tipping of the bucket is of known resolution and is stored together with the time data thanks to the internal clock. The sum of the pulses stored provides the total precipitation of the rainfall event, and the temporal datum allows the construction of the corresponding curves of height and intensity of precipitation. The rain gauges are installed on an aluminium pole 1.5 m high with a wedge base driven into the ground, a support for the cylinder on the horizontal plane, three steel wires fixed to the support and anchored to the ground with punches, made visible with white and red ribbon bands.

Particular importance took the attention in positioning the instruments, aimed at preventing other atmospheric phenomena (wind in particular) or the morphology of the rock walls to create conditions that disproportionately affect the vertical fall of precipitation. The choice of the location has therefore been influenced by two factors:

- 1) the distance from the cliffs that might intercept the rain;
- 2) the distance from the sections of detachment of the wind currents, where inevitably motions of air circulation are created, in such a way to affect the vertical fall of water;

The rain gauges, model HD 2013, are made by the Delta Ohm Company: tipping bucket rain gauge, with an area of 400 cm<sup>2</sup>, suitable at temperatures from +1 ° C to +60 ° C, and with a resolution of 0.5 mm of precipitation. Each sensor is equipped with a data logger with LCD display, lithium battery 3.6 V, able to read and store 128,000 pulses. Visualization and data processing on computer is possible with the supplied software DELTALOG 6.

The three rain-gauges are respectively located (Figure 5.2, chapter 5.1):

- 1) on a detrital slope, a scree with sparse mountain pine, underneath the head of the Bartoldo peak, near the c01 debris flow channel;
- 2) on a high-altitude grassland near the Pomagagnon peak, and upstream the triggering area of the c01 debris flow channel;



- 3) on the triggering section of the c04 "Dimai" debris flow, that is part of the instrumentation of a more complex monitoring station.

### 6.6.2. Rainfall data analysis

The data collected from two of the three rain gauges during summer 2011 (the "Bartoldo scree" instrumentation resulted broken), in which the events here studied occurred, were analyzed for the study of the critical threshold of precipitation for the triggering of a debris flow due to channel-bed failure. The data come from the Pomagagnon pass rain-gauge and from the Dimai monitoring station rain-gauge (Figure 6.21).



Figure 6.21 Rain-gauge, part of the debris flow monitoring station on the c04 Dimai channel.

At first, the periods of precipitation identifiable as storm were individuated: they are those in which it is possible to recognize values of precipitation, relative to the sampling time of 5 minutes, on average larger than 0.8 mm, corresponding to an average intensity of 9.6 mm/hour without solution of continuity. Values of precipitation smaller than 1 mm at the beginning and at the end of the storm have been excluded because they contribute marginally to runoff, but can significantly change the average value of intensity of precipitation (Gregoretti and Dalla Fontana, 2007). The hyetograph has then been built for the identified events. From the hyetograph, the average intensity of precipitation of each single storm has been calculated, and has been compared with two curves of mean rainfall intensity versus time for the debris flow triggering due to channel-bed failure. These thresholds were obtained

by Gregorette and Dalla Fontana (2007), from the study of historical rainfall data of 30 by now defined debris flows that occurred in six watersheds of the Dolomites:

$$I_{ave} = 13D^{-0.9} \quad (6.46)$$

$$I_{ave} = 21D^{-0.55} \quad (6.47)$$

where D is the duration of precipitation.

The critical rainfall was established by comparing a modeled hydrological response with the known times of occurrence of the debris flows and with the critical values of runoff for the initiation of mass transport phenomena identified through laboratory experiments.

Equation (6.46) has been identified as the most suitable to describe the precipitation of a critical rainfall of long duration, i.e. for durations longer than 1 hour and with a return period of approximately 1 year, while equation (6.47) has been found more suitable to describe rainfall events of the "storm" type. Equation (6.47) can be approximated by a rainfall depth duration frequency curve corresponding a return period of three years. Where the value of average intensity of each storm exceeds the threshold, the conditions for the initiation of a debris flow for channel-bed failure of the channel are reached. Consequently, the analysis of the average rainfall intensity of each storm considered two different values of precipitation:

- the duration of the entire rainfall event, which includes the values of intensity of 2.4 mm/h in the range of sampling, without solution of continuity;
- the duration of each intense storm, which includes only the time intervals with hourly intensity values larger than or equal to 9.6 mm/h.

The study has been carried out on the precipitations occurred in the days previous to the debris flow event. Only one rainfall event has been recognised as storm event, the one that occurred on the evening of the 4th of July, from 21:15 to 22:15 on Dimai station and from 21:00 to 21:26 on Pomagagnon pass station. The intensity of the *total* duration of rainfall has been compared to the curve of eq (6.46), while the *intense* storm (only from 22:15 to 21:50 on Dimai station and from 21:17 to 21:26 on Pomagagnon pass station), has been compared to the curve of equation (6.47).

For the calculation of the triggering hydrograph of the phenomenon, the yetograph has been considered only in the interval of 40 minutes in which the precipitation intensity was  $\geq 9.6\text{mm/h}$ . The return period of the precipitation resulted of 4.5 year (using the Gumbell distribution and the method of the moments - refer to Dalla Fontana (2009)).

As shown in figure (Figure 6.22), for Dimai station, both the total and the intense durations exceeded the relative thresholds, while for the Pomagagnon pass station only the total

duration reached this result. As the intense precipitation registered at Dimai exceeded by far the threshold curve, it has been chosen as main input to be used in the hydrological modelling of the debris flow event.

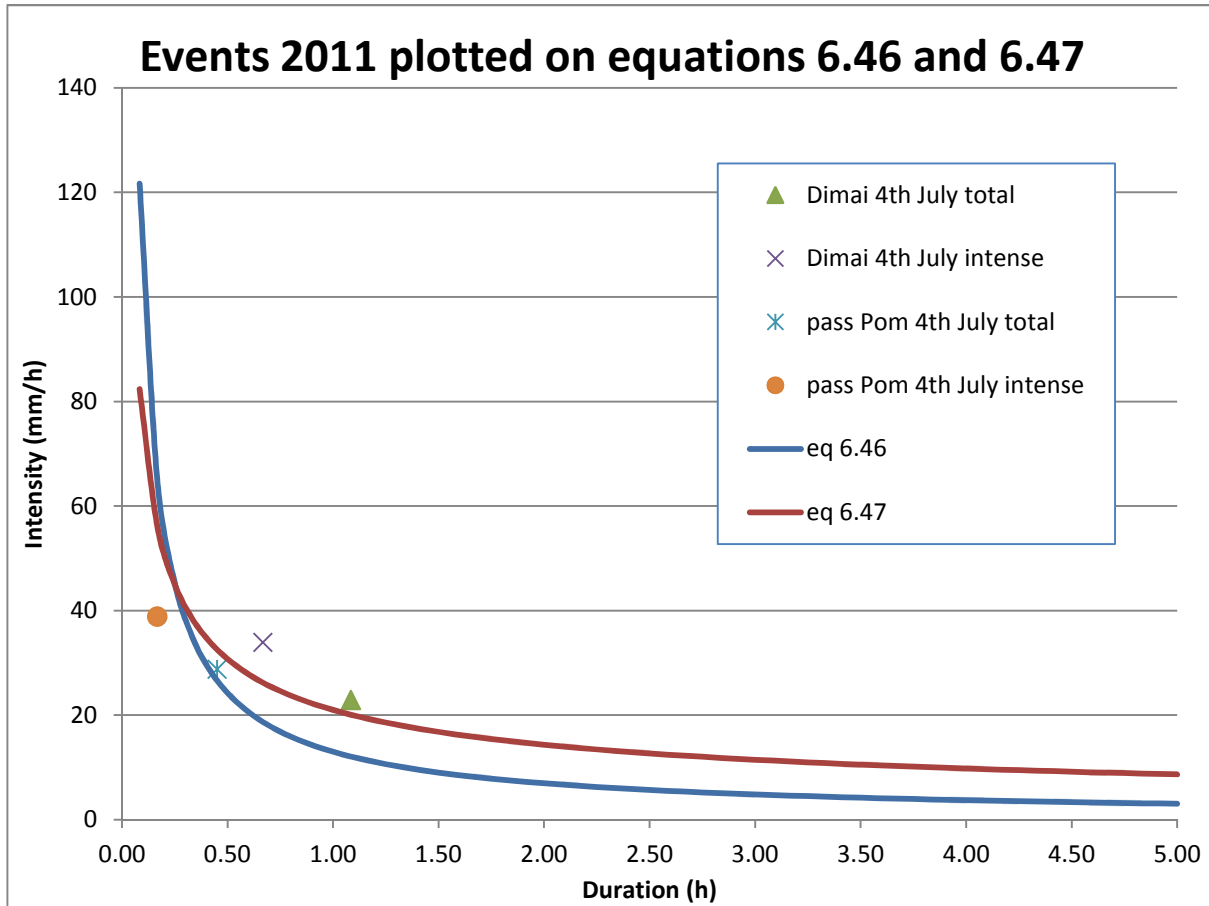


Figure 6.22 The rainfall events analyzed for the individuation of the triggering precipitation of the 4<sup>th</sup> July debris flow. The data are plotted on the curves of mean rainfall intensity for the triggering of a debris flow due to channel-bed failure developed by Gregoretti and Dalla Fontana (2007).

According to Orlandini and Lamberti (2000), unknown spatial and temporal distribution of rainfall input is one of the most significant reasons causing errors in runoff simulations: indeed perturbed airflows and potential airflows over barriers (such as rock cliffs) can cause a precipitation enhancement, and the consequent higher precipitation intensity can lead to a higher infiltration excess runoff production mechanism, increasing the rainfall excess. As a consequence, the consideration of possible effects of wind on the rainfall distribution close to high peaks and rocky cliffs in mountain areas, lead to the increasing of measured rainfall depth. Furthermore, wind can significantly lower the amount of precipitation intercepted by a rain-gauge, in a measure up to the 70%. As a consequence, the possibility of precipitations



10%, 20% and 30% higher have been considered, providing for the following simulation, together with the normal data, three modified (mod+%) hyetographs, that are shown in figure Figure 6.23.

The return time of the mod+30% precipitation, considering only the interval of 40 minutes in which the precipitation intensity was  $\geq 9.6\text{mm/h}$  (Table 6-9), resulted 10.7 years.

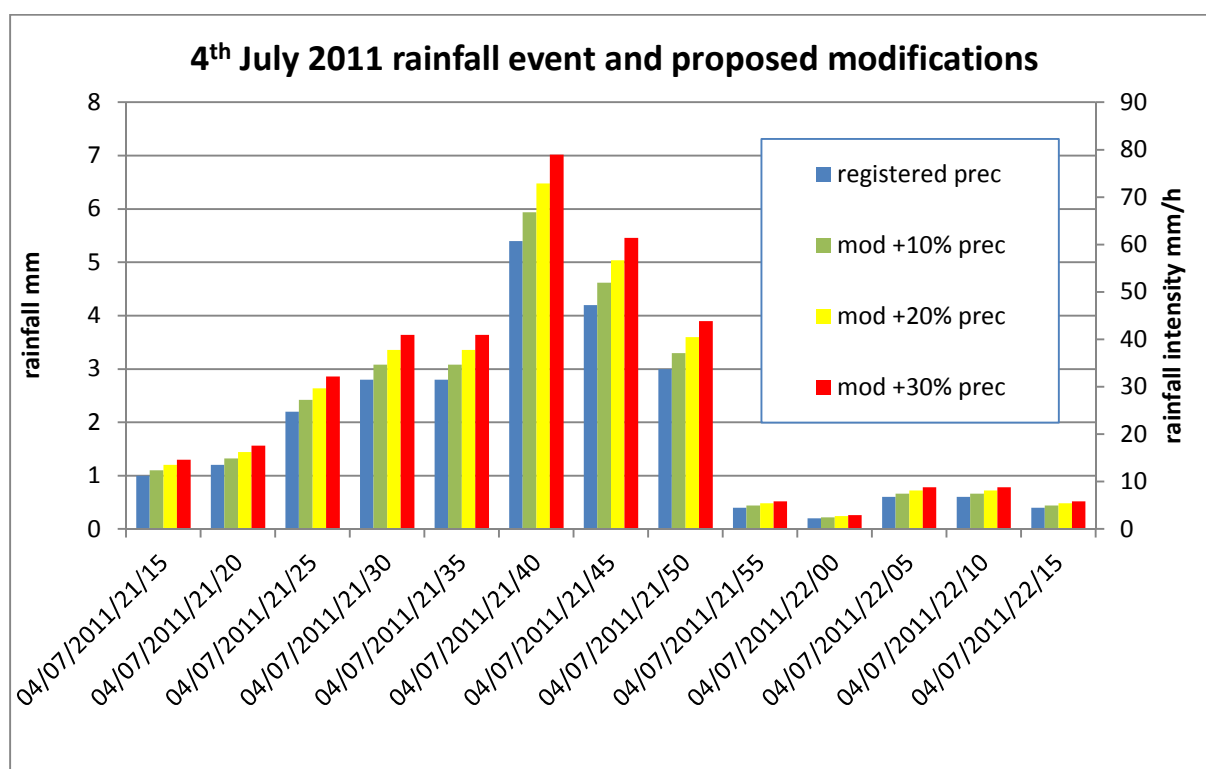


Figure 6.23 The normal and modified yetographs used for the simulations.

Table 6-9 The yetograph mod+30% used for the simulations, considering only the intervals of precipitation with rainfall intensity greater than 9.6 mm/h. The related return period is 10.7 years.

Time	Rainfall mod +30% mm	Intensity mm/h
04/07/2011 21:15	1.3	15.6
04/07/2011 21:20	1.56	18.72
04/07/2011 21:25	2.86	34.32
04/07/2011 21:30	3.64	43.68
04/07/2011 21:35	3.64	43.68
04/07/2011 21:40	7.02	84.24
04/07/2011 21:45	5.46	65.52
04/07/2011 21:50	3.9	46.8

## 6.7. Preliminary GIS analysis

### 6.7.1. Introduction to GIS processing

The GIS software used for the analysis and elaboration of the data consists of:

- AdB Toolbox, a free open source software created by the spin-off “Geomatica e Ambiente” with the participation of the Department of Land and Agro-Forest Environment of the University of Padua. It is a graphic application that can be used for visualizing and elaborating spatial datasets, characterized by a user friendly interface and simplicity. It's provided with a set of tools for topographical, morphological and hydrological analysis.
- ArcMap version 10.0.

The GIS software made possible to process the GIS field data in the way to obtain a representation of the topography of the channel surface before and after a debris flow event: one surface representing the pre-event, one surface representing the post-event. The procedure involved the creation of a TIN, Triangular Irregular Network, from which further obtain a DTM, a Digital Terrain Model of the surface of interest on raster environment.

Triangular irregular networks (TIN) have been used by the GIS community for many years and are a digital means to represent surface morphology. TINs are a form of vector-based digital geographic data and are constructed by triangulating a set of vertices (points). The vertices are connected with a series of edges to form a network of triangles. There are different methods of interpolation to form these triangles, such as Delaunay triangulation or distance ordering. For this work the software ArcGIS has been used, that supports the Delaunay triangulation method.

The resulting triangulation satisfies the Delaunay triangle criterion, which ensures that no vertex lies within the interior of any of the circum-circles of the triangles in the network. If the Delaunay criterion is satisfied everywhere on the TIN, the minimum interior angle of all triangles is maximized. The result is that long, thin triangles are avoided as much as possible.

The edges of TINs form contiguous, non-overlapping triangular facets and can be used to capture the position of linear features that play an important role in a surface, such as ridgelines or stream courses. Because nodes can be placed irregularly over a surface, TINs can have a higher resolution in areas where a surface is highly variable or where more detail is desired and a lower resolution in areas that are less variable.

The input features used to create a TIN remain in the same position as the nodes or edges in the TIN. This allows a TIN to preserve all the precision of the input data while

simultaneously modeling the values between known points. It is possible to include precisely located features on a surface, such as mountain peaks, roads, and streams, by using them as input features to the TIN nodes (ArcGIS 10 manual).

A TIN map can be converted to a raster map with square cells with floating data type (the output raster will use 32-bit floating points of the centre of the cell with real values). The method used to convert a TIN map into a raster map is a linear interpolation of the triangles to calculate the square values.

Each raster map has the same extent and is snapped on the first map obtained for the study area.

The difference in elevation between the two relative DTMs gave a third raster output able to show the areas of erosion, the areas of deposition and the magnitude of the two processes.

### **6.7.2. Data filtering**

A total of 1911 x,y,z geo-referenced points in 2010 (before the event) and 1491 points in 2011 (just after the 4<sup>th</sup> July event) has been acquired and registered with the GPS to describe with high definition (up to 5 centimetres of precision on the vertical coordinate, 2-4 on the horizontal one) the evolution of the surface topography of the channel routed by a debris flow event.

However, data collected with GPS need to be filtered, for different reasons, and wrong or not useful data must be eliminated. In the specific:

- some errors occurred during the field data acquisition so that the geo-referenced points are clearly set out of acceptable ranges of precision and accuracy (GDOP values minor than 4. The Geometric Dilution of Precision is a measure of how errors in the measurement will affect the final state estimation). The errors can be related to momentary lacks of signals between the rover and the satellites or between the rover and the base, or to problems of scattering of the signal on the bare rock/sediment, or to improper use of the GPS instrument by the operator (i.e. pole not vertical, battery connections not kept clean).

The wrong data are founded during the GIS analysis:

- from the comparison of the points' elevations among other close GPS points or, when possible, among close Lidar points: differences over 0.5 m of elevation have to be checked for their plausibility;
- from evident errors on the horizontal coordinates of the points: this is possible thanks to the spatial structure of the surveys, made in linear

sections, each one perpendicular to the flow direction in the channel bed.

Points out of the section lines have to be considered wrong.

- some data have to be considered dangerous because of their possible strong and wrong influence on the algorithms that will interpolate them when elaborating the digital surface on the GIS, creating topographic features not corresponding to the reality. Question of single points, isolated from the points ordered in sections or groups, that would create triangles in excess and false shapes in the TIN interpolation. This situation can be described by the example in figure (Figure 6.24).

After the filtering, 1330 out of 1911 points relative to the year 2010 were verified and kept for the simulation, and 1392 out of 1492 points relative to the 2011 event.

The description contained in the metadata (point description) of each point allowed to draw the profiles of the banks, of the channel bed, of the talweg (the deepest portion of the channel bed), of in-channel deposits, of out-banks deposits.

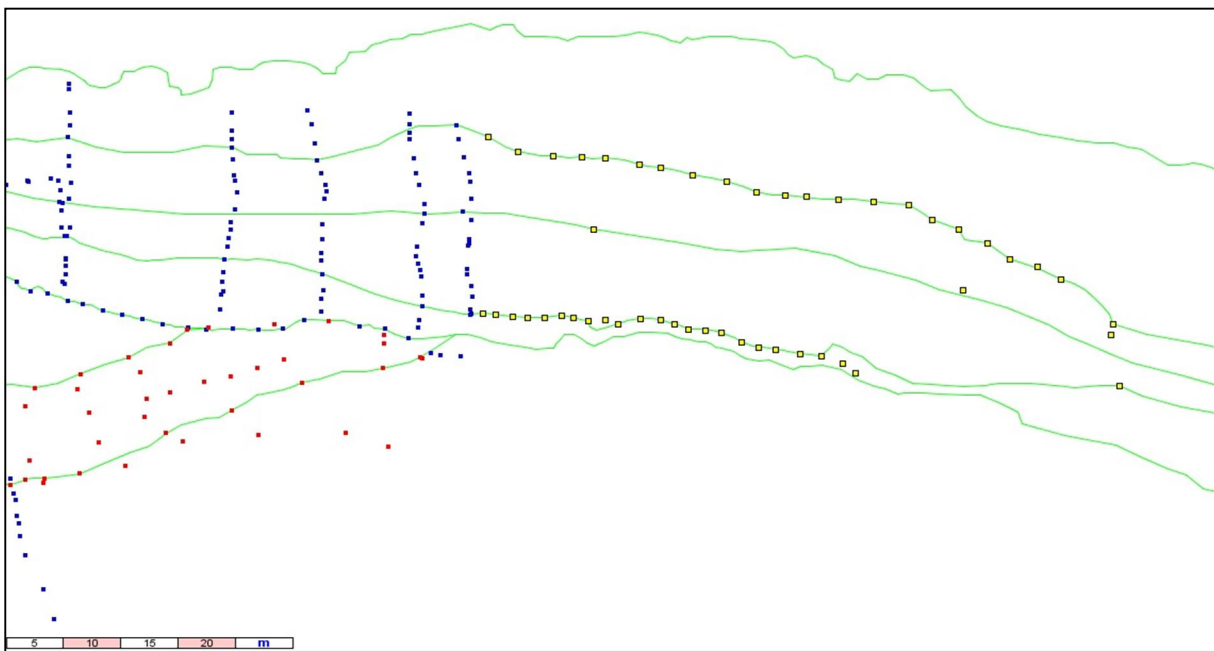


Figure 6.24 The figure shows the GPS points taken close to the triggering area of the c08 channel: blue dots are correct points, red dots are points that have been eliminated because of a wrong GPS acquisition procedure (the vertical elevation resulted 2-3 m displaced in comparison with blue points and with the surrounding Lidar points), yellow dots are points that have been eliminated because of their dangerous influence on the interpolation algorithm, green lines represents the banks, the channel bed, the talweg. The yellow points, in particular, have been excluded from the surface reconstruction algorithm because of the lack of similar points in the surroundings (on the banks and within the channel bed): the TIN interpolation in such a case could create triangles developed in the orthogonal direction to the flux, creating barrier-like features.

### 6.7.3. Creation of the DTM for pre and post event

The process of creation of the DTM surfaces representing the pre-event and the post-event topography required to select and operate with three sets of features:

1. the GPS points related to the surface of the channel and of the deposits, divided into two distinct sub-dataset:
  - one sub-set representing the pre-event surface,
  - one sub-set representing the post-event surface;
2. the Lidar points related to the surface outside of the channel and of the deposits, therefore representing the surface that has not been interested by the processes of erosion and deposition of the case study event. The presence of a Lidar spatial dataset in the immediate surroundings of the GPS dataset allows, in addition, to avoid deviating triangles when interpolating these marginal points.

Merging the two sets, allowed to represent the entire surface topography of the channel through discrete points with x,y,z coordinates. Two total surfaces have hence been created, one describing the pre-event situation, one describing the post event situation.

These discrete features have then been interpolated to create a TIN surface model through the ArcGis tool:

➤ 3D Analyst Tools > TIN Management > Create TIN

The TIN has then been converted into a raster DTM file through the ArcGis tool, using the linear interpolation method:

➤ 3D Analyst Tools > Conversion > From TIN > TIN to float Raster

A resolution of 1x1 m has been chosen for the creation of the DTM.

To work within the software AdB Toolbox the raster files have been converted into a floating raster type through the ArcGis tool:

➤ Conversion Tools > From Raster > Raster to Float.

The following figures (Figure 6.25, Figure 6.26, Figure 6.27, Figure 6.28, Figure 6.29, Figure 6.30) represent the process, from the selection of the points to the creation of the raster DTM, for the post-event surface. The same procedure has been carried out for the pre-event surface.

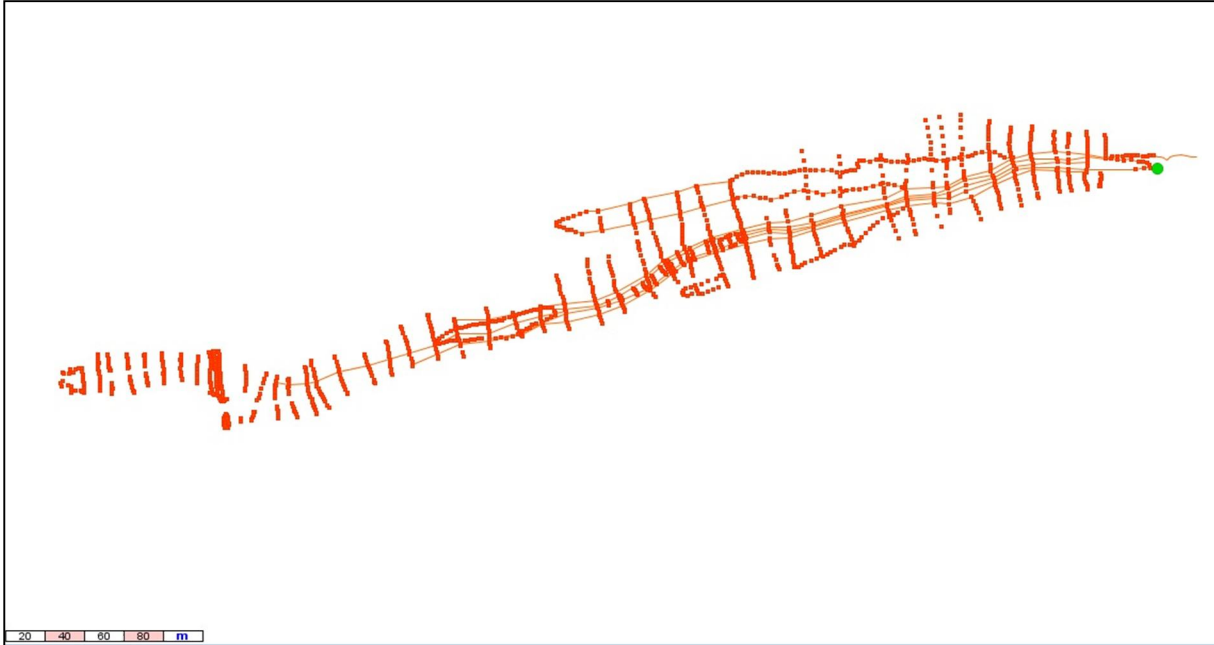


Figure 6.25 The figure shows the red points, representing the GPS points of the post-event surface, and the linear features representing the banks, the channel bed and the talweg, after the filtering process. The triggering area is represented with a green dot.

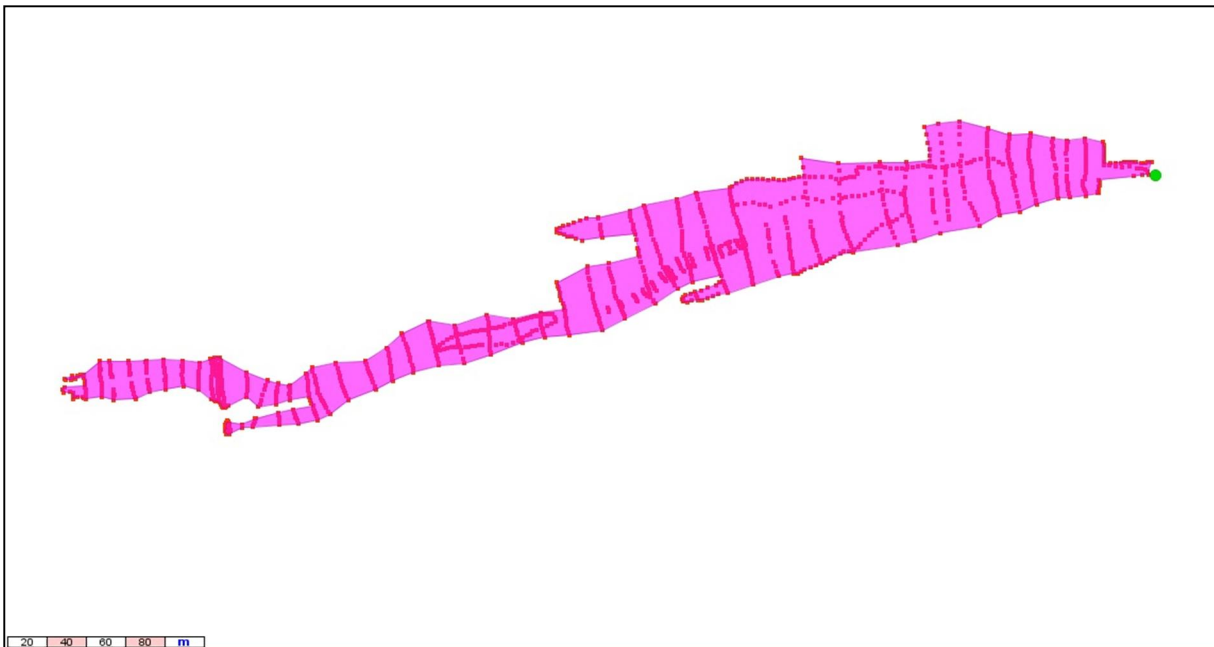


Figure 6.26 The figure shows the mask that has been created to select and operate with the GPS post-event points.

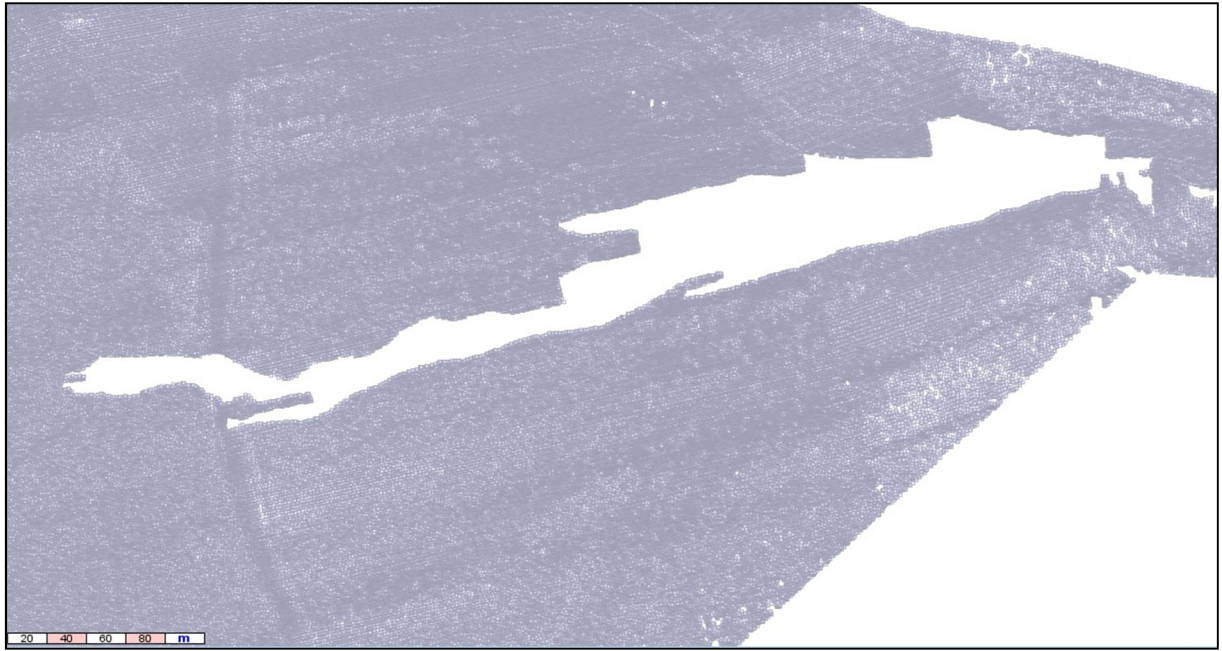


Figure 6.27 The figure shows the Lidar dataset representing the area of the fan not interested by the erosion/deposition processes of the 4<sup>th</sup> July debris flow event. It has been obtained subtracting to the total Lidar dataset the Lidar points intersecting with the mask of the post-event GPS points.

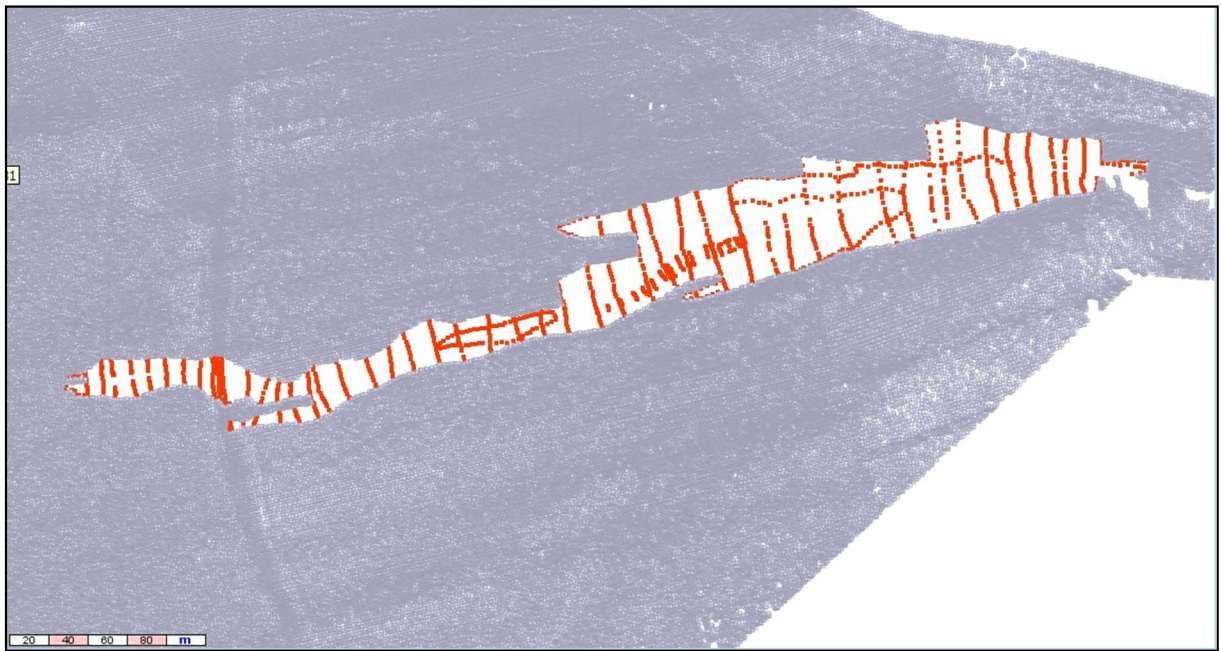


Figure 6.28 The figure shows the total set of points representing the surface of the fan after the case study event, obtained merging the GPS points of Figure 6.25 and the Lidar points of Figure 6.27.



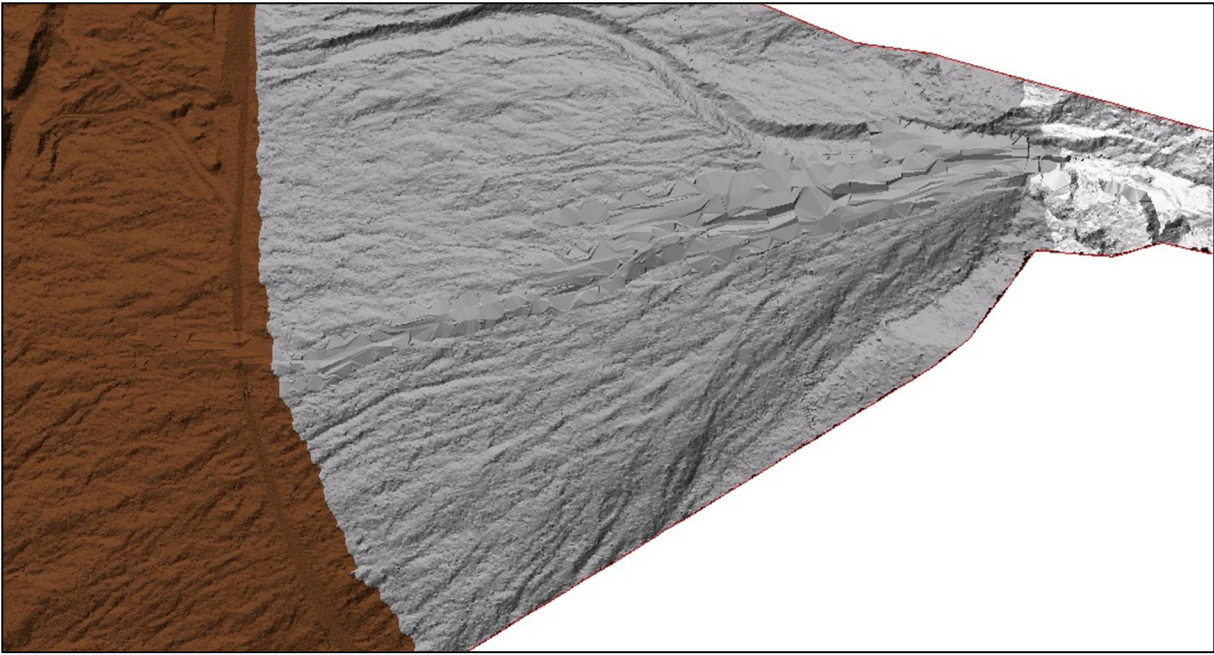


Figure 6.29 The figure shows the TIN obtained from the interpolation of the total set of points representing the post-event surface (of Figure 6.28).

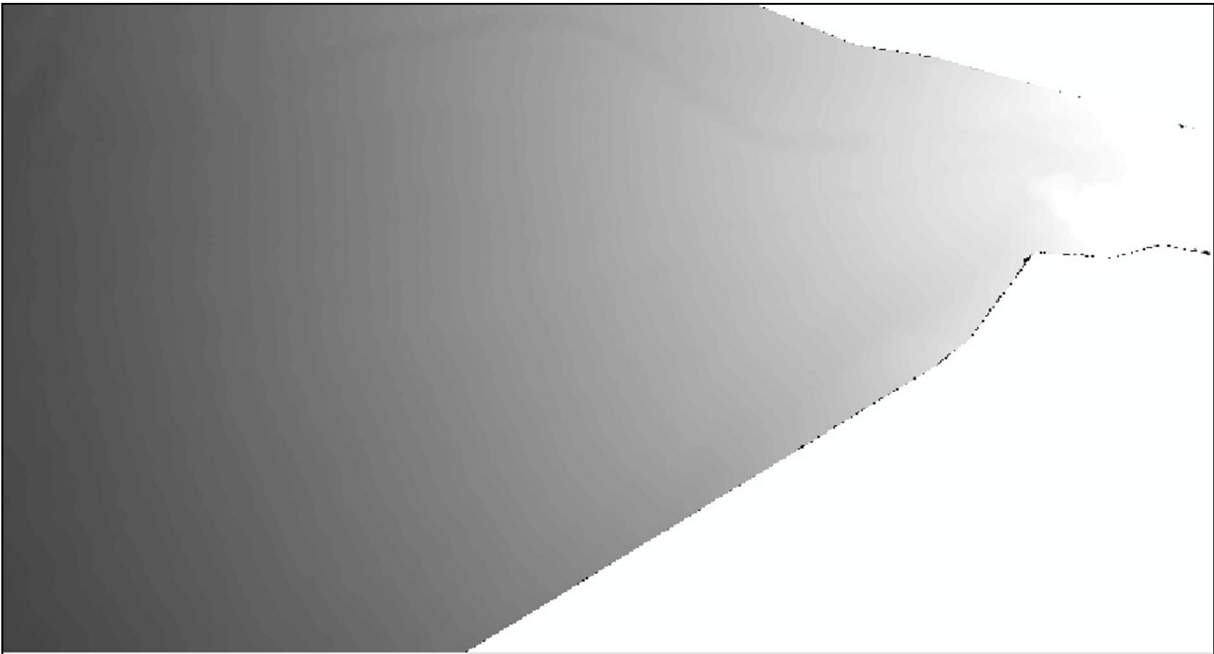


Figure 6.30 The figure shows the DTM obtained from the conversion to a raster file of the TIN of the total post-event surface of Figure 6.29.



#### 6.7.4. Creation of erosion/deposition maps

The algebraic difference between the post-event DTM and the pre-event DTM has been elaborated with the raster calculator tool (AdB Toolbox). The operation provides the relative difference in elevation of the cells of the two surfaces: an increase in elevation of the post-event surface, compared to the pre-event surface, would indeed mean that in that area the deposition of sediment occurred; vice-versa, a decrease in elevation of the post-event surface, compared to the pre-event surface, would mean that a process of erosion occurred. Therefore, the output of the difference of the two raster surfaces provides the map of the processes occurred during the specific debris flow event, visualizing the areas subjected to erosion and those subjected to deposition, and the relative value of magnitude (in m) for each cell.

As mentioned in chapter 5.6 the volume of the event resulted considering two hypothesis:

- hypothesis 1) the same debris flow first obstructed the old channel, then deviated toward the new path, depositing a total (a) of about 7600 cubic meters of sediment material: 6700 (b) of them coming from the triggering and transport reaches of the channel, 900 of them (c) coming from erosion and subsequent deposition in the transition zone between the transport reach and the deposition reach, that has been covered by the field survey;
- hypothesis 2) a total (a) of about 5600 cubic meters of sediment material deposited after encountering an already present obstruction in the old channel: 4700 (b) of them coming from the triggering and transport reaches of the channel, 900 (c) of them coming from erosion and subsequent deposition in the transition zone between the transport reach and the deposition reach, that has been covered by the field survey.

The Automata model is thought to simulate the routing and deposition processes of a debris flow but not erosion. Really a marked distinction between the end of one process and the beginning of the other does not absolutely exist, so that on the field erosion and deposition both occur in a transition zone, where the input source cells for the Automata model must be set.

To be coherent with the possibilities of the Automata model, that works with the input volume coming from the triggering and transport reaches ( $b = a - c$ ) and then routing it to deposition as output, the volume of sediment eroded and then deposited (c) in the area covered by the field survey has not been accounted for the simulations: according to this abstraction, the maps of the distribution of the simulated deposits have been compared with the map of the distribution of the total measured deposits (a) deducted by the volume of sediments eroded and then deposited (c), so obtaining a map ideally representing the

deposition of the only input volume from the triggering and transport reaches (b). The deduction has been calculated on the total measured volume of each cell, multiplying it by a deduction factor (d) equal to:

$$d = 1 - \frac{a - b}{a} = 1 - \frac{c}{a}$$

The deduction factor (d) use for hypothesis 1 resulted 0.8352, the one use for hypothesis 2 resulted 0.8819.

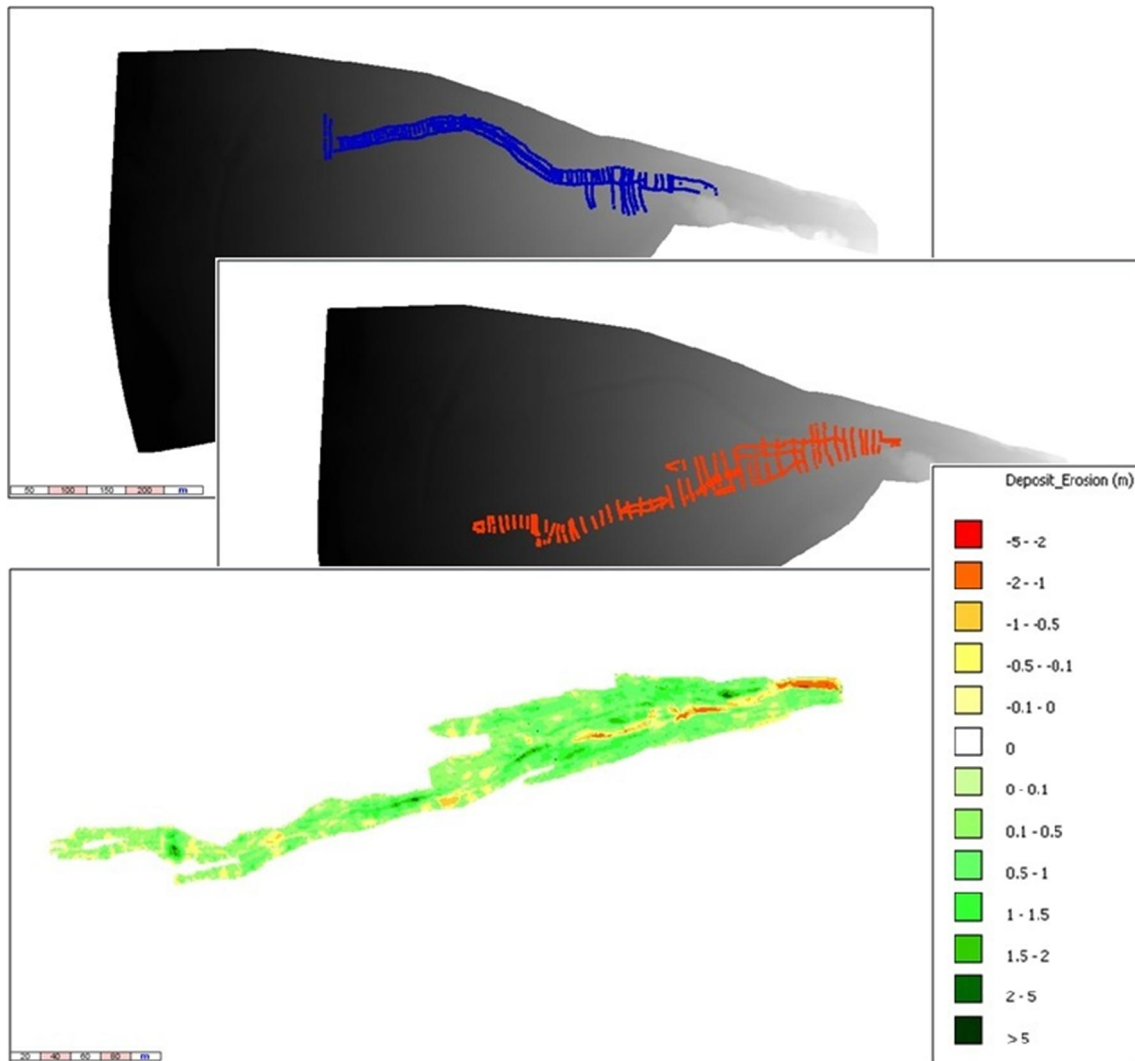
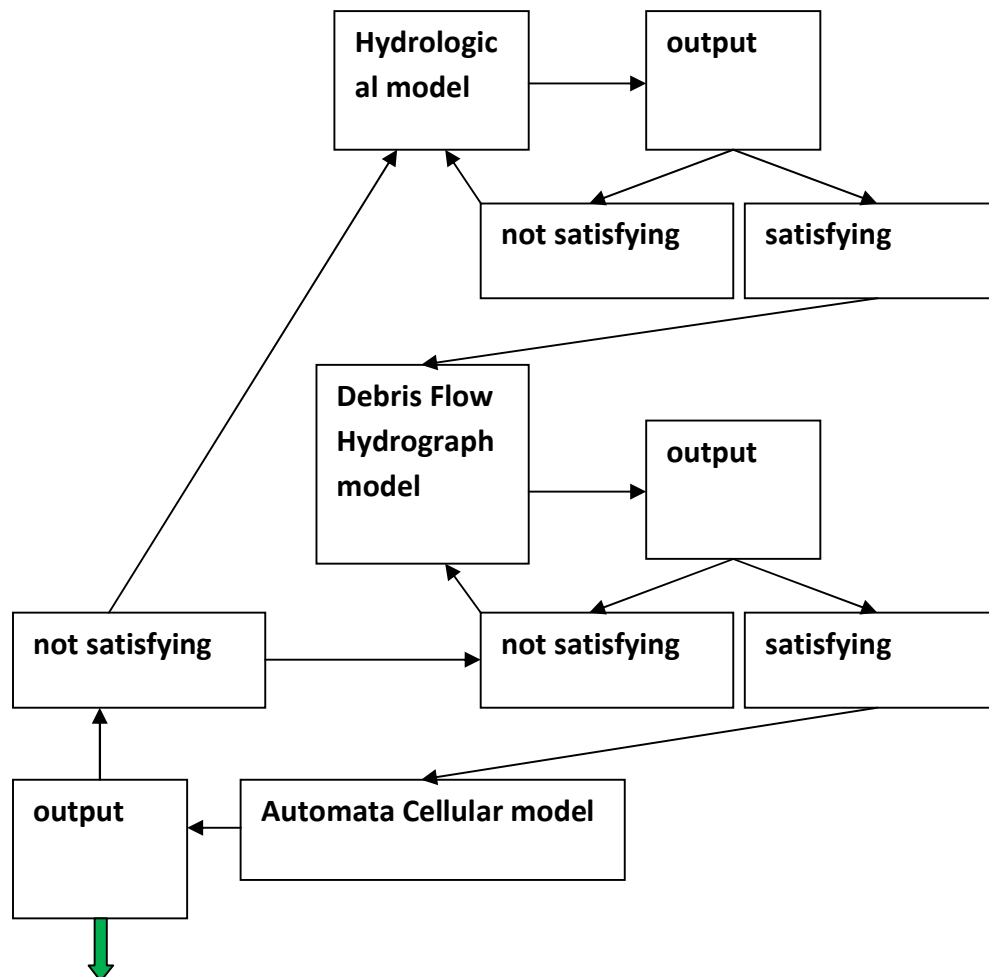


Figure 6.31 The figure show the process through which the estimation of the erosion and of the deposition processes of the 4th July debris flow event happened: the difference in elevation between the post-event DTM (upper frame, indicated together with the red GPS post-event points) and the pre-event DTM (median frame, indicated together with the blue GPS pre-event points) has been elaborated with the raster calculator tool of Adb Toolbox. The bottom frame shows the result of the calculation, with the areas interested by deposition in green tones, and the areas interested by erosion in red tones.

The GPS survey resulted useful to reconstruct the pre-event and the post-event digital surfaces of the channel, in order to estimate the mobilized material, but a higher density of points (or a post event Lidar survey - optimal by the point of view of the quantity of data, but prohibitive by the costs point of view) would be required to increase precision.

## 7. RESULTS AND DISCUSSIONS

Field measurement and GIS elaboration of field data provided the inputs to the "Hydrologic model" for computing runoff hydrograph, that is main input for the "Debris flow Hydrograph model" or "Triggering model", that represents in turn the main input for the "Automata cell model" for the simulation of routing and deposition phases of the debris flow. Hence, the search for the parameters to simulate the event of the 4<sup>th</sup> of July 2011 that best fit with the measured field data took the necessity of producing a set of results to be tested, corrected and re-tested with an iterative procedure involving all the three models at the same time, using the not satisfying results as a basis for new simulations at the root cause (a conceptual scheme is shown below).



## 7.1. The hydrological model

The hydrographs to trigger the two hypothesized volumes of 4700 and 6700 m<sup>3</sup> have been searched: they have been called respectively hypothesis 1 and hypothesis 2.

### 7.1.1. Hypothesis 1

The procedure for the elaboration of the hydrograph has been conducted as it follows.

1. The land use or land-cover map (Figure 7.1) has been obtained through the interpretation of an orthophoto of the area. The procedure has been carried out working drawing a vectorial file and the converting it to a raster map. The need for a high definition, in comparison to land use maps such as the "Corine land cover", comes from the particular requirements of a distributed kinematic-hydrologic model when working on a basin characterized by small dimensions. Working on a catchment with an area of less than 1 km<sup>2</sup>, even small local variations in the land cover can have strong influences on the results of the simulations.

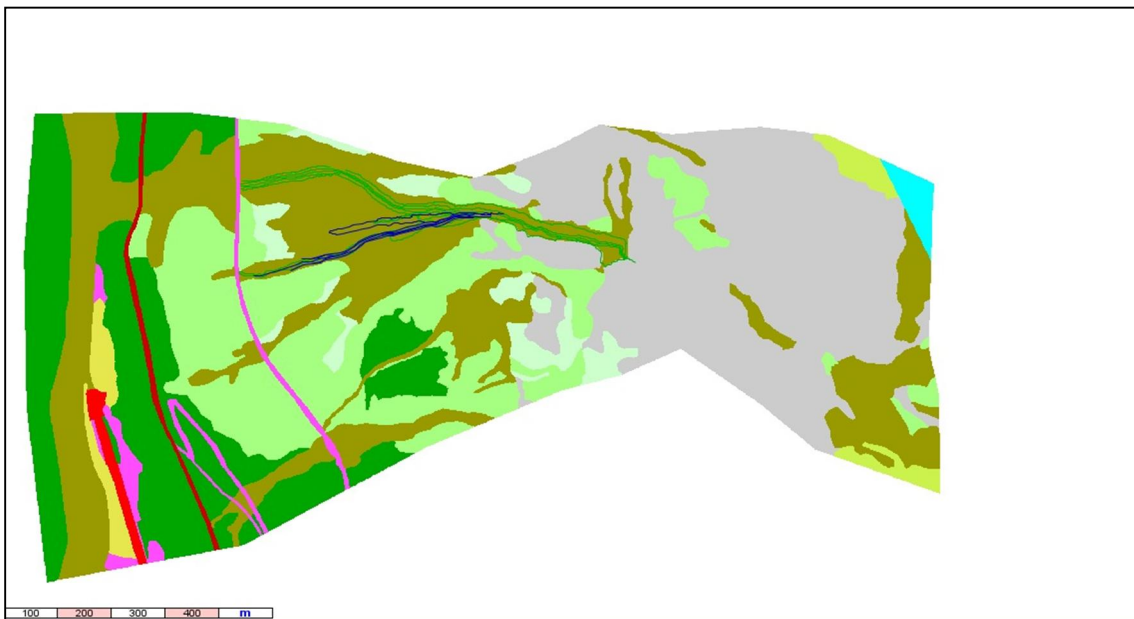


Figure 7.1 c08 land-cover map.

2. The map of the hydrologic groups (Figure 7.2) has been obtained through the procedure explained in chapter 6.1.1.

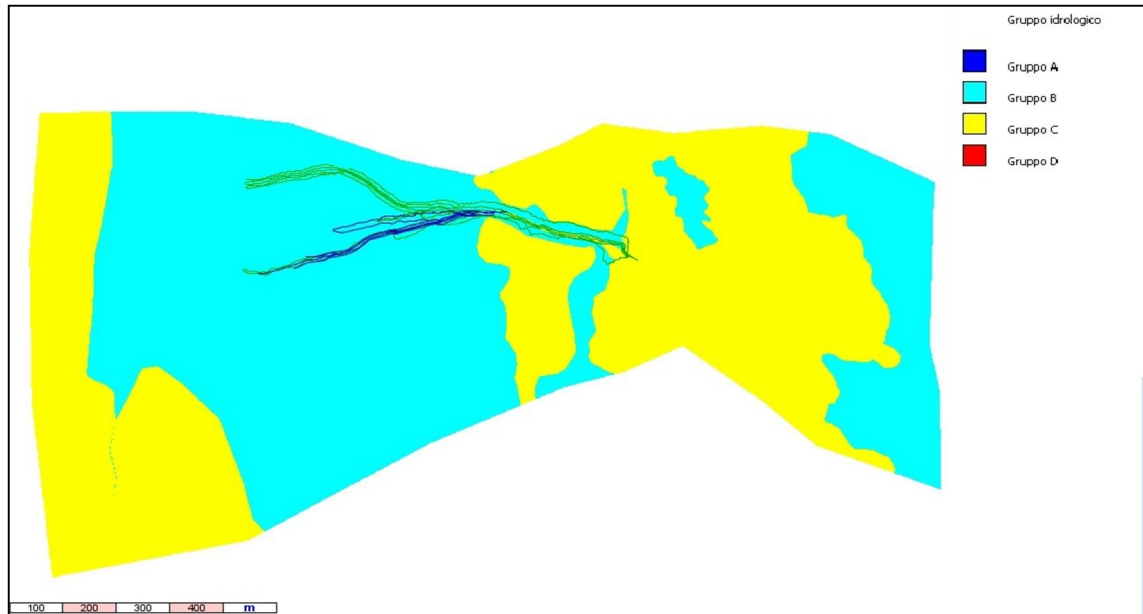


Figure 7.2 c08 hydrologic groups map.

3. Through the combination of the land-cover map and of the hydrologic groups map, operated by the "CN" tool as explained in chapter 6.1.1, the map of the distribution of the Curve Number value for the c08 area has been built (Figure 7.3). The statistics are in Figure 7.4.

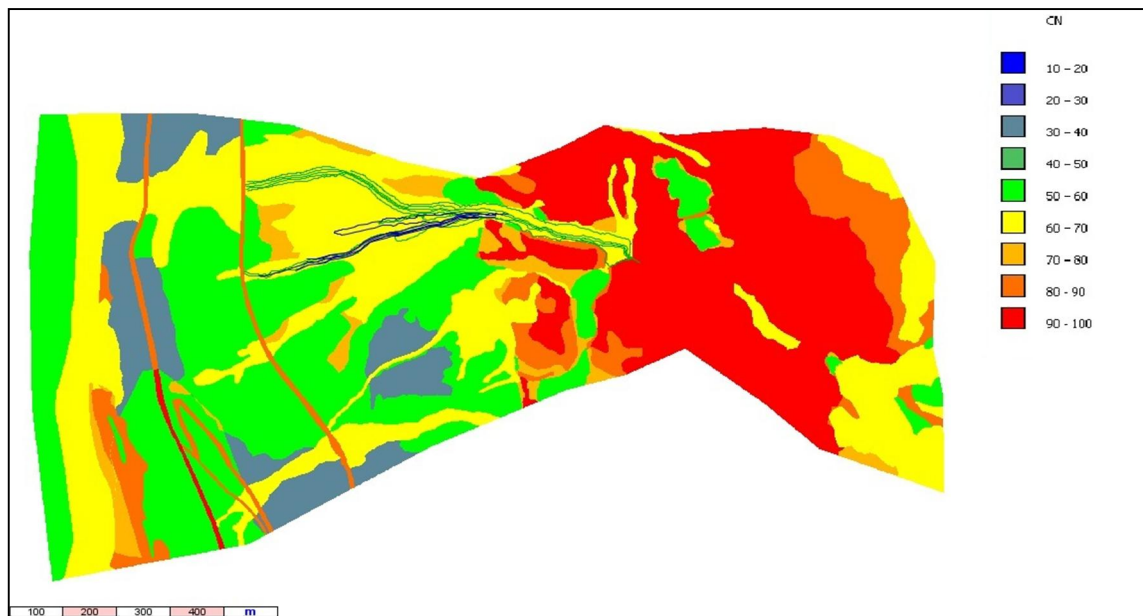


Figure 7.3 c08 Curve Number (CN) map.

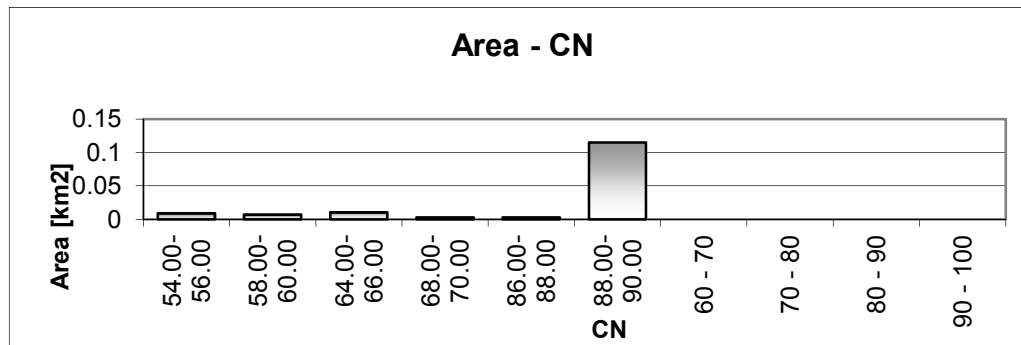


Figure 7.4 Area/CN class of the basin closing at the B section.

- The "Upslope area 1" tool gave the values of drainage area contributing to each cell (Figure 7.5) using, as default, the D8 algorithm to calculate the flow directions.

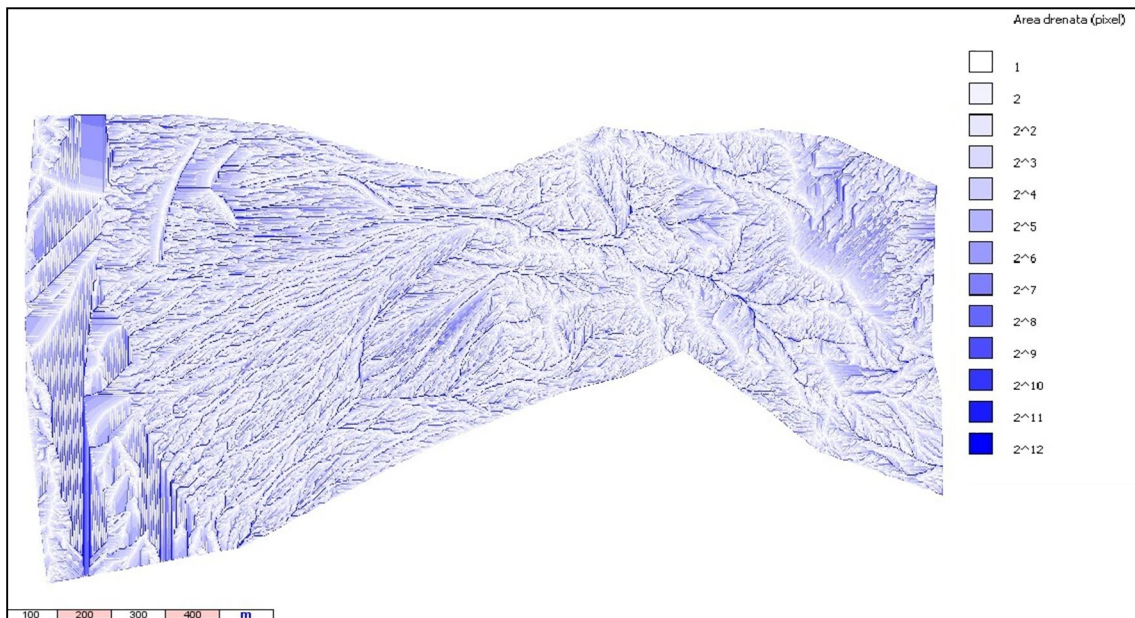


Figure 7.5 c08 upslope area 1.



5. The upslope area 1 raster map allowed to use the "Watershed" tool to extract the borders of the catchment draining water to the outlet, that has been set to coincide with the triggering section of the debris flow: as described in chapter 5.5, two distinct triggering sections have been individuated during the field surveys, one (B), lower, just before the channel exits the rocky cliffs, the other (A), 45 m higher in elevation, 87 m upstream. The watershed relative to both the two sections has been individuated (Figure 7.6 and Figure 7.7), allowing to identify the portion of the territory that contribute to the critical discharge for the triggering of the c08 debris flow.

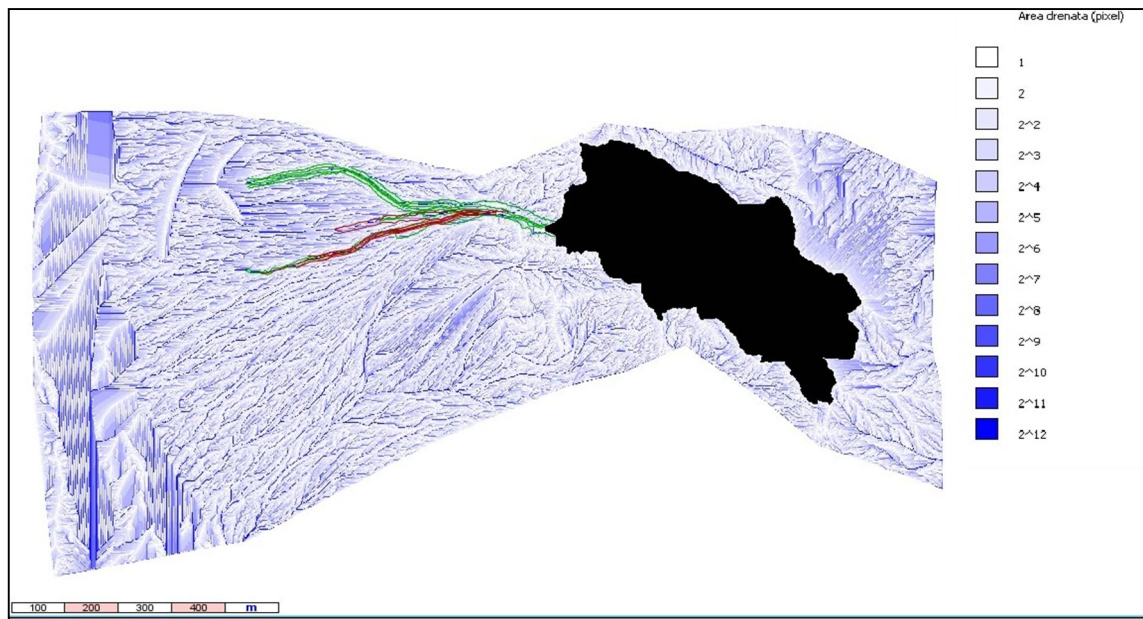


Figure 7.6 c08 watershed mask to the higher (A) outlet.

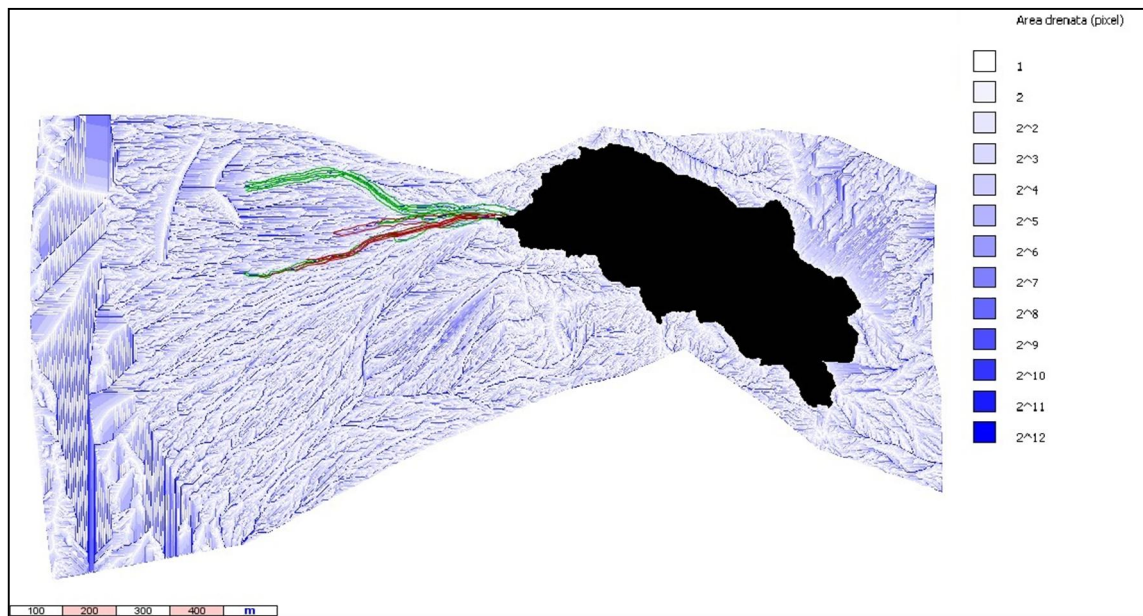


Figure 7.7 c08 watershed mask to the lower (B) outlet.

6. Through the "Upslope area 2" tool two sets of three raster maps have been produced, for the outlets A and B:
- the flow directions: from each cell choosing the D8 algorithm (selecting, among the 8 surrounding cells, the steepest slope direction);
  - the flow distances: it represents the distance in m from each cell, passing through the centre, to the outlet, according to the flow directions (Figure 7.9);
  - the "upslope area 2" (Figure 7.8) drainage area of the catchment relative to the outlet sections: in the output raster file each cell has an assigned value, corresponding to the number of pixels that constitute the drainage area upstream the cell itself. The counting is automatic and runs summing, along the flow directions, the number of pixels included between the cell originating the flow and the considered cell. The source cells will have, draining no pixels upstream,, a value of 1; the cell at the outlet section, draining the entire upstream area, will have a value corresponding to the entire number of cells.

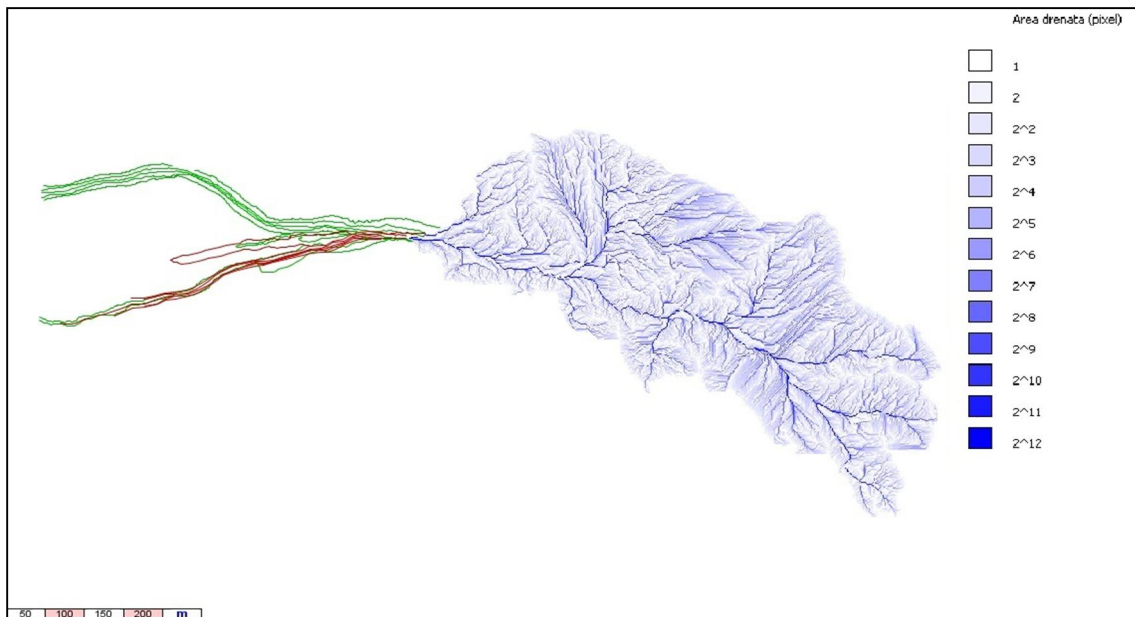


Figure 7.8 c08 upslope area 2, calculated with the D8 algorithm, for the B triggering section



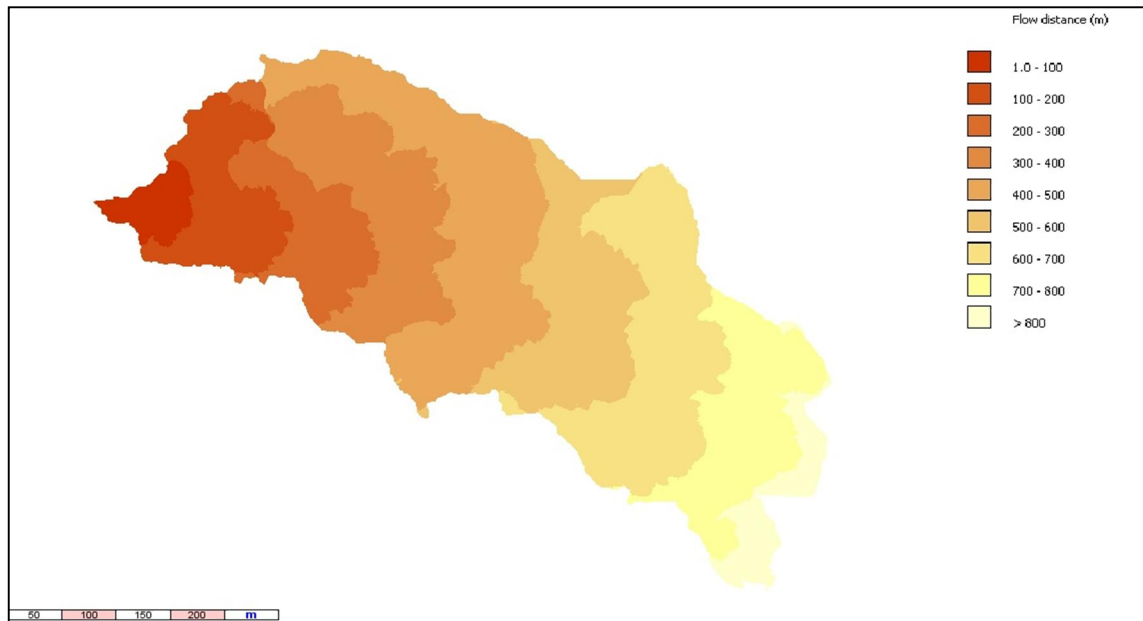


Figure 7.9 c08 flow distances map to the triggering section B.

7. The "Routing" tool has been routed using the just produced Flow direction, Upslope area 2 and Landcover raster maps, setting as threshold drainage area to individuate the network cells at 5000 m<sup>2</sup>, and providing the values of initial flow velocity on the network as 1.26 m/s for the outlet A case, 1.31 m/s for the outlet B case.

The tool provided as result two set of raster maps, concerning the two outlets:

- routing time son the hillslope;
- routing times on the network;
- flow velocities;
- network cells (Figure 7.10).

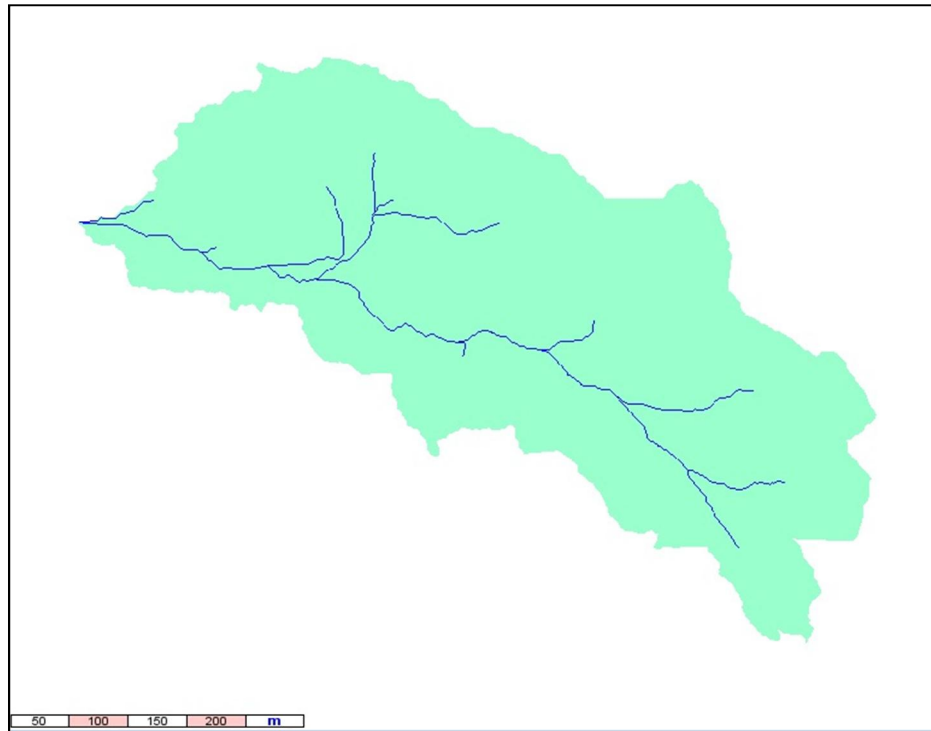


Figure 7.10 Synthetic drainage network individuated for the outlet section B, with a drainage threshold of 5000 m<sup>2</sup>. The network is coloured on blue, the hillslope in light blue.

8. The final step for building the runoff hydrograph required a set of input maps and parameters, and the rainfall data:

- the hillslope routing times: obtained through the "Routing" tool;
- the network routing times: obtained through the "Routing" tool;
- the CN map: obtained through the "CN" tool;
- the geometric characteristics of the outlet section, described in Table 7-1;
- the "advanced parameters" of the hyetograph and of the hydrological characteristics of the watershed, described in Table 7-2. Two simulations have been used: considering two different values of "Initial abstractions (IA)": 0.1 and 0.05S;
  - the file with the temporal distribution of the precipitation: the procedure by attempts to find the input that would have triggered the debris flow in the "Triggering model" imposed the necessity of testing different combinations of data: as reported in chapter 6.6.2, four different hyetographs have been used, the one provided directly by the rain-gauge and the three modified considering the effects of wind and rock cliffs, with an increases of 10, 20 and 30% in the quantiles of precipitation (called respectively mod+10%, mod+20%, mod+30%).

Initially four simulations have been carried out for each outlet section, considering the four hyetographs with a value of initial abstraction of 0.1, therefore eight runoff hydrographs have been produced and tested within the Triggering model. Since the results were not satisfying (the occurrence conditions for debris flow were not reached), two new hydrographs have been computed by considering the hyetograph mod+30% and initial abstractions of 0.05S, both for A and B outlet.

Hereafter is reported the hydrograph that gave the best results in terms of discharge (Table 7-3 and Figure 7.11), the one referred to the outlet section B, using the mod+30% hyetograph and with an initial abstraction value of 0.05S: the larger contributing area and the lower value of initial abstraction indeed provided for greater runoff and larger runoff excess, able to mobilize the 4450 m<sup>3</sup> of sediment of hypothesis 1 with the Triggering model.

Resuming, a total of ten combinations of parameters has been tested, the comparison of their main results is shown in Table 7-4.

To anticipate the computations of the next chapter, the triggering discharge resulted by the Debris Flow Hydrograph model, that should be reached by the input runoff discharge for enough time to mobilize the input sediment is:

- 0.381 m<sup>3</sup>/s for section A
- 0.496 m<sup>3</sup>/s for section B

Table 7-1 Geometric characteristics of the outlet sections

<b>Parameters</b>	<b>Used values: Section A</b>	<b>Used values: Section B</b>
Initial network velocity	1.58 m/s	1.65 m/s
Channel bed slope	42.7%	49%
Channel width	5.57 m	5.95 m
Right and left side slopes	0.66 right, 0.36 left	0.54 right, 2.01 left
Gauckler-Strickler roughness coefficient	9 m <sup>1/3</sup> /s	9 m <sup>1/3</sup> /s
Tolerance	0.04	0.04

Table 7-2 Advanced parameters of the hyetograph and the watershed

Parameters	Used values: Simulation 1	Used values: Simulation 2
Hyetograph shape	Alterned blocks	Alterned blocks
Peak position	0.75	0.75
Rain step	5 min	5 min
Out step	1 min	1 min
AMC	1, constant	1, constant
$Q_0$ - base flow	automatic	automatic
Recession Constant	$6 \cdot 10^6$	$6 \cdot 10^6$
Reduction factor	0.9	0.9
Initial abstractions (IA)	0.1S	0.05S
Max slope velocity	0.3 m/s	0.3 m/s

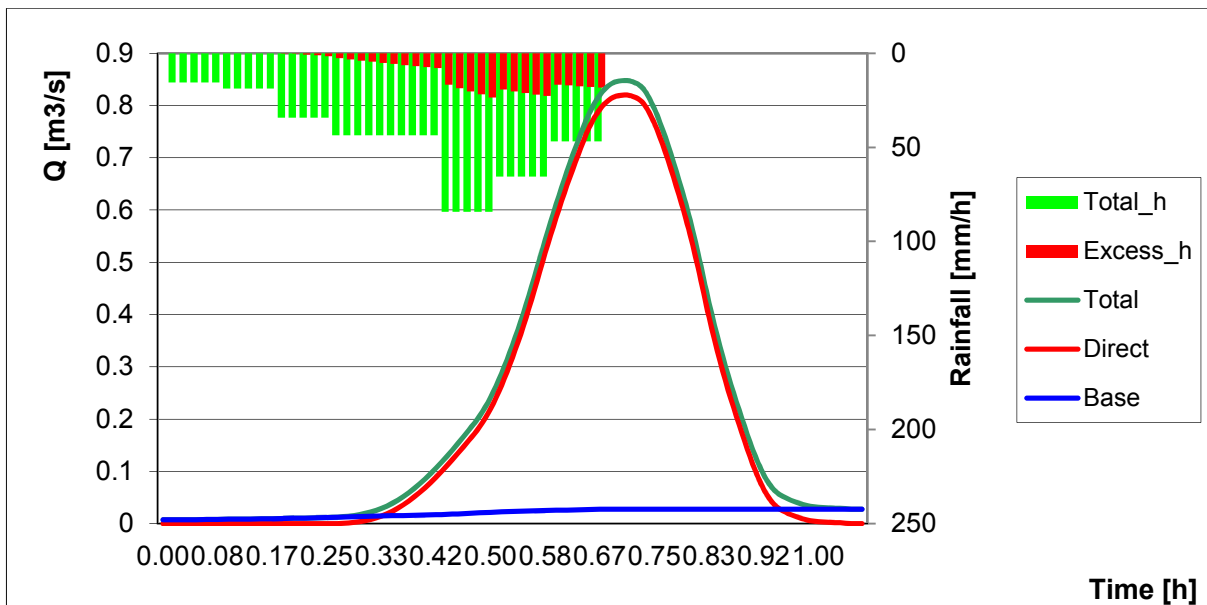


Figure 7.11 The runoff hydrograph of the 4th July event that has been used for the final simulation, referred to the outlet section B, using the mod+30% hyetograph and considering a constant value of initial abstraction of 0.05.

Table 7-3 Discharge and rainfall values for the entire duration of the simulated event of the 4<sup>th</sup> of July, referred to the outlet section B, using the mod+30% hyetograph and initial abstractions equal to 0.05S.

DISCHARGE AND RAINFALL								
Time (h)	Discharge m <sup>3</sup> /s			Precipitation mm				Storage
	Total	Direct	Base	Total	Excess	Total_h	Excess_h	
0.00	0.007	0	0.007	0	0	0	0	8.33311
0.02	0.007	0	0.007	0.26	0	15.6	0	8.59011
0.03	0.008	0	0.008	0.26	0	15.6	0	8.84701
0.05	0.008	0	0.008	0.26	0	15.6	0	9.10383
0.07	0.008	0	0.008	0.26	0	15.6	0	9.36055
0.08	0.008	0	0.008	0.26	0	15.6	0	9.61718
0.10	0.008	0	0.008	0.312	0	18.72	0	9.92572
0.12	0.009	0	0.009	0.312	0	18.72	0	10.23415
0.13	0.009	0	0.009	0.312	0	18.72	0	10.54246
0.15	0.009	0	0.009	0.312	0	18.72	0	10.85067
0.17	0.01	0	0.01	0.312	0	18.72	0	11.15876
0.18	0.01	0	0.01	0.572	6E-05	34.32	0.0036	11.72668
0.20	0.01	0	0.01	0.572	0.0047	34.32	0.2844	12.28972
0.22	0.011	0	0.011	0.572	0.0122	34.32	0.7296	12.84514
0.23	0.011	1E-05	0.011	0.572	0.0195	34.32	1.1694	13.39302
0.25	0.012	4E-05	0.012	0.572	0.0267	34.32	1.6002	13.93353
0.27	0.013	0.0004	0.012	0.728	0.0441	43.68	2.6448	14.61243
0.28	0.014	0.0016	0.013	0.728	0.0551	43.68	3.3066	15.28006
0.30	0.018	0.004	0.013	0.728	0.0658	43.68	3.9474	15.93677
0.32	0.022	0.0081	0.014	0.728	0.0762	43.68	4.5696	16.58288
0.33	0.029	0.0145	0.015	0.728	0.0862	43.68	5.1732	17.21869
0.35	0.039	0.0238	0.015	0.728	0.096	43.68	5.7576	17.84453
0.37	0.052	0.0361	0.016	0.728	0.1054	43.68	6.3264	18.46067
0.38	0.067	0.0511	0.016	0.728	0.1147	43.68	6.8796	19.06737
0.40	0.086	0.0688	0.017	0.728	0.1236	43.68	7.4148	19.66492
0.42	0.106	0.0891	0.017	0.728	0.1323	43.68	7.9368	20.25356
0.43	0.129	0.1112	0.018	1.404	0.2789	84.24	16.7364	21.37133
0.45	0.154	0.1348	0.019	1.404	0.3089	84.24	18.5358	22.45871
0.47	0.179	0.1592	0.02	1.404	0.3376	84.24	20.2542	23.51705
0.48	0.206	0.1855	0.021	1.404	0.3655	84.24	21.9276	24.54712
0.50	0.242	0.2201	0.022	1.404	0.392	84.24	23.5188	25.5503
0.52	0.287	0.2649	0.023	1.092	0.3226	65.52	19.3548	26.31053
0.53	0.341	0.3181	0.023	1.092	0.3376	65.52	20.2542	27.05548
0.55	0.402	0.3784	0.024	1.092	0.352	65.52	21.1212	27.78572
0.57	0.471	0.4465	0.024	1.092	0.3659	65.52	21.9552	28.5018
0.58	0.543	0.5183	0.025	1.092	0.3795	65.52	22.7712	29.20401
0.60	0.611	0.5852	0.026	0.78	0.2792	46.8	16.7538	29.69427
0.62	0.674	0.6479	0.026	0.78	0.2859	46.8	17.1552	30.17765
0.63	0.732	0.7055	0.027	0.78	0.2924	46.8	17.5428	30.6544
0.65	0.784	0.7568	0.027	0.78	0.2987	46.8	17.919	31.12472
0.67	0.82	0.7926	0.027	0.78	0.3048	46.8	18.2898	31.58869
0.68	0.841	0.8131	0.028	0	0	0	0	31.57731
0.70	0.847	0.8196	0.028	0	0	0	0	31.56595
0.72	0.845	0.8176	0.028	0	0	0	0	31.55458
0.73	0.831	0.8036	0.028	0	0	0	0	31.54322

0.75	0.794	0.7657	0.028	0	0	0	0	31.53187
0.77	0.739	0.711	0.028	0	0	0	0	31.52052
0.78	0.674	0.6459	0.028	0	0	0	0	31.50917
0.80	0.602	0.574	0.028	0	0	0	0	31.49783
0.82	0.517	0.4888	0.028	0	0	0	0	31.48649
0.83	0.422	0.3948	0.028	0	0	0	0	31.47515
0.85	0.339	0.3115	0.028	0	0	0	0	31.46382
0.87	0.266	0.2385	0.028	0	0	0	0	31.45249
0.88	0.202	0.1743	0.028	0	0	0	0	31.44117
0.90	0.142	0.1142	0.028	0	0	0	0	31.42985
0.92	0.094	0.0661	0.028	0	0	0	0	31.41854
0.93	0.064	0.0359	0.028	0	0	0	0	31.40723
0.95	0.05	0.022	0.028	0	0	0	0	31.39592
0.97	0.041	0.0134	0.028	0	0	0	0	31.38462
0.98	0.035	0.0069	0.028	0	0	0	0	31.37332
1.00	0.032	0.0039	0.028	0	0	0	0	31.36202
1.02	0.03	0.0024	0.028	0	0	0	0	31.35073
1.03	0.029	0.0018	0.028	0	0	0	0	31.33945
1.05	0.028	0.0003	0.028	0	0	0	0	31.32817
1.07	0.028	1E-05	0.028	0	0	0	0	31.31689

Table 7-4 Comparison of the simulation parameters and of the resumed results of the ten runoff hydrographs simulated to search for the best triggering conditions for hypothesis 1.

<b>Outlet A, normal rainfall, IA 0.1S</b>					
SIMULATION PARAMETERS			SIMULATED RUNOFF		
Base flow initial (m3/s)	0.007		Direct	Base	Total
Base flow recession	6	Rainfall (mm)	3.096	21.704	24.8
AMC	1	Initial discharge (m3/s)	0	0.007	0.007
Appearing CN	76.698	Maximum discharge (m3/s)	0.368	0.024	0.391
Watershed Area (km2)	0.135	Average discharge (m3/s)	0.079	0.014	0.016
Contributing area (%)	81.381	Time to peak (h)	0.72	1.10	0.72
<b>Outlet B, normal rainfall, IA 0.1S</b>					
SIMULATION PARAMETERS			SIMULATED RUNOFF		
Base flow initial (m3/s)	0.007		Direct	Base	Total
Base flow recession	6	Rainfall (mm)	3.051	21.749	24.8
AMC	1	Initial discharge (m3/s)	0	0.007	0.007
Appearing CN	76.537	Maximum discharge (m3/s)	0.394	0.026	0.42
Watershed Area (km2)	0.147	Average discharge (m3/s)	0.084	0.015	0.017
Contributing area (%)	80.295	Time to peak (h)	0.73	1.10	0.73
<b>Outlet A, rainfall mod+10%, IA 0.1S</b>					
SIMULATION PARAMETERS			SIMULATED RUNOFF		
Base flow initial (m3/s)	0.007		Direct	Base	Total
Base flow recession	6	Rainfall (mm)	3.115	21.745	24.86
AMC	1	Initial discharge (m3/s)	0	0.007	0.007
Appearing CN	76.695	Maximum discharge (m3/s)	0.457	0.024	0.481
Watershed Area (km2)	0.135	Average discharge (m3/s)	0.111	0.014	0.016
Contributing area (%)	81.381	Time to peak (h)	0.70	0.68	0.70
<b>Outlet B, rainfall mod+10%, IA 0.1S</b>					
SIMULATION PARAMETERS			SIMULATED RUNOFF		
Base flow initial (m3/s)	0.007		Direct	Base	Total
Base flow recession	6	Rainfall (mm)	3.07	21.791	24.86
AMC	1	Initial discharge (m3/s)	0	0.007	0.007
Appearing CN	76.534	Maximum discharge (m3/s)	0.49	0.026	0.517
Watershed Area (km2)	0.147	Average discharge (m3/s)	0.119	0.015	0.017
Contributing area (%)	80.295	Time to peak (h)	0.72	0.68	0.72

Outlet A, rainfall mod+20%, IA 0.1S					
SIMULATION PARAMETERS			SIMULATED RUNOFF		
Base flow initial (m3/s)	0.007		Direct	Base	Total
Base flow recession	6	Rainfall (mm)	3.84	23.281	27.12
AMC	1	Initial discharge (m3/s)	0	0.007	0.007
Appearing CN	76.519	Maximum discharge (m3/s)	0.552	0.025	0.578
Watershed Area (km2)	0.135	Average discharge (m3/s)	0.137	0.014	0.016
Contributing area (%)	83.363	Time to peak (h)	0.70	0.68	0.70
Outlet B, rainfall mod+20%, IA 0.1S					
SIMULATION PARAMETERS			SIMULATED RUNOFF		
Base flow initial (m3/s)	0.007		Direct	Base	Total
Base flow recession	6	Rainfall (mm)	3.783	23.337	27.12
AMC	1	Initial discharge (m3/s)	0	0.007	0.007
Appearing CN	76.343	Maximum discharge (m3/s)	0.591	0.028	0.619
Watershed Area (km2)	0.147	Average discharge (m3/s)	0.145	0.015	0.018
Contributing area (%)	82.226	Time to peak (h)	0.70	0.68	0.70
Outlet A, rainfall mod+30%, IA 0.1S					
SIMULATION PARAMETERS			SIMULATED RUNOFF		
Base flow initial (m3/s)	0.007		Direct	Base	Total
Base flow recession	6	Rainfall (mm)	5.946	23.434	29.38
AMC	1	Initial discharge (m3/s)	0	0.007	0.007
Appearing CN	75.562	Maximum discharge (m3/s)	0.635	0.026	0.66
Watershed Area (km2)	0.135	Average discharge (m3/s)	0.167	0.014	0.018
Contributing area (%)	100	Time to peak (h)	0.67	0.68	0.67
Outlet B, rainfall mod+30%, IA 0.1S					
SIMULATION PARAMETERS			SIMULATED RUNOFF		
Base flow initial (m3/s)	0.007		Direct	Base	Total
Base flow recession	6	Rainfall (mm)	4.62	24.759	29.38
AMC	1	Initial discharge (m3/s)	0	0.007	0.007
Appearing CN	76.354	Maximum discharge (m3/s)	0.648	0.027	0.674
Watershed Area (km2)	0.135	Average discharge (m3/s)	0.163	0.014	0.017
Contributing area (%)	83.363	Time to peak (h)	0.70	0.68	0.70



Outlet A, rainfall mod+30%, IA 0.05S					
SIMULATION PARAMETERS			SIMULATED RUNOFF		
Base flow initial (m3/s)	0.007		Direct	Base	Total
Base flow recession	6	Rainfall (mm)	5.946	23.434	29.38
AMC	1	Initial discharge (m3/s)	0	0.007	0.007
Appearing CN	75.562	Maximum discharge (m3/s)	0.635	0.026	0.66
Watershed Area (km2)	0.135	Average discharge (m3/s)	0.167	0.014	0.018
Contributing area (%)	100	Time to peak (h)	0.67	0.68	0.67
Outlet B, rainfall mod+30%, IA 0.05S					
SIMULATION PARAMETERS			SIMULATED RUNOFF		
Base flow initial (m3/s)	0.007		Direct	Base	Total
Base flow recession	6	Rainfall (mm)	5.864	23.516	29.38
AMC	1	Initial discharge (m3/s)	0	0.007	0.007
Appearing CN	75.319	Maximum discharge (m3/s)	0.82	0.028	0.847
Watershed Area (km2)	0.147	Average discharge (m3/s)	0.221	0.015	0.019
Contributing area (%)	100	Time to peak (h)	0.70	0.68	0.70

### 7.1.2. Hypothesis 2

The results of the Hydrological model for hypothesis 1 in the Triggering model were barely able to mobilize only 4700 cubic meters. Hence, the initiation of the movement of the debris flow with the hypothesis of 6700 cubic meters of deposited material had no way of being tested without introducing heavy abstractions in the parameters of the models.

In this case, the positive response of the Triggering model to the hydrograph input of the Hydrological model has been provided only using a false CN map with a constant distributed value of 91 (appearing CN 81), the precipitation mod+30% and with IA = 0.05S, against an average CN value on the true map, used in hypothesis 1, of 84 (appearing CN 75).

Due to this unreal forcing of the input, the final results have not been considered. Here are reported just for completeness (Table 7-5).

Table 7-5 The resumed results of the runoff hydrograph simulated to search for the best triggering conditions for hypothesis 2.

<b>Outlet B, CN91, rainfall mod+30%, IA 0.05S</b>					
SIMULATION PARAMETERS		SIMULATED RUNOFF			
Base flow initial (m3/s)	0.007		Direct	Base	Total
Base flow recession	6	Rainfall (mm)	8.079	21.301	29.38
AMC	1	Initial discharge (m3/s)	0	0.007	0.007
Appearing CN	80.94	Maximum discharge (m3/s)	1.091	0.026	1.117
Watershed Area (km2)	0.147	Average discharge (m3/s)	0.304	0.015	0.02
Contributing area (%)	100	Time to peak (h)	0.68	0.68	0.68

## 7.2. The triggering model

As in the previous simulations, the search for the parameters to simulate the debris flow event of the 4<sup>th</sup> of July 2011 that best fit with the measured field data took the necessity of producing a set of results to be tested. The aim of this procedure has been in particular to find the parameters able to simulate the quantity of deposited sediment found on the field with hypothesis 1 and 2, then to test their routing with the Automata model.

The output of the Triggering model has been tested considering:

- the outlet section: A or B;
- the hydrograph type: normal precipitation, mod+10%, mod+20%, mod+30%, mod+30% and IA 0.05S;
- average sediment size sampled in the triggering sections: 0.047 or 0.074 m (as founded by the grain size analysis of the sampled material, operated with the software Campion (Gregoretti, 2010));
- saturation discharge: 0.07 or 0.045 m<sup>2</sup>/s (as founded by Gregoretti and Dalla Fontana, 2008) ;
- the option of considering only the volume to be deposited or both the volume and its volumetric concentration.
- the shape of the solid-liquid hydrograph: since the distance between the outlet sections A,B and the points at which the starting of the deposition has been set vary from 35 to 120 m (respectively from outlet B and outlet from A), both the solid-liquid hydrograph shape QR1 and QR2 have been tested: QR1 applies to the hydrograph of a starting debris flow in the triggering section and in the first routing metres, QR2 refers to the shape of a well formed debris flow front, with a very steep rising limb and gentle declining limb.

### 7.2.1. Hypothesis 1

Among all the combinations of parameters regarding the hypothesis 1, two simulations resulted useful to trigger the movement of the input volume, differing only in the grain size diameter:

- the one using the mod+30% hydrograph at triggering section B, with IA of 0.05S, saturation discharge of  $0.045 \text{ m}^2/\text{s}$ , average grain size in the triggering section on  $0.047 \text{ m}$ , considering only the volume datum of  $4700 \text{ m}^3$  as input in the Triggering model: the mobilized volume resulted of 4700 cubic meters, exactly as the input. A successive simulation to test for the limit of volume entrainable by the provided hydrograph resulted with a threshold of 5000 cubic metres, a little more than for hypothesis 1, but much less than for hypothesis 2;
- the one using the mod+30% hydrograph at triggering section B, with IA of 0.05S, saturation discharge of  $0.045 \text{ m}^2/\text{s}$ , average grain size in the triggering section on  $0.074 \text{ m}$ , considering only the volume datum of  $4700 \text{ m}^3$  as input in the Triggering model: the mobilized volume resulted 4452 cubic meters, a little less than expected but in a range of acceptability.

Both of the results have been tested both with QR1 and QR2 solid-liquid hydrograph shape, bringing the number of successful triggering simulations to four, but this parameter resulted not influent on the values of output volumes. Nevertheless, all the four different outputs have been considered as input in the Automata model to test for the hydrograph shape influence in the routing phases.

The results of all the combinations for hypothesis 1 are resumed in Table 7-6 for outlet A and Table 7-7 for outlet B. Were the runoff has not been able to trigger the debris flow it has been indicated that the maximum discharge  $Q_{\text{max}}$  were inferior to the critical discharge  $Q_{\text{crit}}$ .

Table 7-6 Comparison of the simulation parameters and of the resumed results of the Triggering model for outlet A, searching for the input to be used in the Automata cell model for routing and deposition phases.

	outlet A				
	Precipitation file	Average sediment size (m)	saturation discharge (m <sup>2</sup> /s)	Volume (Vm <sup>3</sup> ) or Volume+sediment Concentration(Vm <sup>3</sup> C)	Simulated deposited sediment (m <sup>3</sup> )
Hyp 1	prec norm	0.047	0.07	V4700 C05012	Qmax < Qcrit
				V4700	Qmax < Qcrit
			0.045	V4700 C05012	Qmax < Qcrit
				V4700	Qmax < Qcrit
		0.074	0.07	V4700 C05012	Qmax < Qcrit
				V4700	Qmax < Qcrit
			0.045	V4700 C05012	Qmax < Qcrit
				V4700	Qmax < Qcrit
	prec mod+10%	0.047	0.07	V4700 C05012	Qmax < Qcrit
				V4700	Qmax < Qcrit
			0.045	V4700 C05012	844
				V4700	1646
		0.074	0.07	V4700 C05012	Qmax < Qcrit
				V4700	Qmax < Qcrit
			0.045	V4700 C05012	Qmax < Qcrit
				V4700	Qmax < Qcrit
	prec mod+20%	0.047	0.07	V4700 C05012	699
				V4700	1362
			0.045	V4700 C05012	1314
				V4700	2561
		0.074	0.07	V4700 C05012	Qmax < Qcrit
				V4700	Qmax < Qcrit
			0.045	V4700 C05012	853
				V4700	1663
	prec mod+30%	0.047	0.07	V4700 C05012	1340
				V4700	2610
			0.045	V4700 C05012	1740
				V4700	3391
		0.074	0.07	V4700 C05012	282
				V4700	549
			0.045	V4700 C05012	1361
				V4700	2652
	prec mod+30%, IA 0.05S mm/s	0.047	0.07	V4700 C05012	1387
				V4700	2702
			0.045	V4700 C05012	1953
				V4700	3805
		0.074	0.07	V4700 C05012	282
				V4700	549
			0.045	V4700 C05012	1415
				V4700	2757

Table 7-7 Comparison of the simulation parameters and of the resumed results of the Triggering model for outlet B, searching for the input to be used in the Automata cell model for routing and deposition phases.

	outlet B				
	Precipitation file	Average sediment size (m)	saturation discharge (m <sup>2</sup> /s)	Volume (Vm <sup>3</sup> ) or Volume+sediment Concentration(Vm <sup>3</sup> C)	Simulated deposited sediment (m <sup>3</sup> )
Hyp 1	prec norm	0.047	0.07	V4700 C05012	Qmax < Qcrit
				V4700	Qmax < Qcrit
			0.045	V4700 C05012	345
				V4700	672
		0.074	0.07	V4700 C05012	Qmax < Qcrit
				V4700	Qmax < Qcrit
			0.045	V4700 C05012	Qmax < Qcrit
				V4700	Qmax < Qcrit
	prec mod+10%	0.047	0.07	V4700 C05012	Qmax < Qcrit
				V4700	Qmax < Qcrit
			0.045	V4700 C05012	840
				V4700	1637
		0.074	0.07	V4700 C05012	Qmax < Qcrit
				V4700	Qmax < Qcrit
			0.045	V4700 C05012	Qmax < Qcrit
				V4700	Qmax < Qcrit
	prec mod+20%	0.047	0.07	V4700 C05012	1016
				V4700	1980
			0.045	V4700 C05012	1488
				V4700	2900
		0.074	0.07	V4700 C05012	Qmax < Qcrit
				V4700	Qmax < Qcrit
			0.045	V4700 C05012	1107
				V4700	2151
	prec mod+30%	0.047	0.07	V4700 C05012	1504
				V4700	2930
			0.045	V4700 C05012	1911
				V4700	3723
		0.074	0.07	V4700 C05012	972
				V4700	1895
			0.045	V4700 C05012	1247
				V4700	3263
	prec mod+30%, IA 0.05S	0.047	0.07	V4700 C05012	2240
				V4700	4364
			0.045	V4700 C05012	2592
				V4700	4700
		0.074	0.07	V4700 C05012	1196
				V4700	3760
			0.045	V4700 C05012	2285
				V4700	4452

### 7.2.2. Hypothesis 2

As mentioned before, the triggering of the debris flow with the hypothesis of 6700 cubic meters of deposited material has been recognized not possible with the set of parameters used for the hypothesis 1 (the maximum entrainable volume resulted 5000 m<sup>3</sup>), even if they have been pushed to the limits of plausibility founded by experimental data or in literature. Therefore, the triggering for hypothesis 2 has been obtained only introducing heavy abstractions in the parameters of the Hydrological model, in particular on the CN map. In addition, the 6700 cubic metres have been triggered only considering an average sediment size of 0.047 m and a saturation discharge 0,045 m<sup>2</sup>/s (inferior triggering conditions).

Due to this unreal forcing of the input, the final results have not been considered.

## 7.3. The event simulations with the Automata model

### 7.3.1. Hypothesis 1

As explained in chapter 7.2.1 a total of four solid-liquid hydrograph from the Triggering model simulations resulted able to mobilize the 4700 cubic metres of hypothesis 1. They have been used as input in the Automata model. They have been identified with a code for simplicity, as reported in Table 7-8.

Table 7-8 Parameters of the triggering hydrograph with the relative code

PARAMETERS OF THE TRIGGERING HYDROGRAPH	CODE
Triggering section B, precipitation mod+30%, IA 0.05S mm/s, average grain size diameter <b>0.074 m</b> , saturation discharge 0.045 m <sup>2</sup> /s, <b>QR2</b> , volume 4700 m <sup>3</sup>	alfa
Triggering section B, precipitation mod+30%, IA 0.05S mm/s, average grain size diameter <b>0.047 m</b> , saturation discharge 0.045 m <sup>2</sup> /s, <b>QR2</b> , volume 4700 m <sup>3</sup>	beta
Triggering section B, precipitation mod+30%, IA 0.05S mm/s, average grain size diameter <b>0.074 m</b> , saturation discharge 0.045 m <sup>2</sup> /s, <b>QR1</b> , volume 4700 m <sup>3</sup>	gamma
Triggering section B, precipitation mod+30%, IA 0.05S mm/s, average grain size diameter <b>0.047 m</b> , saturation discharge 0.045 m <sup>2</sup> /s, <b>QR1</b> , volume 4700 m <sup>3</sup>	delta

The options and the parameters for routing the Automata model explained in chapter 6.3.2 have been tested to model the debris flow event by giving the four results of the Triggering model. Some of them have been kept constant in all the simulations:

- the Courant number, constant to the minimum value of 0.5, to decrease oscillations, improve accuracy and decrease numerical dispersion;
- the ending simulation velocity, constant to 0.01 m/s, to be coherent with the magnitude classes proposed by the PAI methodology (chapter 6.3.2) whose first class inferior limit is set to 0.02 m/s;
- the dry sediment volumetric concentration, constant to 0.62, as resulted from experimental data on the material sampled on the field;

The effects of varying the other parameters have been tested with a set of consecutive simulations (sensitivity test):

- the duration in real time of the simulation: according to the duration of the solid-liquid hydrograph of the Triggering model;
- the Chezy a-dimensional relationship;
- the initiation angle;
- the number and the position of the input cells for the deposits: two different section of cells have been tested:
  - section A5, composed of 5 input cells, about 30 metres upstream the triggering area B. The location of the section A has been decided on the field, observing the presence of deposits considered belonging to the case study event. The number of cell has been chosen to cover the width of the channel;
  - section A8, in the same place of section A5 but composed of 8 cells. The number of cells have been chosen just to evaluate the influence of the number of input cells (the solid-liquid hydrograph, when routing in the Automata model, is partitioned in each of the input cells);
  - section B5, about 30 metres downstream the triggering area B, just where the measured deposits begin. The location of this input section has been decided on GIS, after analyzing the measured dataset and the output of the first simulations (the reason will be soon treated).

The pre-event DTM (see chapter 0) that should have been used as the digital surface on which to route the Automata model showed a problem in the first simulations: the sediment material obstructing the old channel was not working as a wall, and so not preventing the

simulated debris flow to route WWS as observed in the field. In order to have the possibility to compare the simulated area and volume with those measured, the pre-event DTM has been modified on GIS (Adb Toolbox > tools > hydraulic analysis > channel-bed analysis > modify raster values), increasing the height of the cells forming the obstruction. Many trials have been conducted to adjust the DTM, the working result is in Figure 7.12. Figure 7.12 Hillshade of the pre-event DTM, used for the Automata simulation, modified increasing the height of the cells forming the obstruction on the old debris flow channel: the black line represent the modified wall..

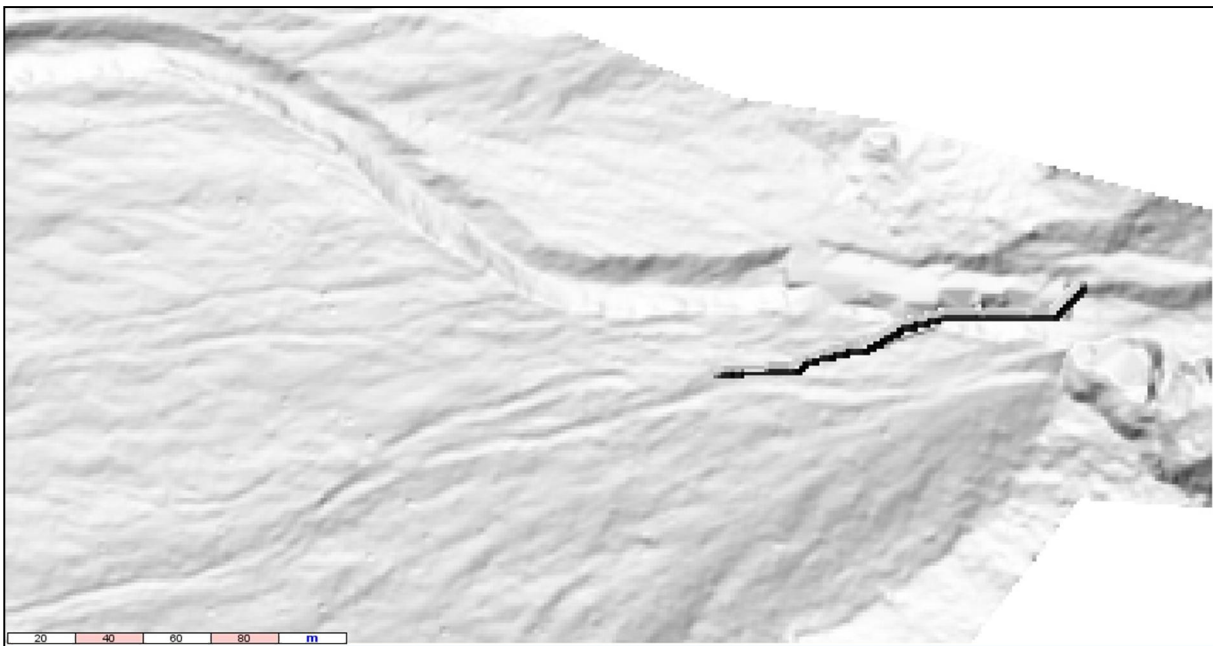


Figure 7.12 Hillshade of the pre-event DTM, used for the Automata simulation, modified increasing the height of the cells forming the obstruction on the old debris flow channel: the black line represent the modified wall.



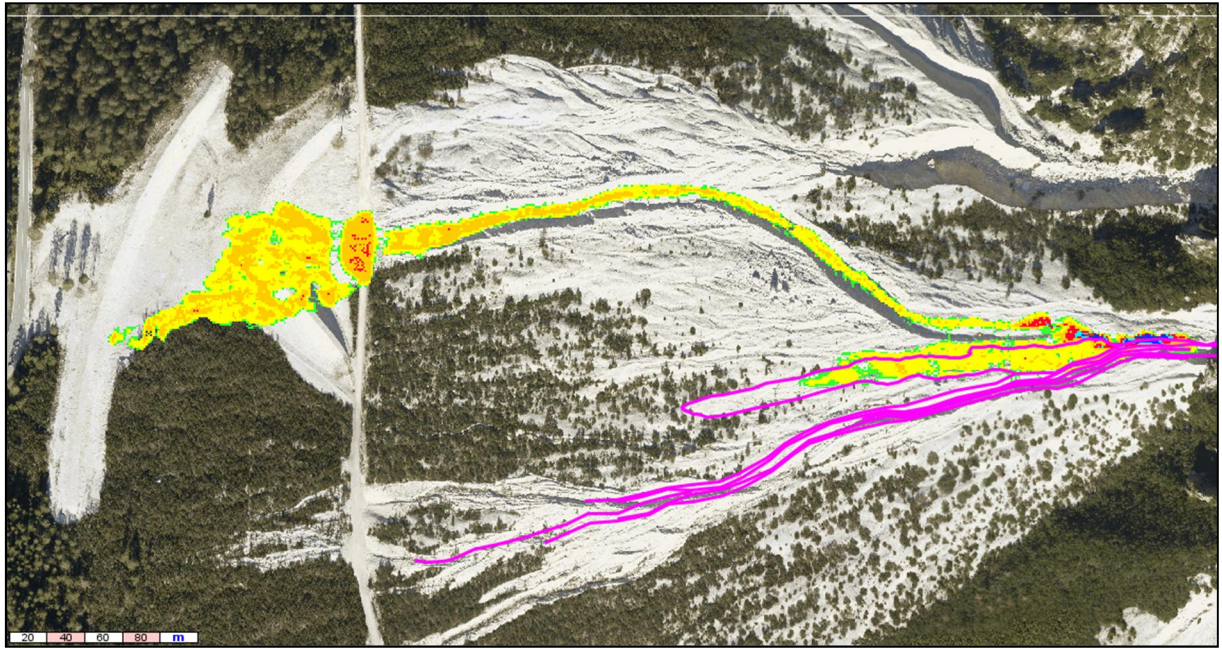


Figure 7.13 Outcome of the simulation with the parameters of sim 20 (see Table 7-11) using the not modified digital surface: to be observed that, being absent the fake wall of Figure 7.12, the model would allocate the major part of the sediment material on the old channel, compromising the result. The routing zones of the 4<sup>th</sup> July event are coloured in purple.

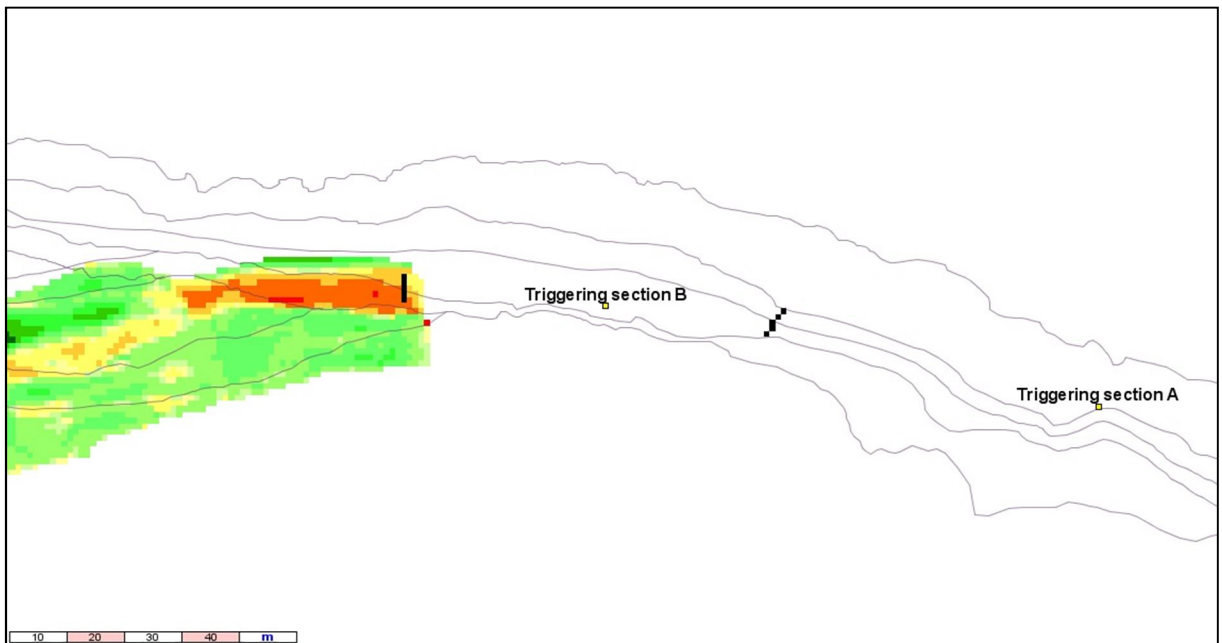


Figure 7.14 Disposition of the triggering sections A and B used to calculate the solid-liquid hydrograph and of the input section for the deposition phases with the Automata model, input section A5 and B5. Input section A8 is located in the same place of section A5. The first measured deposits are coloured on the left side.

A set of simulations (sim) with changing parameters has been conducted to find the best ones. A resume of the simulations and the relative parameters is shown in the following Tables: Table 7-9, Table 7-10, Table 7-11. The quality of each simulation has been preliminary evaluated through a rough visual comparison, on GIS, of the output sediment

deposition depth raster map with the map of the deposits measured on the field. The first element to evaluate the kindness of the simulation was the distribution of the deposits, considering both area and depth distributions. This comparison has been made possible adopting the same depth classes and colour model for the maps to be compared.

Initially only one input triggering hydrograph (alfa) has been used, in order to take confidence with the parameters and observe their influence on the results. Once in the range of goodness, also the other three hydrographs have been tested.

The model works with a constant Chezy roughness coefficient on the whole area: for the case study area it should be equal to 2 (as suggested by Gregoretti, 2000) but also values of 1 and 3 have been tested.

Great importance has been discovered for the location of the input sections: with the A8 and A5 cells a large portion of the simulated volume stopped too high in elevation, out of the range of the measured deposits. The input section B5, so, has been chosen as the best for this case study. Even if the number of input cells play an important role on the total discharge passing through them (the triggering hydrograph is automatically partitioned on each of the cells), the difference in the range of those considered (5 and 8) has been observed as not influent.

The duration of the simulation has been progressively increased from 3200 to 3900 seconds to avoid still flowing material at its end, but too high simulation time required also very long processing times on the computer, so they have been adjusted to 3500-3600 seconds.

The initiation angle has been found playing an important role in the spatial distribution of the simulated deposits, especially in combination with the grain size diameter: in general, input files with lower average grain size required lower initiation angles (because of a greater triggering hydrograph): the final simulations regarding the lower sediment size (29 and 31) are best routed with an initiation angle of  $47^\circ$ , while the simulations regarding the higher sediment size (28 and 30) are best routed with an initiation angle of  $48^\circ$ .

The shape of the input triggering hydrograph did not influenced the two simulations regarding the lower sediment size (29 and 31), while it was influencing the dispersion of sediment in the simulations regarding the higher sediment size (28 and 30): the simulation routed with QR2 (sim28) indeed, have less sediment deposited in the very initial part of the simulated deposition area. According to this observation seems that a well developed solid-liquid hydrograph shape, in a range of average grain size diameter around that used (0,074 m in this case), disperse more the sediment volume than a still developing debris flow front.

Table 7-12 contains the four simulations, with the relative parameters, that best fit with measured data at the rough visual analysis.

Table 7-9 Simulations 1-9 with the relative parameters.

Parameter	Sim1	Sim2	Sim3	Sim4	Sim5	Sim6	Sim7	Sim8	Sim9
<b>Triggering hydrograph</b>	alfa	alfa	alfa	alfa	alfa	alfa	alfa	alfa	alfa
<b>Sim time (s)</b>	3200	3200	3200	3200	3200	3400	3400	3400	3400
<b>Input cells</b>	A8	A8	A8	A8	A8	A8	A8	A8	A8
<b>Chezy rel.</b>	1	1	1	1	1	2	2	2	2
<b>Initiation angle (°)</b>	35	40	45	47	50	35	40	45	50

Table 7-10 Simulations 10-18 with the relative parameters.

Parameter	Sim10	Sim11	Sim12	Sim13	Sim14	Sim15	Sim16	Sim17	Sim18
<b>Triggering hydrograph</b>	alfa	alfa	alfa	alfa	alfa	alfa	alfa	alfa	alfa
<b>Sim time (s)</b>	3400	3400	3400	3400	3400	3400	3900	3900	3900
<b>Input cells</b>	A8	A8	A8	A8	A5	B5	A8	A8	B5
<b>Chezy rel.</b>	2	2	2	2	2	2	2	2	2
<b>Initiation angle (°)</b>	46	47	48	49	45	46	46	47	46

Table 7-11 Simulations 19-27 with the relative parameters.

Parameter	Sim19	Sim20	Sim21	Sim22	Sim23	Sim24	Sim25	Sim26	Sim27
<b>Triggering hydrograph</b>	alfa	alfa	beta	beta	beta	gamma	gamma	beta	delta
<b>Sim time (s)</b>	3900	3500	3500	3500	3500	3500	3500	3500	3500
<b>Input cells</b>	B5	B5	B5	B5	B5	B5	B5	B5	B5
<b>Chezy rel.</b>	2	2	2	2	2	2	2	2	2
<b>Initiation angle (°)</b>	47	48	50	47	45	48	46	48	46

Table 7-12 Final simulations 28-31, with the best parameters for the four triggering hydrographs.

Parameter	Sim28	Sim29	Sim30	Sim31
Triggering hydrograph	alfa	beta	gamma	delta
Sim time (s)	3500	3600	3500	3600
Input cells	B5	B5	B5	B5
Chezy rel.	2	2	2	2
Initiation angle (°)	48	47	48	47

The output raster maps of the final step of the four simulated debris deposition depths have been reported. As emerges from the visual comparison of the maps in Figure 7.15 and Figure 7.16, the measured deposits with a depth higher than 1 m (indicated by black arrows in Figure 7.15) are more distributed on the surface, in zones characterized by a less steep slope; the simulated deposits higher than 1 m (indicated by black arrows in Figure 7.16) are instead concentrated upstream, just after the input cells used to route Automata model.

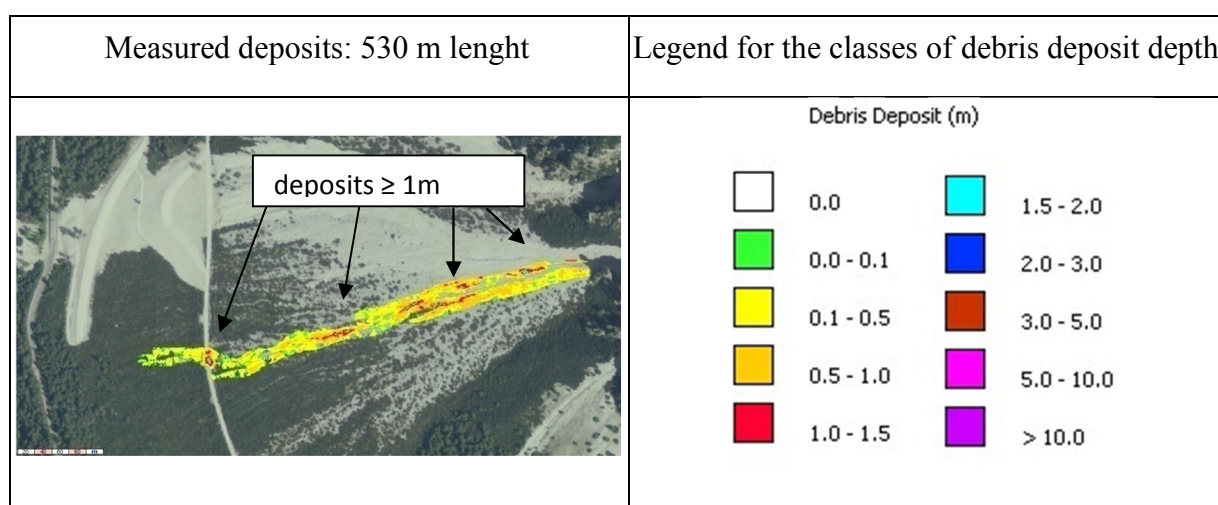


Figure 7.15 Raster map of the measured deposits (with the deduction factor, see chapter 0) used as comparison with the output of the simulations. On the right the legend used for the classes of debris deposit depth is indicated.



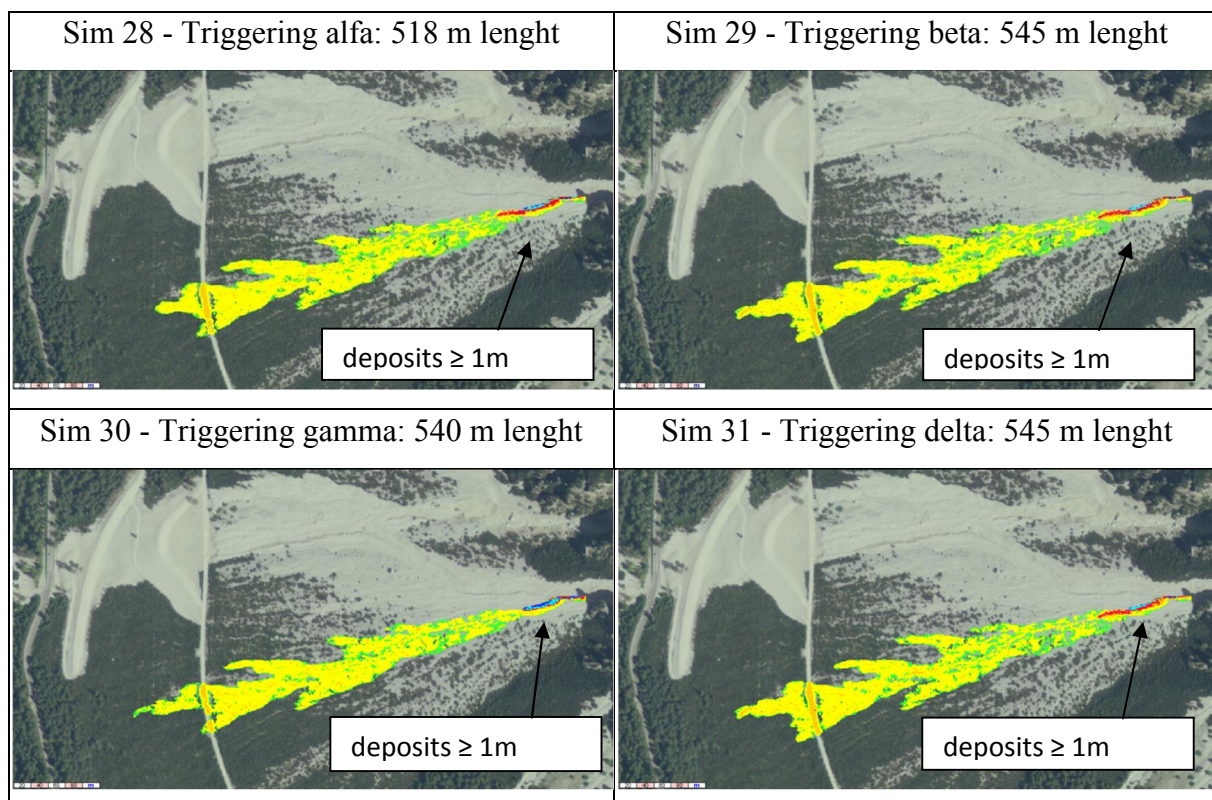


Figure 7.16 The raster maps of the last step simulations of the four calculated are compared (indicating also the debris flow hydrograph that generated them: alfa, beta, gamma, delta) .

The following steps, after the visual analysis, has been to compare analytically the measured deposition depths with the simulated deposition depths. The comparison has been made with the tool "Confronta\_depotiti" (translated: Deposit\_Comparison) elaborated by Gregoretti (2012).

The tool compares the simulated and the measured deposit depths. First it compares the measured area ( $B [X,Z]$  in Figure 7.17) and the simulated area ( $B [X,Y]$  in Figure 7.17) and the corresponding volumes, Then it splits the measured depths in classes and one by one it compares both the area and the volume with the corresponding simulated. As output are produced a text file with the results (the indexes  $\alpha$ ,  $\beta$ ,  $\gamma$ ,  $\epsilon$ ,  $\Omega$  of Scheidl and Rickenmann (2010) and the index F-Fit% of Bates and De Roo (2000)) of predicted deposition and non-deposition zones and volumes, resumed in Table 7-14).

Also four raster maps are provided:

- map of the measured deposits in the defined classes;
- map of the simulated deposits in the defined classes
- map of the overlap. It shows:

- the overlapping area of measured and simulated deposits, with correctly simulated (deposition depth in the same class);
- the overlapping area of measured and simulated deposits, with volumes not correctly simulated (volume > 0 but deposition depth not in the same class as measured);
- the areas with deposits measured but not simulated;
- the areas with deposit simulated but not measured.
- map of the correct overlap. It shows only:
  - the overlapping area of measured and simulated deposits, with volumes (per classes) correctly simulated;
  - the overlapping area of measured and simulated deposits, with volumes (per classes) not correctly simulated (volume > 0 but not in the same class as measured);

Four classes of deposit depths (m) have been considered (taking into account that 2.4 m was the higher measured deposit value and 4.5 m the higher simulated deposit value) :

class 1: 0 - 0.5m; class 2: 0.5 - 1m; class 3: 1 - 1.5m; class 4: 1.5 - 4.5m.

The calculated results regarding the total area and total volume compared, for the four simulations, are described in Table 7-13. The percentages are always referred to the measured area and volume. The percentage of area with both measured deposits and simulated deposits (not considering the depths) shows a very good overlap, lining up to 76-77% for all four final simulations, and with the best result of sim 28 (77.7%). Regarding the total measured volume, the 76-79% is located in this area correctly simulated, with the best result of sim 28 (78,9%), while the 39-43% of simulated volume lays in the same area, with the best result of sim 30 (43.3%).

The used F index (Fit%) is equal to:

$$F = \frac{Area_{measured} \cap Area_{modeled}}{Area_{measured} \cup Area_{modeled}} * 100 \quad (7.1)$$

and is equal to 100% when the two areas coincide, while it penalises over- and under-prediction of the area by the model. For the four simulations it ranges between 76 and 77% on the overall measured area, and 34% on the measured area correctly simulated by deposition depths.

The used evaluation factor  $\Omega$  is value describing the overall accuracy of the simulated events, (calculated as  $\Omega = \alpha - \beta - \gamma + \epsilon$ , with  $2 \leq \Omega \leq 2$ ). The best fit simulation is characterized by  $\Omega = 2$ , then the simulated deposition pattern equals the observed deposition

pattern. On the contrary, a value of  $\Omega = -2$  implies no overlap-ping between the simulated and the observed deposition area. The values of  $\Omega$  in the four simulations range between -0.271 and -0.074, indicating an overall medium-low correspondence between measured and simulated deposit.

In Table 7-15 the results are resumed per classes. The classes allows to understand which are the deposition depth that have been best simulated. Considering the comparison among depth classes, the 46-47% of the total measured deposition area has been correctly simulated with matching classes, with the best result of sim 28 (47.2%): into the specific, the 45.7-46% only within the first class (0 - 0.5 m of depth), and the remaining 0.9-1.2% in the second class (0.5 - 1 m of depth); higher deposit depths have not been correctly simulated. The 21-22% of total simulated volumes resulted in the same depth class as measured deposits, with the best result of sim 30 (22.8%): into the specific, the 19.7-21.7% only within the first class (0 - 0.5 m of depth), and the remaining 1.1-1.8% in the second class (0.5 - 1 m of depth); higher deposit depths have not been correctly simulated. In the first class the 71-72% of the area and the 57-63% of the volume have been correctly simulated, among the four simulations. The first class with the greater area correctly simulated is that one of sim 28 (72.6%), while that with the greater volume correctly simulated refers to sim 30 (63.7%).

The F index has also been calculated in each depth class, with a positive result of 0.508-0.512 in the first class among the four simulations.

Table 7-13 Statistics on the comparison of total area and total volume among the simulated deposits and the measured deposits, with the results of the four final simulations 28, 29, 30 and 31.

simulation		28-alfa	29-beta	30-gamma	31-delta
area corresponding to the measured deposits		10631	10631	10631	10631
area corresponding to the simulated deposits		18411	19313	17554	19313
volume of measured deposits		4700.28	4700.28	4700.28	4700.28
volume of the simulated deposits		4441.089	4675.86	4454.615	4675.86
volume of the simulated deposits in the measured area		1925.572	1853.053	2036.803	1853.053
percentage of area with measured deposits and simulated deposits		77.735	76.032	77.265	76.032
percentage of area with measured deposits and no simulated deposits		22.265	23.968	22.735	23.968
percentage of area with no measured deposits and simulated deposits		95.447	105.634	87.856	105.634
percentage of measured volumes respect to the measured volume in the area correctly simulated		78.911	76.3	78.476	76.3
percentage of simulated volumes respect to the measured volume in the area correctly simulated		40.967	39.424	43.334	39.424
percentage of measured deposition area correctly simulated		47.183	46.919	46.562	46.919
percentage of measured deposition volume correctly simulated		22.198	21.538	22.874	21.538
percentage of simulated deposition area with depths out of the range of those measured		0	0	0	0
percentage of simulated deposition volume with depths out of the range of those measured		0	0	0	0
Global F index (correctly predicted)		0.344	0.341	0.343	0.341
Global F index (overall deposition)		0.777	0.760	0.773	0.760
Indexes of Scheidl and Rickenman (2010)	positive area prediction accuracy $\alpha$	0.777	0.760	0.773	0.760
	negative area prediction accuracy $\beta$	0.954	1.056	0.879	1.056
	non-area prediction accuracy $\gamma$	0.223	0.240	0.227	0.240
	volume prediction accuracy $\epsilon$	0.266	0.265	0.259	0.265
	evaluation factor $\omega$ (overall deposition)	-0.134	-0.271	-0.074	-0.271



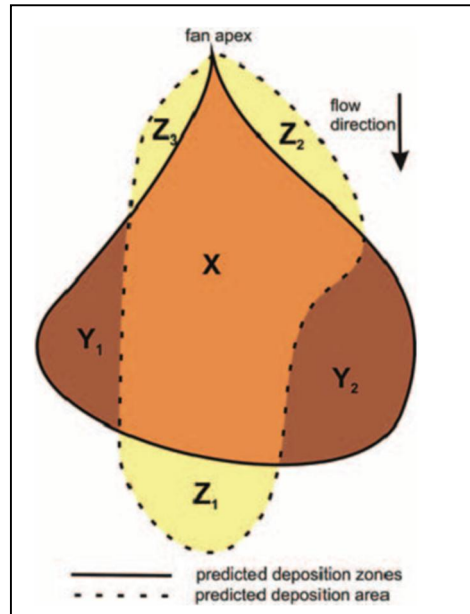


Figure 7.17 Subareas (X, Y, Z) comparing predictive hazard zones with mapped hazard zones on a schematic debris-flow fan.

Table 7-14 Accuracy matrix of evaluation concept with  $B_{\lambda} = \sum_{i=1}^{n\lambda} \lambda_i$ ,  $\lambda[X,Y,Z]$ , as founded in Scheidl and Rickenmann (2010).

	Predicted deposition zones		Non-predicted deposition zones	
	Area	Volume	Area	Volume
Observed deposition area	Positive accuracy (X) $\alpha = \frac{B_X}{B_{\text{observed}}}$	Positive accuracy (X) $\varepsilon = \frac{V_{BX}}{V_{\text{observed}}}$	Missing (non) accuracy (Z) $\gamma = \frac{B_Z}{B_{\text{observed}}}$	Missing (non) accuracy (Z) $\phi = \frac{V_{BZ}}{V_{\text{observed}}} = 1 - \varepsilon$
Non-deposition area	Negative accuracy (Y) $\beta = \frac{B_Y}{B_{\text{observed}}}$	Negative accuracy (Y) $\phi = \frac{V_{BY}}{V_{\text{observed}}} = 1 - \varepsilon$	—	—

Table 7-15 Statistics on the comparison of area and volume per classes among the simulated deposits and the measured deposits, with the results of the four final simulations 28, 29, 30 and 31. The F index is indicated on the first column on the right.

percentage of correctly simulated area and volume for each class respect to the class and the total					
sim28 - alfa					
Depth classes	Area-class	Volume-class	Area/total	Volume/total	Index F of Bates and De Roo (2000)
0 <h< 0.5	72.586	60.632	46.101	20.693	0.508
0.5 <h< 1	3.614	3.174	1.082	1.504	0.030
1 <h< 1.5	0	0	0	0	0
1.5 <h< 4.5	0	0	0	0	0
sim29 - beta					
Depth classes	Area-class	Volume-class	Area/total	Volume/total	Index F of Bates and De Roo (2000)
0 <h< 0.5	71.919	57.802	45.678	19.727	0.512
0.5 <h< 1	4.148	3.82	1.242	1.81	0.032
1 <h< 1.5	0	0	0	0	0
1.5 <h< 4.5	0	0	0	0	0
sim30 - gamma					
Depth classes	Area-class	Volume-class	Area/total	Volume/total	Index F of Bates and De Roo (2000)
0 <h< 0.5	71.934	63.664	45.687	21.728	0.502
0.5 <h< 1	2.923	2.418	0.875	1.146	0.025
1 <h< 1.5	0	0	0	0	0
1.5 <h< 4.5	0	0	0	0	0
sim31 - delta					
Depth classes	Area-class	Volume-class	Area/total	Volume/total	Index F of Bates and De Roo (2000)
0 <h< 0.5	71.919	57.802	45.678	19.727	0.512
0.5 <h< 1	4.148	3.82	1.242	1.81	0.032
1 <h< 1.5	0	0	0	0	0
1.5 <h< 4.5	0	0	0	0	0

The tool "Confronta Depositi" that compared the results of the four final simulations with the measured deposits, provided the maps of the correct overlapping (Figure 7.18). It shows:

- the areas correctly simulated (whose measured deposits fell within the same class as measured ones): these are almost all located in the zones in which the measured deposits resulted in the first class of depth (0 - 0.5 m);
- the area not correctly simulated (whose simulated deposits are  $> 0$  but not in the same class as measured ones): these refer to the measured depths laying sparse on the debris flow deposition area, where a decrease of slope or of flow velocity allowed for thick layer to stop; the model was not able to simulate these features since all their major deposits are located within the first hundreds of meters (of the total 550 m of the simulated debris flow);
- the area with measured but not simulated deposits: these are mainly located outside the banks in very initial parts of survey, where the model was not able to generate avulsion. These deposits indeed were not simulated because the input cells chosen to start the simulation have been set very close to the first measured deposits;
- the areas with simulated but non measured deposits: these are mainly simulated lateral avulsion, or the zones within the channel in which erosion has been measured (the model cannot simulate erosion).

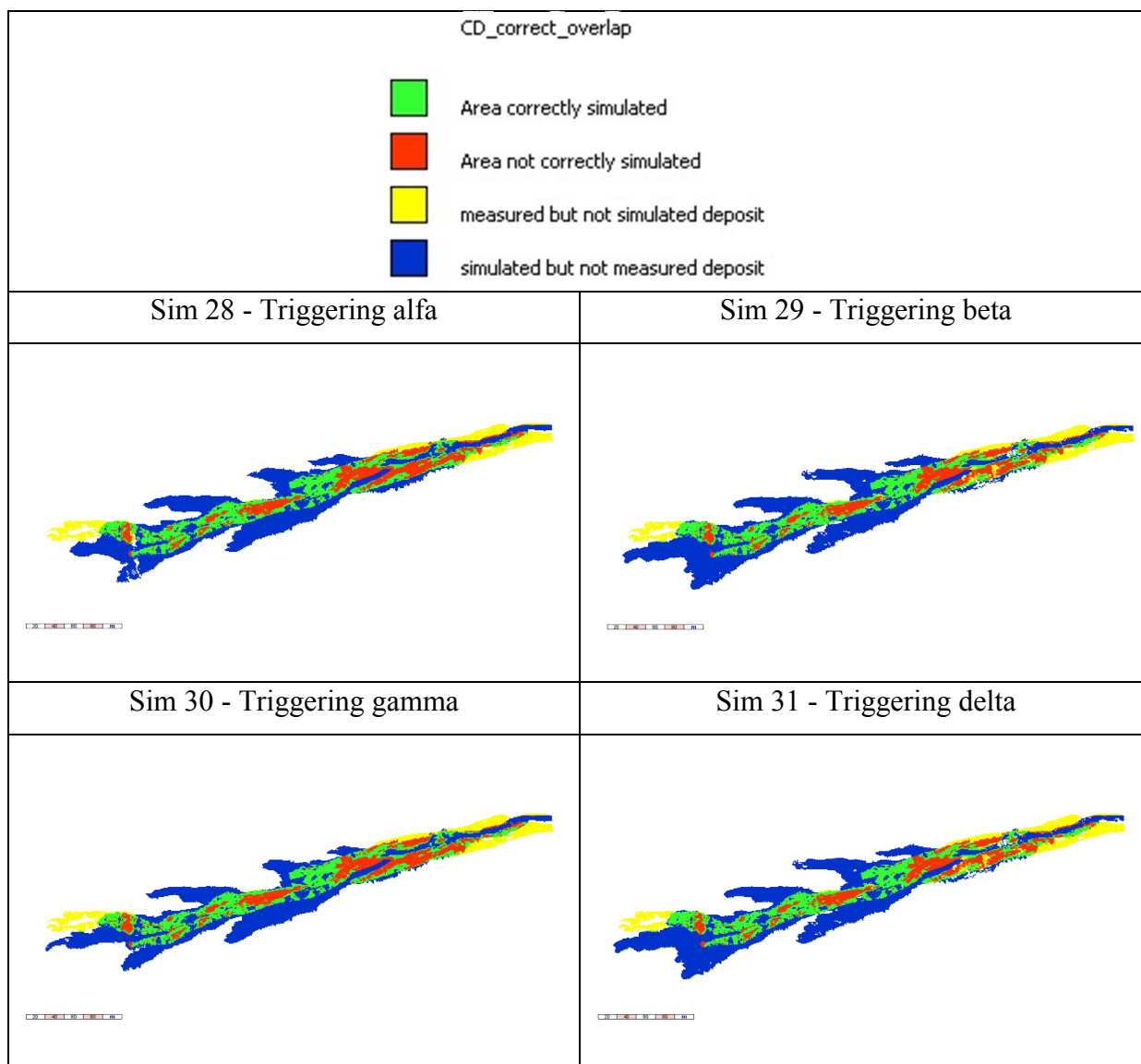


Figure 7.18 Output maps of the tool "Confronta Depositi" that compared the results of the four final simulations with the measured deposits.

The Figure 7.19 shows the four final raster maps of the maximum simulated flow velocities, whose value have been used, with the maximum values of flow depth, to build the magnitudo matrices. Higher velocities are simulated in the initial routing phases and spatially along the central channel.

Since the velocity of the phenomenon is always in the third class, the output magnitudo classes (maps reported in Figure 7.20) resulted as follows:

Debris flow Magnitudo		Velocity class
		3
Geometric severity class	3	9
	2	6
	1	3

The magnitudo estimation may not have a big importance for a little localized debris flow like that of the simulation, but when dealing with storm events characterized by a larger return time, able to mobilize many thousands of cubic metres of sediment (and the c08 channel show the evidence that such kind of events already interested its area), the mapping of the estimated magnitudo could gain great importance when projecting defensive structures, like the detention basin now in place. Even greater importance could be given to hazard mapping if considering the actual scenario and the possible future ones: observing Figure 7.21 it is clear that the last debris flows (other two events occurred after that one of the 4<sup>th</sup> of July) proceeded in the same WWS direction, following the steepest slope path, bypassing on the left the detention basin and pointing unstopped at the SS 51 road.

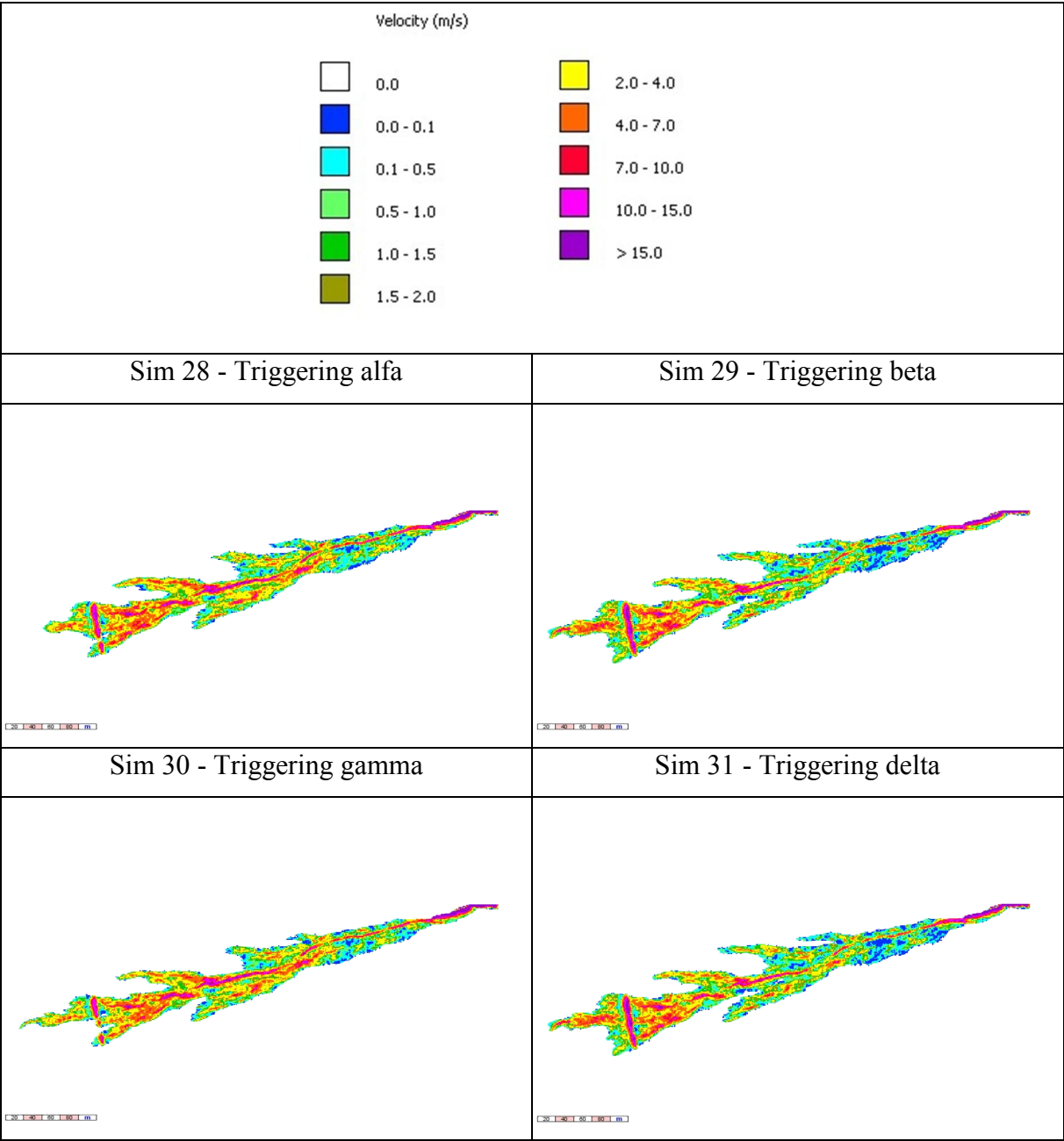


Figure 7.19 Raster map of the maximum simulated flow velocity. The legend for the classes of velocity is provided.

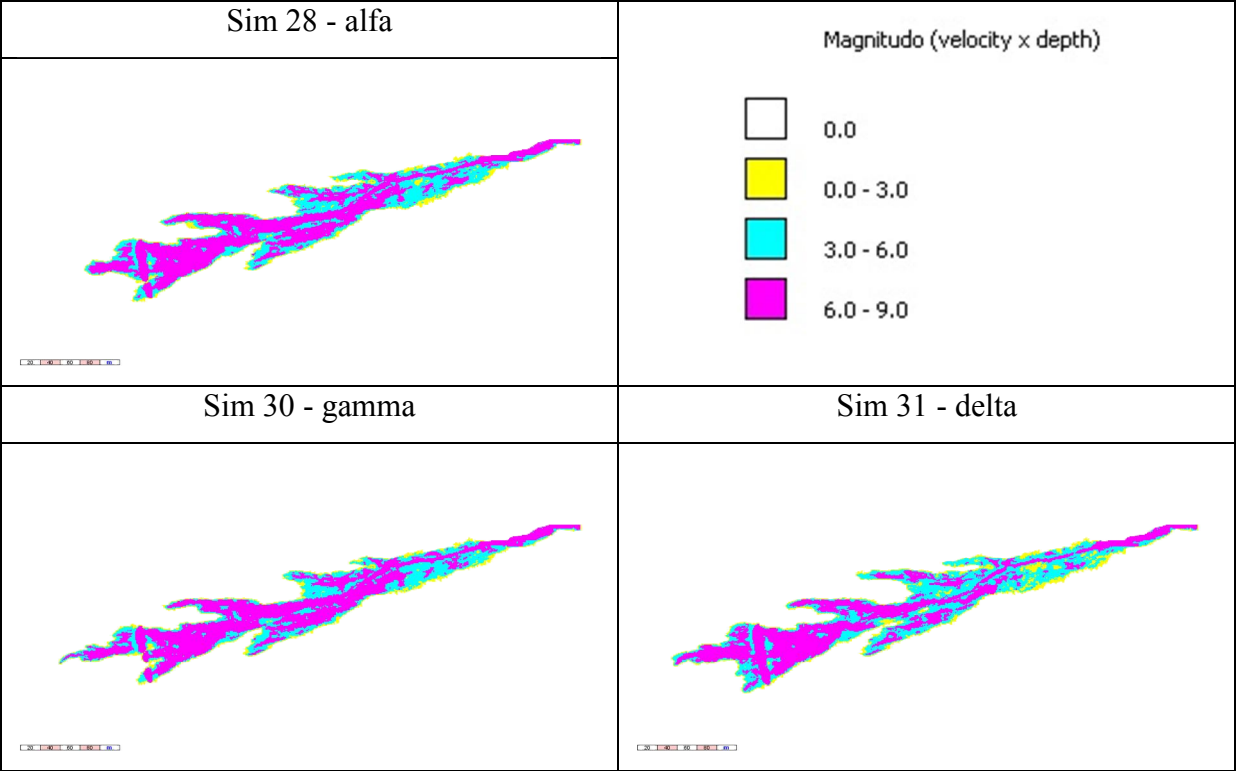


Figure 7.20 Magnitudo classes calculate by the Automata model.

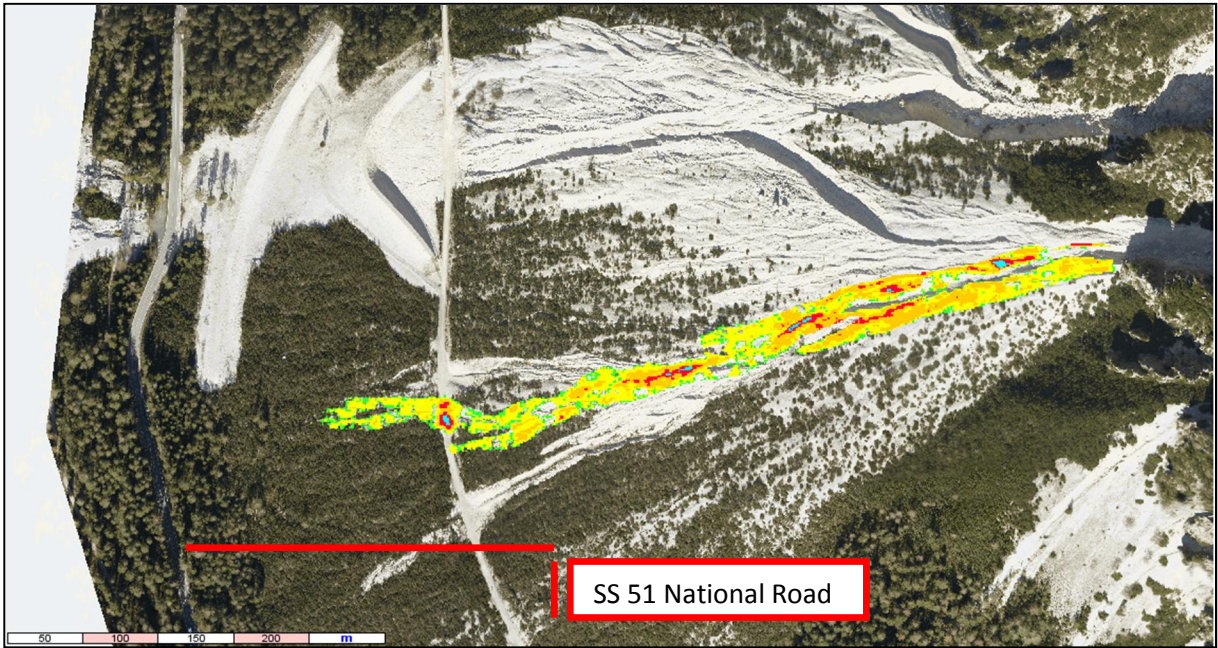


Figure 7.21 Actual scenario of the c08 debris flow channel

Each simulation provides for each desired time step to check for its evolution: here in Figure 7.22 are reported as an example the output maps representing the depth of debris deposits every 75seconds for simulation 28.

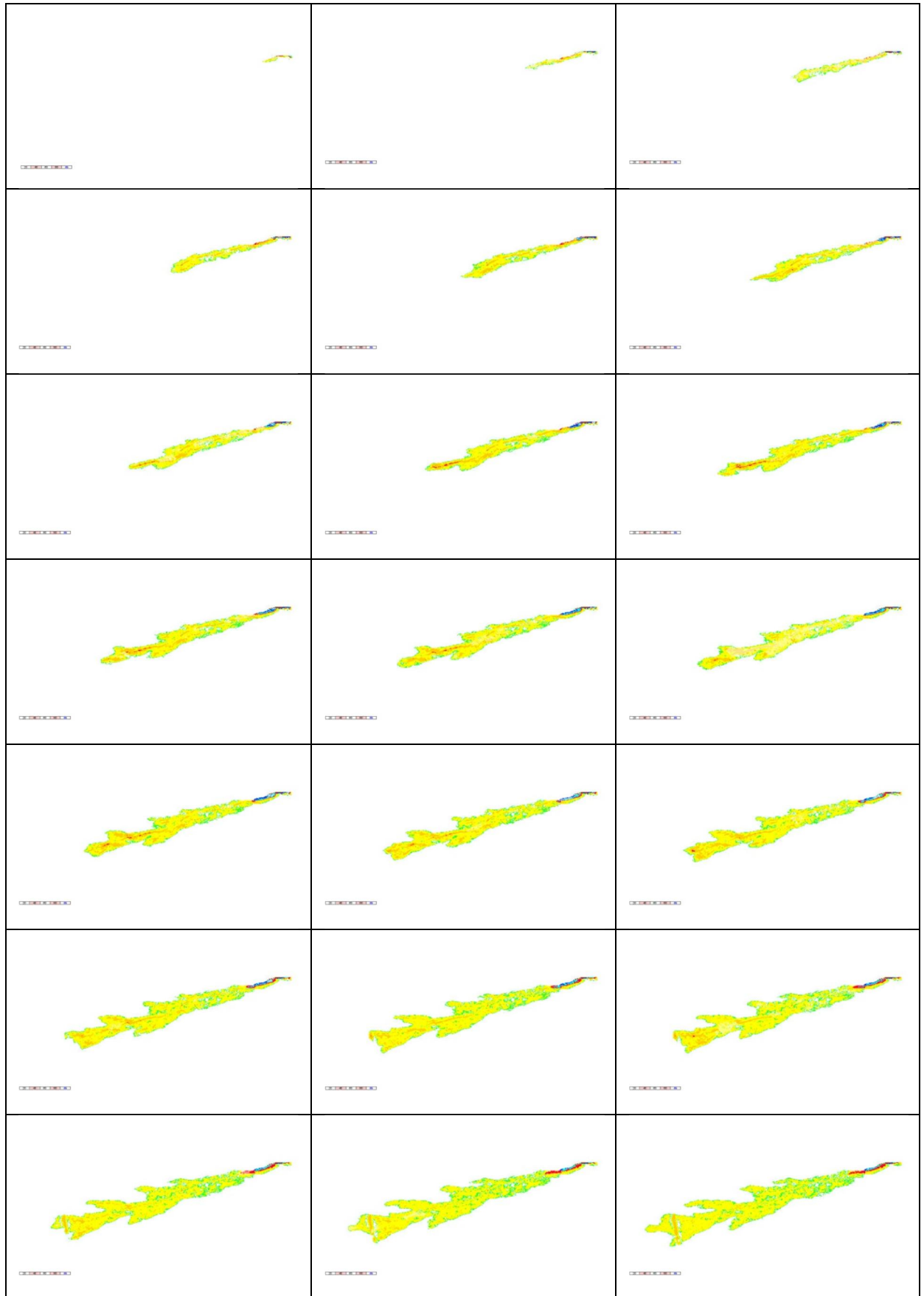


Figure 7.22 Raster map of the distribution of deposits of simulation 28 every 75 time steps (s).

### 7.3.2. Hypothesis 2

With the liquid hydrograph provided for hypothesis 1, whose parameters have been pushed to the limits, the Triggering model was not able to simulate the movement of 6700 cubic metres of sediment (the maximum entrainable material resulted 5000 m<sup>3</sup>).

The debris flow hydrograph for hypothesis 2 have been provided only using a false CN map with a constant distributed value of 91 (appearing CN 81), the precipitation mod+30% and with IA = 0.05S. With this hydrograph, the movement of 6700 cubic metres have been made possible only using an input average sediment size of 0.047 m and a saturation discharge of 0.045 m<sup>2</sup>/s.

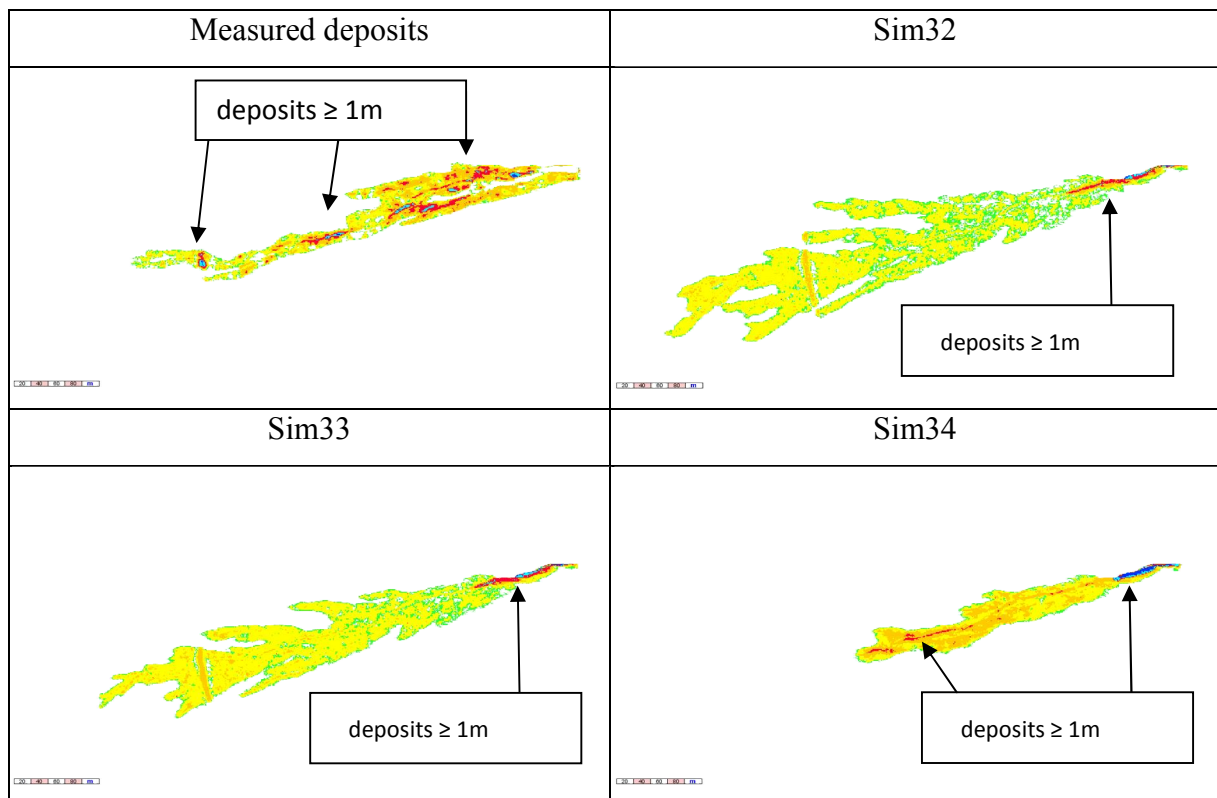
With the aim of observing and commenting the behaviour of the model with this input, some simulations have been run, but their output won't be considered as a result.

Table 7-16 Simulation parameters used for hypothesis 2.

Parameter	Sim32	Sim33	Sim34
Sim time (s)	3600	3600	3600
Input cells	B5	B5	B5
Chezy rel.	2	2	2
Initiation angle (°)	46	48	50

The best simulation that seems to represent the measured deposit for hypothesis 2 is the number 33. Its input solid-liquid hydrograph considers an average grain size diameter of 0.047m, a saturation discharge of 0.045 m<sup>2</sup>/s, QR2, like sim 29 for hypothesis 1. The output is in line with the observations made for hypothesis 1 since the same input cells, initiation angle and Chezy coefficient have been used. The position of the obstruction has however not been simulated correctly, and the majority of the thicker layer lay still too upstream (as for hypothesis 1).





7.23 The simulation routed for hypothesis 2, compared with the map of the measured deposits for the same hypothesis

### 7.3.3. Final considerations

At the end many considerations can be done:

- the influence of the shape of the solid-liquid hydrograph (input: alfa, beta, gamma, delta), given the same input liquid hydrograph and the same input volume to be deposited, seems not to have great influence on the distribution of the simulated deposits, since the percentage difference in all the just considered parameters ranges in only 1-3%, but a little tendency for QR1 debris flow hydrograph to deposit thick layers upstream. In the considered range of parameters and conditions, all the four founded Triggering hydrographs seem able to simulate the 4<sup>th</sup> July debris flow event;
- the parameter "initiation angle" and the average grain size diameter of the solid-liquid hydrograph have to work in direct relationship: the lower the sediment size, the lower the initiation angle required to gain the same spatial distribution of deposits. This is due to the fact that a triggering hydrograph with an input lower average sediment size would mobilize a greater sediment volume;
- a Chezy coefficient of 2 (as suggested by Gregoretti, 2000) is able to work with the input data and with the provided initiation angles to simulate the measured deposits;

- the model is able to simulate with good approximation the deposition area (76-77% of the measured deposits). The simulation of the volume distribution works still with good approximation if dealing with the lower depths, well representing the 71-72 % of the first class deposits (0 - 0.5 m), but shows many difficulties when dealing with larger deposition depth: the deposits in the second class (0.5 - 1 m) are well represented only in the 1-2% of the total; the distribution of higher deposition depths is not correctly simulated, since they tend to stop, in general, too upstream.

## 8. MODELING OF A DESIGN SCENARIO

### 8.1. Introduction to the design scenario

The next step after the search for the best parameters working on the c08 channel has been the simulation of possible future scenarios.

From historical rainfall data it is possible to develop Depth Duration Frequency Curves (DDFC) in the form:

$$h = at^n$$

in which the height (mm) of precipitation, for a given duration (t) and for a given return time can be estimated through the parameters "a" and "n", obtained interpolating historical rainfall series for different durations. The implementation in the Hydrological model for a module that gives the possibility of using this kind of relationships as rainfall input would allow to take into consideration a design precipitation.

The parameters of the DDFC for the area of Fiames have been calculated by Gregoretto (2012) for the return times asked by the PAI methodology. Results are in Table 8-1 and Table 8-2.

Table 8-1 Parameters "a" and "n" of the DDFC for the return periods of 30,100 and 300 years.

Return periods (years)	n	a
30	0.5625	46.3259
100	0.5798	57.3909
300	0.5910	67.4290

Table 8-2 Rainfall heights calculated with the DDFC for the return periods of 30, 100 and 300 years, and for the indicated durations.

duration (hours)	0.083	0.25	0.5	0.45	1	2	3	6	12	24
Rainfall height (mm)	11.45	21.24	31.37	29.56	46.33	68.42	85.94	126.92	187.44	276.82
	13.59	25.69	38.40	36.12	57.39	85.78	108.51	162.19	242.41	362.32
	15.53	29.72	44.76	42.06	67.43	101.57	129.07	194.42	292.85	441.11

Applying a runoff hydrograph obtained from a design precipitation in the Debris Flow Triggering model, with the set of parameters just provided by this study, allowed to simulate the possible entrainable volume and the possible routing and deposition phases of a design

debris flow event characterized by a given return period. Given the delicate situation of the area, in which a much busy national road as the SS 51 could be soon encountered by future events on the c08 channel, this set of models would represent a complete tool to draw hazard maps.

## 8.2. Modeling the design scenario

First, a design runoff has been simulated by the hydrological model thanks to the same parameters used for the successful simulation of the previous chapters (resumed in Table 8-3). To assume the worst possible conditions the AMC conditions have been set to a value of 3.

Three design runoff hydrographs (Table 8-4) have been produced with the three return periods considered by the PAI methodology.

Table 8-3 Advanced parameters of hyetograph and watershed B (one the left) and outlet B characteristics (on the right) used to simulate the runoff.

Advanced Parameters	Used values:		Outlet Parameters	Used values: Section B
Hyetograph shape	Alterned blocks		Initial network velocity	2 m/s
Peak position	0.5		Channel bed slope	49%
Rain step	5 min		Channel width	5.95 m
Out step	1 min		Right and left side slopes	0.54 right, 2.01 left
AMC	3, constant		Gauckler-Strickler roughness coefficient	9 m <sup>1/3</sup> /s
Q <sub>0</sub> - base flow	0.007 m <sup>3</sup> /s		Tolerance	0.04
Recession Constant	6*10 <sup>6</sup>			
Reduction factor	0.9			
Initial abstractions (IA)	0.05S			
Max slope velocity	0.3 m/s			

Table 8-4 Resumed results of the Hydrological model for the three design runoff.

Return period 30 years			
SIMULATED RUNOFF			
	Direct	Base	Total
Rainfall (mm)	10.87	10.099	20.966
Initial discharge (m3/s)	0	0	0
Maximum discharge (m3/s)	2.338	0.009	2.347
Average discharge (m3/s)	0.7	0.003	0.005
Time to peak (h)	0.27	0.27	0.27
Return period 100 years			
SIMULATED RUNOFF			
	Direct	Base	Total
Rainfall (mm)	14.272	11.062	25.334
Initial discharge (m3/s)	0	0	0
Maximum discharge (m3/s)	3.029	0.01	3.039
Average discharge (m3/s)	0.919	0.003	0.006
Time to peak (h)	0.27	0.27	0.27
return period 300 years			
SIMULATED RUNOFF			
	Direct	Base	Total
Rainfall (mm)	17.496	11.817	29.314
Initial discharge (m3/s)	0	0	0
Maximum discharge (m3/s)	3.669	0.01	3.679
Average discharge (m3/s)	1.127	0.003	0.007
Time to peak (h)	0.25	0.27	0.25

The triggering condition "beta" for the Debris flow Hydrograph model have been used: Triggering section B, precipitation mod+30%, IA 0.05S, average grain size diameter 0.047 m, saturation discharge 0.045 m<sup>2</sup>/s, QR2 debris flow hydrograph shape. Instead of a given volume, the input has been represented by the front sediment concentration obtained by the "beta" triggering simulation, in order to mobilize the maximum quantity of sediment material for the given conditions. A design triggering hydrograph has been produced for each of the three considered return times.

The Automata model have been routed with the provided solid-liquid hydrographs, and with the input parameters of sim 29 (except than for the simulation time, set to 1800 observing the Triggering model results): Chezy coefficient = 2, initiation angle = 47°, minimum routing velocity = 0.01 m/s, dry sediment volumetric concentration = 0.62.

The digital surface of the terrain has been obtained by the same procedure explained in chapter 0, but with the post-event GPS points (post 4<sup>th</sup> July) as reference for elevation on the channel area.

The output maximum flow depths and flow velocities have been automatically used to provide the magnitudo maps according to the PAI classification (Figure 8.4).

The map of the hazard classes, according to PAI methodology (see chapter 6.4) , have been obtained crossing in a matrix the higher magnitudo value for each cell, among the three design events, and the relative return periods (Figure 8.5).

All the design events, according to the simulations, resulted able to follow the new active channel, avoiding to the South the retention basin, (confirming the suppositions made on the field) and to reach the SS 51 depositing on it thick layers of debris ( $\geq 1\text{m}$  depth, in Figure 8.1, Figure 8.2, Figure 8.3). The national road, according to the map in Figure 8.5, resulted in the fourth class (P4) of hazard (the most dangerous).

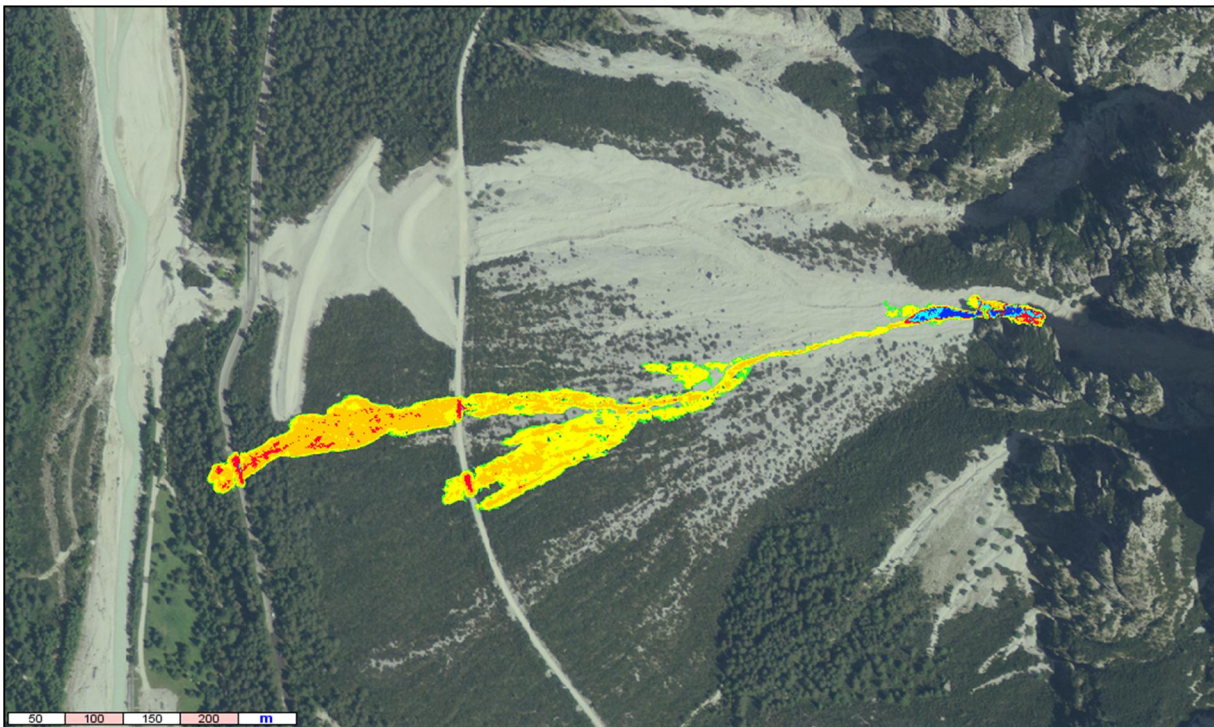


Figure 8.1 Debris deposition depth obtained for the design event with a 30 years return period.



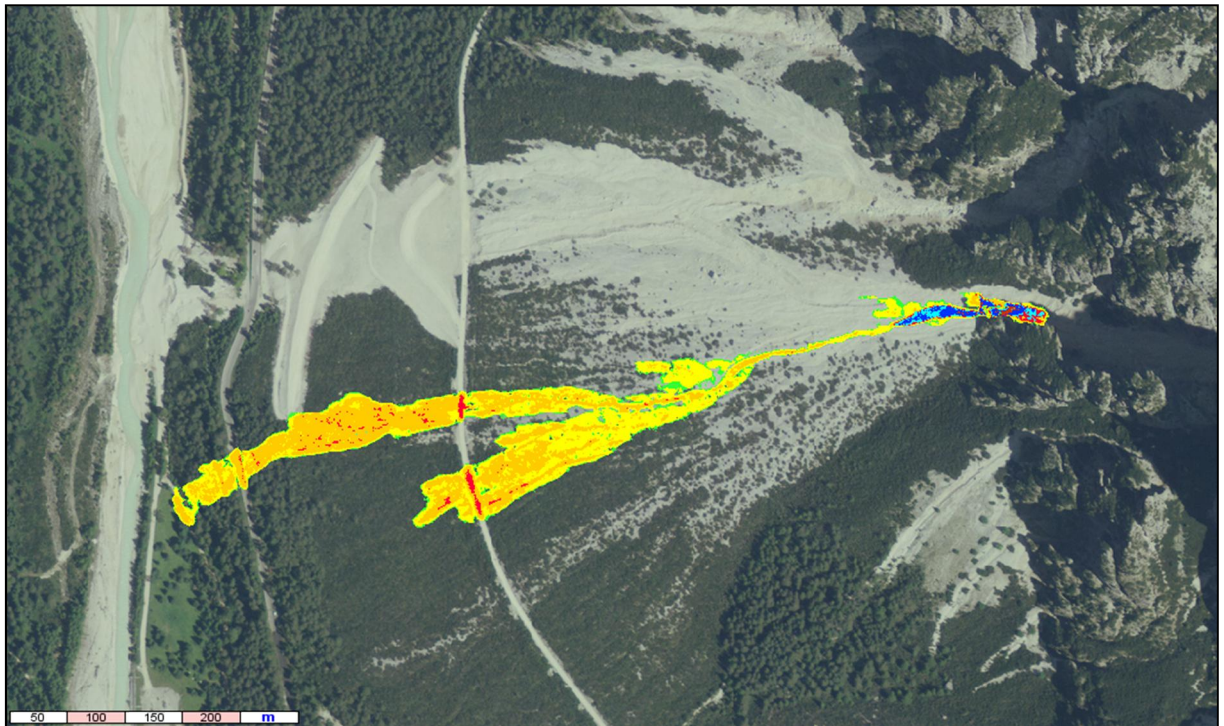


Figure 8.2 Debris deposition depth obtained for the design event with a 100 years return period.

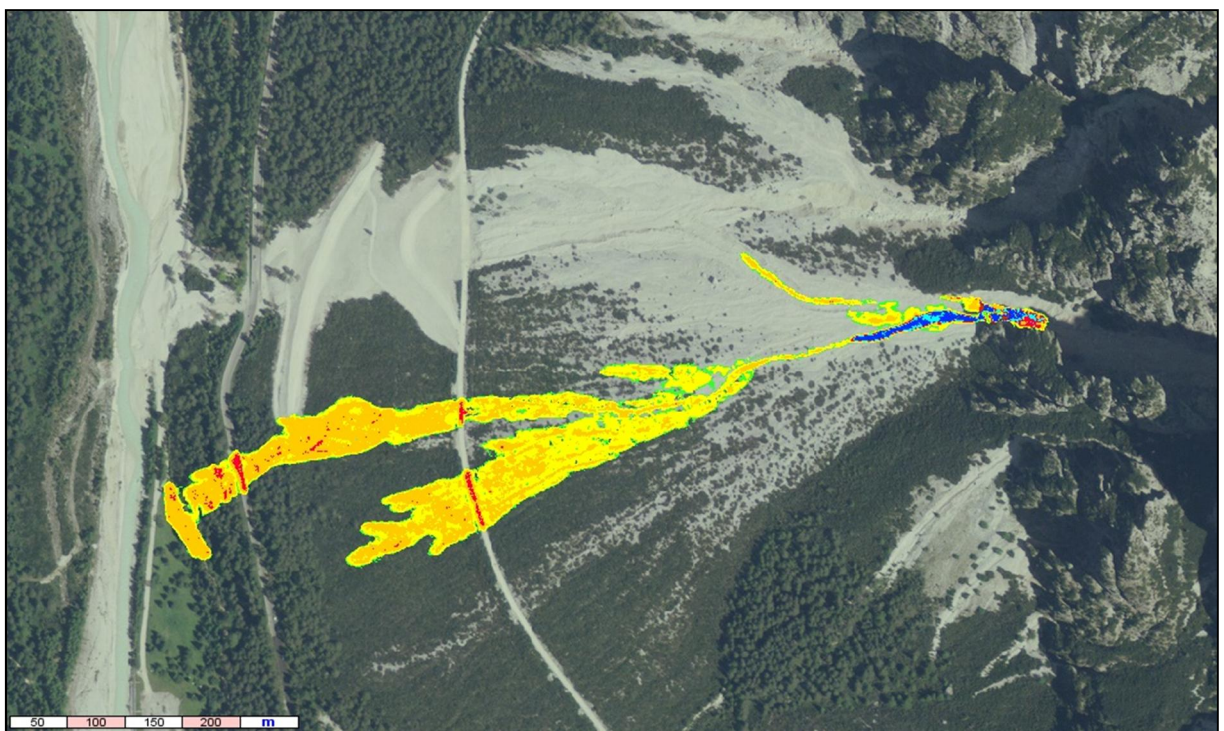


Figure 8.3 Debris deposition depth obtained for the design event with a 300 years return period.



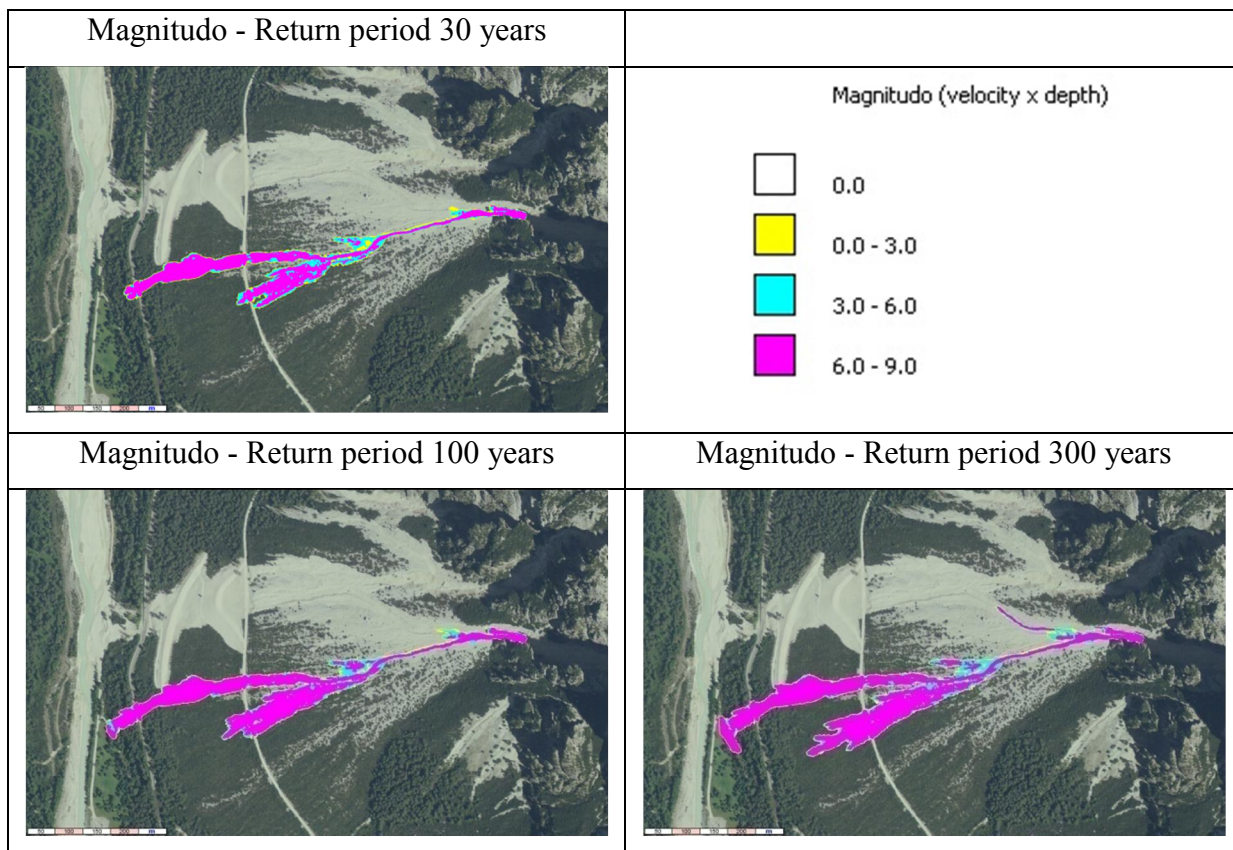


Figure 8.4 Magnitudo maps obtained for the project design with return periods of 30, 100 and 300 years.

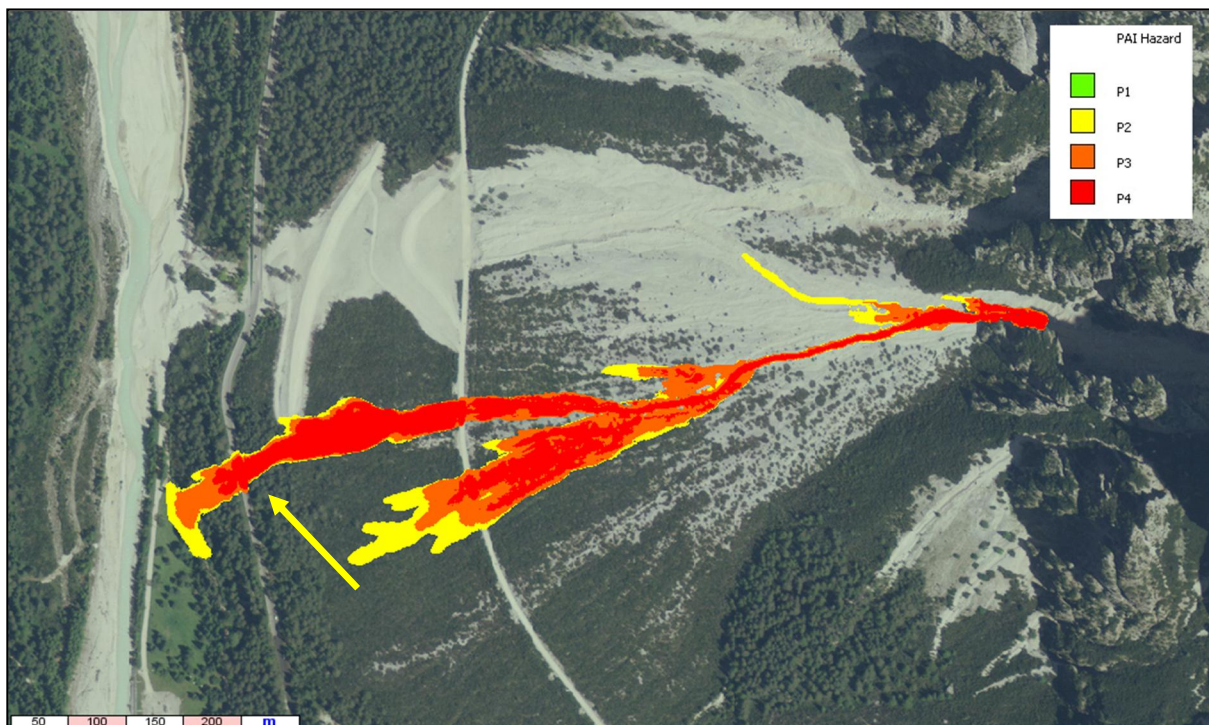


Figure 8.5 Hazard map, according to PAI methodology, obtained crossing in a matrix the higher magnitudo value for each cell, among the three design events, and the relative return periods. The yellow arrow shows the position in which the design events encounter the SS51.



## 9. CONCLUSIONS

The Hydrological model, the Debris Flow Hydrograph model and the Automata Cellular model have been used for estimating the solid-liquid hydrograph and simulating the routing and deposition phases of the debris flow occurred in the evening of the 4<sup>th</sup> of July 2011 at Fiames (Km 109 SS51).

A set of field data, made by both GPS and Lidar dataset, have been used to estimate the sediment material entrained by the case study event, and to build the digital surfaces of the terrain where debris flow simulations run. The GPS survey resulted useful to reconstruct the pre-event and the post-event digital surfaces of the channel, in order to estimate the mobilized material, but a higher density of points (or a post event Lidar survey - optimal by the point of view of the quantity of data, but prohibitive on the point of view of costs) would be required to increase precision.

The search for the parameters to simulate the event that best fit with the measured field data lead to a set of simulations providing results to be tested, corrected and re-tested with an iterative procedure involving all the three models at the same time, using the not satisfying results as a basis for new simulations.

The Hydrological resulted able to simulate runoff that mobilized the hypothesized 4700 cubic metres of material (hypothesis 1), as emerged from field observations and field measurements. after assuming:

- among the two triggering areas hypothesized on the field, the one with the larger contributing area (B) has been chosen;
- the rainfall data registered by the rain-gauge positioned in the Dimai channel, about 1,7 Km South, have been increased by 30% to take into consideration the measurement losses due to wind and the possible barrier effect of the surrounding peaks;
- The Kinematic Routing Excess Rainfall Model (KRERM) applied to calculate the liquid hydrograph have been used considering a value of initial abstraction of 0.05S instead of 0,1S.

The Triggering model has been able to trigger the movement of 4700 cubic metres of material under four set of conditions:

- Triggering section B, precipitation mod+30%, IA 0.05S, average grain size diameter **0.074 m**, saturation discharge 0.045 m<sup>2</sup>/s, **QR2** debris flow hydrograph shape, volume 4700 m<sup>3</sup>;
- Triggering section B, precipitation mod+30%, IA 0.05S, average grain size diameter **0.047 m**, saturation discharge 0.045 m<sup>2</sup>/s, **QR2** debris flow hydrograph shape, volume 4700 m<sup>3</sup>;
- Triggering section B, precipitation mod+30%, IA 0.05S, average grain size diameter **0.074 m**, saturation discharge 0.045 m<sup>2</sup>/s, **QR1** debris flow hydrograph shape, volume 4700 m<sup>3</sup>;
- Triggering section B, precipitation mod+30%, IA 0.05S, average grain size diameter **0.047 m**, saturation discharge 0.045 m<sup>2</sup>/s, **QR1** debris flow hydrograph shape, volume 4700 m<sup>3</sup>.

All the four solid-liquid hydrographs have been used as input in the Automata model for the simulation of routing and deposition phases. As resulting from the visual and analytical comparison, all of them resulted able to simulate with good approximation the measured deposits (simulations 28, 29, 30 and 31). The parameters that most influenced the routing phases were the input solid-liquid hydrograph, in particular the average grain size diameter, and the initiation angle for sediment mobilization, that apparently are in direct relationship. The shape of the input triggering hydrograph did not influenced the two simulations regarding the lower sediment size (sim 29 and 31), while it influenced the dispersion of sediment in the simulations regarding the higher sediment size in the triggering area (sim 28 and 30): the simulation routed with QR2 (sim28) indeed, provided for more sediment deposition depths in the initial portion of the simulated deposition area.

Among the four simulations, the 76-77% of the area with measured deposits have been overlapped by those simulated. Four deposit depth classes have been adopted to compare the volumes: only 20-21% of the deposits depths in the first class (0 - 0.5 m) have been correctly simulated, and 1-2% of the second class (0.5 - 1m). Higher depths were not correctly simulated because the measured thicker layers (up to 2.4 m) were distributed in various zones of the channel (probably where allowed by the slope conditions), and the simulated thicker layer (up to 4m) occurred in the first hundreds of metres of the routing area (550 m is the linear extension of the deposition area).

The hypothesis of a mass movement of 6700 cubic metres have been realized only introducing heavy abstraction in the input of the Hydrological model, in particular providing it with a false CN map with a constant distributed value of 91, +30% modified precipitations and initial abstraction equal to 0.05S. Some simulations have been conducted to observe and comment the outputs but their results have not been considered.

As emerges from the positive results of the comparison among measured and simulated deposits, the set of Hydrological, Debris Flow Hydrograph and Automata models resulted able to simulate the case study event.

Finally, the possibility of simulating possible future scenarios has been tested. The historical rainfall analysis for the area and the construction of depth duration frequency curves has been conducted: using the project precipitations in the model allowed to test it with three design debris flow events, characterized by a return period of respectively 30, 100 and 300 years (according to PAI methodology), and using the input parameters just calibrated with the case study of the 4<sup>th</sup> of July. The output maps of magnitude have been used to generate a hazard map relative to the possible activity of the c08 debris flow channel for the considered return periods. According to the model, resulted that the SS51 national road, where it meets the debris flow, is classified P4, the higher hazard level. The simulated debris front was indeed able to proceed along the new active channel, avoiding to the South the retention basin, and depositing huge quantities of sediment on the road.

Considering the success of the model in simulating with good approximation a case study event and a project event for the construction of hazard maps, it should result helpful in improving hazard management strategies for infrastructures and human settlements protection in the Dolomitic and, in general, in the Alpine areas.



## 10. BIBLIOGRAPHY

- ArcMap ver 10.0 user manual.
- Autorita' di Bacino dei Fiumi Isonzo, Tagliamento, Livenza, Piave, Brenta-Bacchiglione (2007); Piano Stralcio per L'assetto Idrogeologico dei Bacini Idrografici dei Fiumi Isonzo, Tagliamento, Piave e Brenta-Bacchiglione: 32-35.
- Bagante D. (1999) - Studio sperimentale di colate detritiche su pendii drenati ad elevata pendenza, Università di Padova, Facoltà di Ingegneria, Dip. Idraulica, marittima e geotecnica, Tesi di laurea, 97-128 pp.
- Bates P.D., De Roo A.P.J. - A simple raster-based model for flood inundation simulation; Journal of Hydrology 236 (2000) 54-77.
- Berti et al. (2000) - Debris flow monitoring in the Acquabona watershed on the Dolomites (Italian Alps); Phys. Chem. Earth (B), vol 25, n°9, pp. 707-715, 2000.
- Berti M., Genevois R., Simoni A., Tecca P.R., (1998) - Field observations of a debris flow event in the Dolomites; Geomorphology 29 (1999) 265-274.
- Berti, M & Simoni A. (2007) - Prediction of debris flow inundation areas using empirical mobility relationships; Geomorphology, 90: 144-161.
- Blijenberg H.M. (1998) - Rolling Stones. Triggering and frequency of hillslope debris flow in the Bachelard Valley, southern French Alps; Tesi di dottorato, Buren, 25 Agosto 1998, 29-114 pp.
- Convenzione tra La Regione Veneto E L'IRPI – CNR per lo Studio della colata detritica di Fiames (Cortina d'Ampezzo, BL) - Relazione Finale; Università di Padova - Dipartimento di Geologia, Padova - Maggio 2005; pagg. 5-9.
- Dalla Fontana (2009) - Materiale didattico del corso di Sistemazioni Idraulico Forestali, cap. 5 frequenza degli estremi.
- Degetto M., Gregoretti C. (2012) - Debris Flow Modeling Tool User Manual, (2012).
- Gregoretti C. and Dalla Fontana G. (2007) - Rainfall threshold for the initiation of debris flows by channel-bed failure in the Dolomites; Debris-Flow Hazards Mitigation: Mechanics, Prediction and Assessment, Chen & Major, eds, 2007 Millpress, Netherlands.
- Gregoretti C. and Dalla Fontana G. (2008) - The triggering of debris flow due to channel-bed failure in some headwater basins of the Dolomites: analyses of critical runoff; Hydrological Processes, vol. 22, DOI: 10.1002/hyp.6821.

- Gregoretti C.(2000) - Estimation of the maximum velocity of a surge of debris flow propagating along an open channel.
- Gregoretti C., Degetto M. (2012) - Debris Flow Modeling Tool Reference Manual, (2012).
- Gregoretti C., Furlan M., Degetto M.; (2011) - GIS-based cell model for simulating debris flow routing and deposition phases on a fan.
- Hawkins R.H., Ward T.J., Woodward D.E., Van Mullem J.A. (2009) - Curve Number Hydrology: state of the practice; Eds. By American Society of Civil engineers (ASCE).
- Johnson A.M., Rodine J.R. (1984) - Debris Flow; in Brundsen D. e Prio D.B "Slope Instability", J.Wiley, New York, 357-361.
- Paramount Statements (2007); [http://www.paramount-project.eu/index.php?option=com\\_content&view=frontpage&Itemid=1](http://www.paramount-project.eu/index.php?option=com_content&view=frontpage&Itemid=1).
- Rickenmann D. (2005) - Runout prediction methods In Debris-Flow Hazards and Related Phenomena; Jakob M, Hungr O (eds). Praxis Springer: Berlin Heidelberg: 305-324.
- Scheidl C., Rickenmann D., Chiari M. - The use of airborne LiDAR data for the analysis of debris flos events in Switzerland; Natural Hazard and Earth System Sciences,8,1113-1127, 2008.
- Scheidll C., Rickenmann D. (2010) - Empirical prediction of debris-fl ow mobility and deposition on fans; Earth Surf. Process. Landforms 35, 157–173 (2010).
- Takahashi T. (1981) - Debris Flow; in Van Dyke M., Wehauser J.V. and Limley J.L., Annual review of fluid mechanics: Palo Alto, California, Annual reviews, v.13,55-77 pp.
- Takanashi K., Mizuyama T. & Nakano Y. (2007) – A method for delineating restricted hazard areas due to debris flows; Proceedings of the 4<sup>th</sup> International Congress on Debris-Flow Hazards Mitigation, Chengdu 10-13 September: 471-478.